

**MODELING AND FAULT DIAGNOSIS OF BROKEN
ROTOR BAR FAULTS IN INDUCTION MOTORS**

By

Kenneth Ikponmwosa Edomwandekhoe

A thesis submitted to the

School of Graduate Studies

In partial fulfillment of the requirements for the degree of

Master of Engineering

Faculty of Engineering and Applied Science

Memorial University of Newfoundland

Oct. 2018

St. John's

Newfoundland

Abstract

Due to vast industrial applications, induction motors are often referred to as the “workhorse” of the industry. To detect incipient faults and improve reliability, condition monitoring and fault diagnosis of induction motors are very important. In this thesis, the focus is to model and detect broken rotor bar (BRB) faults in induction motors through the finite element analysis and machine learning approach.

The most successfully deployed method for the BRB fault detection is Motor Current Signature Analysis (MSCA) due to its non-invasive, easy to implement, lower cost, reliable and effective nature. However, MSCA has its own limitations. To overcome such limitations, fault diagnosis using machine learning attracts more research interests lately. Feature selection is an important part of machine learning techniques.

The main contributions of the thesis include: 1) model a healthy motor and a motor with different number of BRBs using finite element analysis software ANSYS; 2) analyze BRB faults of induction motors using various spectral analysis algorithms (parametric and non-parametric) by processing stator current signals obtained from the finite element analysis; 3) conduct feature selection and classification of BRB faults using support vector machine (SVM) and artificial neural network (ANN); 4) analyze neighbouring and spaced BRB faults using Burg and Welch PSD analysis.

Acknowledgements

The author would like to express his solemn appreciation to his supervisor, Dr. Xiaodong Liang for her tremendous supervision and support to this research. The author is appreciative and pleased with her for inspiring him and putting her prized knowledge during the course of his research work in M.Eng at Memorial University of Newfoundland. The successful completion of this program would be almost impossible unless for her guidance and supervision.

The author would like to thank all entities that provided financial support for this research in the two years stipulated of M.Eng program.

The author would also like to thank Memorial University of Newfoundland for all kind of support to this research.

The author would like to express profound gratitude to his family members, and friends for their encouragement and emotional supports.

Table of Contents

Abstract.....	ii
Acknowledgements	iii
List of Tables.....	vi
List of Figures.....	vii
List of Symbols.....	xi
List of Abbreviations.....	xiv
Chapter 1: Introduction.....	17
1.1 Background.....	17
1.2 Components of Induction Motors	18
1.3 Operation Principles of Induction Motors	20
1.4 Thesis Organization	21
Chapter 2: Literature Review	27
2.1 Non-Parametric Approach	28
2.2 Artificial Intelligence Methodology	33
Chapter 3 : Current Spectral Analysis of Broken Rotor Bar Faults for Induction Motors.....	81
Chapter 4: Advanced Feature Selection for Broken Rotor Bar Faults in Induction Motors.....	99
Chapter 5: Burg and Welch PSD analysis of Neighbouring and Spaced Broken Rotor Bar Faults for Induction Motors.....	131

5.1	Burg PSD Signal Analysis	137
5.2	Welch PSD Technique	140
	Chapter 6: Conclusion and Future Work	151
6.1	Contribution	151
6.2	Future Work	153

List of Tables

Table 2.1: Performance Comparison of the AAC, MLFF, and the ANFIS [18]	39
Table 2.2: Fault Survey Results for Induction Motors from IEEE-IAS and EPRI [25]	44
Table 2.3: Stator end winding insulation failure due to broken rotor bar fragment in a 6.6-kV 500-kW induction motor [28]:	45
Table 2.4: FSC values: (a) FSC vs. the number of BRBs, (b) FSC vs. sample number using TLS ESPRIT [37].	50
Table 2.5: Frequency Bands for High Order Wavelet Signals [34]	55
Table 3.1: Specifications of Induction Motor Used in the Simulation	86
Table 3.2: AMPLITUDES FOR DIFFERENT BRB FAUCLTS USING THOMSON	93
Table 3.3: Amplitudes for Different BRB Faults Using Welch PSD Estimation	93
Table 3.4: Feature Selected Using Welch PSD Estimation Technique for SVM Classification	96
Table 4.1: Comparison of Three Spectral Analysis Techniques (FFT, YUL-AR, AND MP)	109
Table 4.2: Amplitudes for Different BRB Condition Using FFT	110
Table 4.3: Amplitudes for Different BRB Faults Using YUL-AR	113
Table 5.1: The basic motor information used in the simulation	137
Table 5.2: Comparative Features of Burg and Welch PSD Technique.	140
Table 5.3: (III) Burg PSD analysis	145
Table 5.4: IV Welch PSD analysis	145

List of Figures

Figure 1.1: Three-phase induction motor (ABB motors)	18
Figure 1.2: Squirrel cage rotor vs wound rotor type.....	20
Figure 2.1: Probability distributions: (a) of 1 and 0 s in Det_mat. (b) of T, SNR=-65 dB (normalized) [3].	30
Figure 2.2: Overview of the proposed method for fault detection and diagnosis [5].	31
Figure 2.3: STFT current spectrogram (a) Healthy motor (b) Motor with 1BRB [8].	32
Figure 2.4: Tapered estimate of the PSD of the AR(6) process. (a) Tapered estimate using the Hann taper. (b) Equivalent smoothing kernel $1/\Delta H(f) ^2$ centered at $f\Delta=0.4$. The zoomed-in view of the main lobe is shown on the top left [9] (AR depicts Auto regressive).	33
Figure 2.5: Schematic representation of the pattern standardization and comparison [13]......	35
Figure 2.6: Training data set for 3-dimensional problem after applying PCA (cross- validation 1): red - healthy bars, blue - broken bars (b) Training data set for 2-dimensional problem after applying PCA (cross-validation 1): red - healthy bars, blue - broken bars [15]	37
Figure 2.7: Training and testing data production algorithm [15].	38
Figure 2.8: Test set in the three-dimensional feature space (Fop) after standardization. Healthy machine $\langle\langle \blacksquare \rangle\rangle$, defective machine $\langle\langle \star \rangle\rangle$, bearing failure $\langle\langle \bullet \rangle\rangle$ [19].	39
Figure 2.9: Fault types and percentage of occurrence in induction motors [20]-[24]	44

Figure 2.10: Stator end winding insulation failure due to broken rotor bar fragment in a 6.6-kV 500-kW induction motor [28]	49
Figure 2.11: MCSA results for the same motor with a broken rotor bar under a constant load and a gradual varying load condition [28].	50
Figure 2.12: FSC values: (a) FSC vs. the number of BRBs, (b) FSC vs. sample number using TLS ESPRIT [37].	54
Figure 2.13: Loaded machine with two broken rotor bars. (a) Wavelet analysis of start-up current, (b) FFT analysis of the current in steady state [34].	55
Figure 2.14: Flowchart showing effects of two categories of bearing faults [51].	60
Figure 2.15: Spectrum of vibration velocity of a motor with a healthy bearing [51].	60
Figure 2.16: Spectrum of vibration velocity for a motor with 1500 μ m bearing defect [51].	61
Figure 2.17: DC equivalent circuit of source, motor and DC injection circuit [60].	62
Figure 2.18: Block diagram of mathematical model for induction motors [63].	63
Figure 2.19: Simulation of an asymmetrical induction motor model [66]	64
Figure 2.20: Neural network architecture [69]	67
Figure 2.21: Normalized amplitudes of broken rotor bar components at different loads and motor states (the motor is 1.1 kW) [69].	68
Figure 2.22: The learning curve of NN with eight input feature [70].	68
Figure 3.1: Induction motor FE analysis model at 75% loading: (a) a healthy motor, (b) a motor with 1BRB, (c) a motor with 2BRBs, and (d) a motor with 3 BRBs.	86
Figure 3.2: Simulated induction motor stator current at 75% loading using ANSYS for the four scenarios defined in Fig. 3.1	87

Figure 3.3: Simulated induction motor speed signal at 75% loading using ANSYS for the four scenarios defined in Fig. 3.1.....	87
Figure 3.4: Simulated induction motor torque signal at 75% loading using ANSYS: (a) a healthy motor, (b) a motor with 1BRB, (c) a motor with 2BRBs, and (d) a motor with 3BRBs.....	88
Figure 3.5: Thompson Multitaper estimation for current spectrum: (a) a healthy motor; (b) a motor with 1BRB; (c) a motor with 2BRBs; (d) a motor with 3BRBs.....	92
Figure 3.6: Welch PSD estimation for current spectrum: (a) a healthy motor; (b) a motor with 1BRB; (c) a motor with 2BRBs; (d) a motor with 3BRBs.....	93
Figure 3.7: Welch PSD estimation for power spectrum of x and y peaks; (b) SVM classification model for BRB faults for the induction motor.....	95
Figure 4.1: Induction motor model at 75% loading: (a) a healthy motor, (b) a motor with one BRB, (c) a motor with two BRBs, and (d) a motor with three BRBs.....	105
Figure 4.2: Induction motor stator current at 75% loading.....	106
Figure 4.3: Torques calculated by ANSYS at 75% loading for a healthy motor and motor with one, two and three BRBs.....	106
Figure 4.4: Motor stator current spectra obtained by FFT: (a) a healthy motor, (b) with one BRB, (c) with two BRBs, (d) Motor with three BRBs.....	109
Figure 4.5: SVM 22% failed classifier using FFT features.....	110
Figure 4.6: Motor stator current spectra obtained by YUL-AR: (a) healthy motor, (b) one BRB, (c) two BRBs, (d) three BRBs.....	112
Figure 4.7: Approximated signals obtained by MP: (a) healthy motor, (b) motor with one BRB, (c) motor with two BRBs, (d) motor with three BRBs.....	116

Figure 4.8: The orthogonal MP feature indices for selected coefficients: (a) healthy motor, (b) one BRB, (c) two BRBs, and (d) three BRBs.	117
Figure 4.9: SVM quadratic classification by MP features: (a) RankofSelRank vs Ndxindic class, (b) Coefs vs Ndxindic class, c) Ndzxinfamily vs Familynumber class, d) RankofselRank vs Familynumber.	122
Figure 4.10: SVM quadratic confusion matrix; true positive vs false positive rate.	122
Figure 4.11: ANN model for training and classification output.	122
Figure 4.12: ANN training and classification output.	123
Figure 4.13: Performance for ANN Training	123
Figure 4.14: Target and response for ANN Training.	124
Figure 5.1. IM ANSYS Model under 100% loading; (a) 2-Neighbor BRB, (b) 2-Spaced BRBs, (c) 3-Neighbor BRB, and (d) 3-Spaced BRBs	136
Figure 5.2. The stator current signal: Blue is 2-Neighboring BRB, Yellow is 2-Spaced BRB, Green is 3-Neighboring BRB, and Red is 3-Spaced BRB.	137
Figure 5.3. Burg PSD Estimate; (a) 2-Spaced-BRB; (b) 2-Neighbour-BRB; (c) 3-Spaced-BRB; and (d) 3-Neighbour-BRB	139
Figure 5.4. Welch PSD Spectrum for Healthy Motor Condition.	142
Figure 5.5. Welch PSD Estimate; (a) healthy motor; (b) 2 Spaced BRBs (c) 2 Neighbouring BRBs; (c) 3 Spaced BRBs; (d) 3 Neighbouring BRBs.	143

List of Symbols

B_{xx}^w	Biased Spectral Estimate
Ce_{srp}, Ce_{srn}	Pulsating Torque
$J_M^{(i)}(w)$	Periodogram
W_t	Model Parameter
b_{or}	Rotor slot Opening
b_{os}	Stator slot Opening
μ_0	Magnetic Permeability of Air
ϕB_{rn}	Rotor Flux Fault Density
ϕB_{rp}	Rotor Flux Normal Density
ϕB_s	Stator Flux Density
$1/\sqrt{s}$	Normalization constant
$a \hat{p}$	Estimates of Ar Parameters
B	Shift Operator
D	Dictionary
Det_mat	Binary Representation of Frequency Pattern
F	Frequency
F_b	Bar Frequency
F_{op}	Feature Optimization
g	Airgap
K_r	Coefficient Depending on Cage Rotor Assembly
K_s	Coefficient Depending on Stator Winding

L	Active Length of Magnetic Circuit
M	Length of Sub Samples
N	Numbers of Data
Θ	Contact Angle
P	Model Order
R	Window Hop Size
R	The Average Radius of Air-Gap
R_0	Internal Resistance
S	Scaling
S	Slip
T	Temperature
U	Normalization Factor
U	Shifting
W	Bandwidth
α	Winding Property Constant
Ξ	Modulating
Υ	Index
D_p	Ball Pitch Diameter
\hat{E}_p	Total Least-Square Error of Order P
Fr	Speed of Rotor
I_{rn}	Rotor Negative Current
I_{rp}	Rotor Positive Current
I_s	Stator Current

K/p	1, 2, 3...
R_r	Rotor Resistance
R_s	Stator Resistance
$W(e^{j\omega})$	Spectral Window
$X(t)$	Variant of AR Process
dB	Decibel
$e[n]$	Unobserved Input Data
$w[n]$	Applied Window
$x(n)$	Signal Length
$x[n]$	Observed Output of System
Ψ_j	Coefficient of X_t
β	Beta

List of Abbreviations

AAC	Artificial Ant Clustering
AAS	Artificial Ant System
AC	Alternating Current
AE	Acoustic Emission
AI	Artificial Intelligence
ANFIS	Adaptive Network-Based Fuzzy Interference System
ANN	Artificial Neural Network
BP	Back Propagation
BRB	Broken Rotor Bar
CART	Classification and Regression Tree
CCB	Counter Current Breaking
DB	Ball Diameter
DC	Direct Current
DCT	Discrete Cosine Transform
DFT	Discrete Fourier Transform
DPSS	Discrete Prolate Spheriodal Sequence
DWT	Discrete Wavelet Transform
EEG	Electroencephalogram
EMD	Empirical Mode Decomposition
EPRI	Electric Power Research Institute
FE/FEM	Finite Element/ Finite Element Method
FFA	Relative Humidity

FFT	Fast Fourier Transform
FGPA	Field Programmable Gateway Array
FMM	Finite Min-Max
FN	False Negative
FP	False Positive
FSC	Fault Severity Criterion
HT	Hilbert Transform
IM	Induction Motor
KNN	K-Nearest Neighbour
LDA	Linear Discriminant Analysis
MATLAB	Matrix Laboratory
MCSA	Motor Current Signal Analysis
MLFF	Multilayer Feed Forward
MLP	Multilayer Perceptron
MMF	Magneto Motive Force
MP	Matching Pursuit
MSE	Mean Square Error
MTM	Multitaper Method
MUSIC	Multiple Signal Classification
NB	Number of Balls
OMP	Orthogonal Matching Pursuit
PCA	Principal Component Analysis
PSD	Power Spectral Density

SMO	System Minimal Optimization
SNR	Signal Noise Ratio
ST	Scale Transform
STFT	Short Time Fourier Transform
SVM	Support Vector Machine
TEFC	Totally Enclosed Fan Cooled
TLS-ESPIRIT	Estimation of Signal Parameters via Rotational Invariance Techniques
VFD	Variable Frequency Drive
WPA	Wavelet Packet Analysis
YUL-AR	YULE Auto-Regression
<i>DQ</i>	Direct Quadrature

Chapter 1: Introduction

1.1 Background

In modern societies, our life majorly relies on rugged and efficient machines for fast pace production of goods and services, evident in continual remodeling and enhancement of different machines to enable effective and sustainable delivery of produce in various industrial sectors. The production of goods and services are connected to optimum use of energy. Electrical energy consumes approximately 30% of used energy [1]. Most electrical energy is transformed into mechanical energy through electrical motors, and induction motors are the most vastly applied machines for both home and industrial applications due to their robust design, compactness and ruggedness. For home appliances, small single-phase induction motors are often used and fed from an AC single phase power supply [2]. Three phase induction motors are widely used in industrial facilities.

Recently, variable frequency drives (VFD) have been commonly used for induction motors due to flexibility in production control, soft starting characteristics etc. It is said that the relevance of VFD's is on the increase, with about a 9% growth rate since a decade ago. Application with VFD's are compressors, ventilators, pumps, robotics, and electric vehicles etc [3].

1.2 Components of Induction Motors

An induction motor consists of a stator and a rotor. The stator is a stationary part, and the rotor is the rotating part of the machine. There are two types of rotor design: 1) squirrel cage rotor, and 2) wound rotor. In this thesis, the squirrel cage induction motor is considered. The design of an induction is strived to have less required maintenance, high reliability and good efficiency [4]. Fig. 1.1 shows the internal structure of a three-phase induction motor.

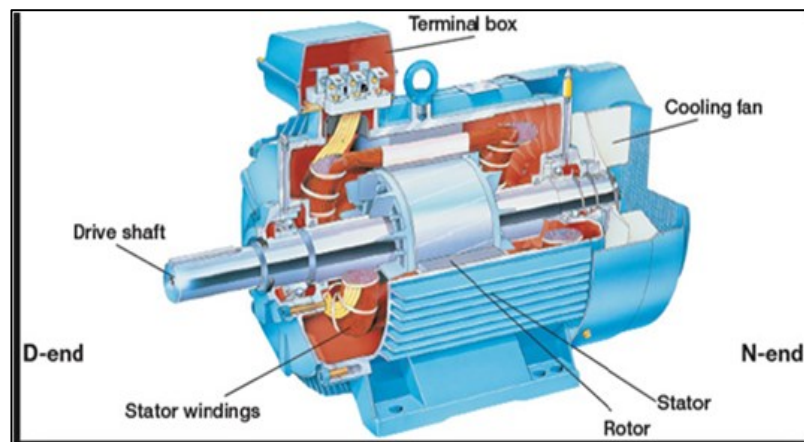


Figure 1.1: Three-phase induction motor (ABB motors)

The stator consists of an outer cylindrical frame with two ends made up of cast aluminum alloy or cast-iron steel laminations. For a higher fundamental frequency, thinner laminations are proposed. The laminated stator slotted magnetic core ensures moderate losses (eddy current and heat loss). The three-phase winding is embedded in the stator core from which the three-phase voltage is supplied. There are six terminals that are connected to the machine box terminal, a pair per phase. All induction motors practically have a cylindrical rotor having a radial airgap existing between the stator and the rotor.

The airgap of induction motors serves as the passage route for the magnetic field generated by the stator. The magnetic field passing through the airgap is responsible for the induction of voltage and current in the rotor. When the passage of the airgap becomes narrower, the magnetomotive force (mmf) within the rotor compartment is smaller. Factors that affect the lower limit of airgaps, g , include: 1) mechanical constraints, 2) the ratio of the stator and rotor slot openings (b_{os} , and b_{or} respectively) to airgap g , and 3) keep the surface core and tooth flux pulsation extra losses to an acceptable level. Wrapping the windings within the core ensures that the magnetization current is reduced and the heat transmission to the core is enhanced. The geometry slot depends on power capacity of induction motors. Slots opening in the motor influences core losses through the flux density manipulations.

Rotor design is supplied with either single or double cage windings as seen in Fig. 1.2. The cage rotor is a product of die cast aluminum for low and medium power machines, while brass or copper for large machines. Medium and high-power motors have their bars welded end to end to provide insulation. To achieve high efficiency, induction motors with copper winding are preferable as they ensure high conductivity, high temperature working tolerance and current density.

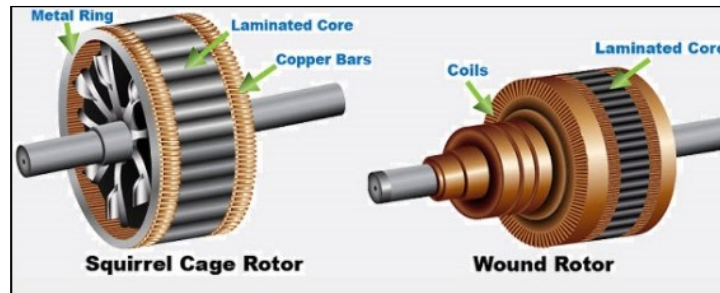


Figure 1.2: Squirrel cage rotor vs wound rotor type.

1.3 Operation Principles of Induction Motors

Due to vast applications of induction motors, incipient fault detection remains a critical tool that can proffer long term solutions against unprecedented breakdown of the motor. Failures in machines can be connected to motor assembling, installation, load tolerance, and maintenance timing. Induction motor faults may arise in three core parts of the machine: bearing, rotor, and stator. Amongst various faults, the broken rotor bar fault causes about 9% of induction motor failures. Due to absence of direct electrical connection between the squirrel cage rotor and the stator, the detection of the broken rotor bars fault is difficult.

This research seeks to develop a mechanism that can help track and pinpoint incipient broken rotor bar faults arising in induction motors. An effective approach will help checkmate and avoid the downsides of machine unscheduled failure due to BRB faults that could have huge negative impacts in the industrial financial sector.

There are three major types of maintenance strategy for induction motors:

1) Scheduled maintenance. This type of maintenance involves a maintenance either based on the manufacturer's prescription or planned timing decided based on machine accumulated workhours. This is one of the most employed known methods of maintenance used by industry, however, it does not guide against emergency motor failure.

2) Breakdown maintenance. This methodology is intended to run the motor to the threshold tolerance until it breaks down, therefore, it is usually the least indulged maintenance technique. Due to breakdown, the motor might be irredeemable but only good for replacement. Thus this methodology is rarely employed in industry today.

3) Condition based maintenance. This is the most viable technique on the rise in factory and commercial industry today. It involves real-time monitoring in most cases, whereby the system condition is being observed while in operation and would detect any anomaly that arises during the system working mode. The indication of the system deviation from normal operation could be done through an alarm system or other means that can inform the system to shut down for analysis and reinstallation.

The real-time condition monitoring technique involves a system that continually monitors working conditions of systems per time and is able to detect any deviation or anomaly that arises. This technique is more viable and effective because it's able to prevent severe damages to the machine and prevent uninterrupted machine breakdown [6-8].

1.4 Thesis Organization

This thesis is dedicated to exploring and modeling methodology that is based on condition-based maintenance culture, which will prevent the untimely interruption of work

process, reduce the process downtime, and narrow the maintenance cost. Various techniques are discussed and reviewed as a precedence to reaching a viable method. A new method credible of diagnosing and predicting fault accurately is hereby proposed for incipient fault detection of BRB faults of induction motors. Various fault conditions with different numbers of BRBs are modeled, and a fault prediction mechanism is proposed to capture healthy and fault conditions.

In the absence of motor experimental/testing data, modeling of an induction motor is a viable way to have access to data through simulation of fault conditions of the machine. The non-invasive condition monitoring technique is a favorable condition monitoring technique. It is known that improper modeling with many assumptions may introduce errors, in this thesis, the finite element analysis is used to model the induction motor due to its proven accuracy in the literature. The finite element software ANSYS is used for modeling and simulation of a healthy motor and the motor with various number of BRBs. ANSYS is a feasible tool that can best represent transiency inherent in induction motor operation. Several parameters can be output from the ANSYS simulation: stator current, power, torque and speed. The simulated stator current signal is used for fault detection in this research. The structure of the thesis is explained in this section.

Chapter 2

In this chapter, various condition monitoring techniques are reviewed, and some content is discussed in the following paper: “*Xiaodong Liang, and Kenneth Ik Edomwandekhoe, “Condition Monitoring Techniques for Induction Motors”, Proceedings*

of 2017 IEEE Industry Applications Society (IAS) Annual Meeting, pp. 1-10, Cincinnati, OH, USA, October 1- 5, 2017.” (Note: This paper is attached to Chapter 2). Different techniques so far employed by researchers are investigated and inference are drawn based on simplicity and reliability of technique. This exercise serves as a formidable guide to finding a more viable technique, either by enhancing an existing technique, or by employing a novelty method, which could inform new insight into other research possibilities.

Chapter 3

In this chapter, the following published paper is attached: “*Kenneth Edomwandekhoe, and Xiaodong Liang, "Current Spectral Analysis of Broken Rotor Bar Faults for Induction Motors", Proceeding of 31st Annual IEEE Canadian Conference on Electrical and Computer Engineering (CCECE 2018), Québec City, Québec, Canada, May 13-16, 2018.*” This chapter unveils the implementation of two signature techniques known as Welch power spectral density (PSD) and Thompson Multitaper (MTM) power spectral density (PSD) estimates. Welch power density data are deployed amid other machine parameters using a linear SVM method for fault classification and prediction. This method is an enhancement methodology of the existing technique and provides a major contribution in terms of feature selection deduced for prediction and identification of BRB faults.

Chapter 4

In this chapter, the following published paper is attached: “*Kenneth Edomwandekhoe, and Xiaodong Liang, "Advanced Feature Selection for Broken Rotor Bar Faults in Induction*

Motors", Proceedings of IEEE 54th Industrial and Commercial Power Systems (I&CPS) Conference, Niagara Falls, ON, Canada, May 8th - 12th, 2018". In this chapter, a new method is proposed that is proven to be a very reliable technique for prognosis and prediction of BRB fault conditions. This manuscript comprises an application of various methods such as the traditional signature analysis method (FFT), which is a parametric method, the statistical method known as Yule walker estimate by Auto regression (YUL AR), which is a non-parametric method, and an advance signature technique known as matching pursuit (MP). The MP technique is more effective and reliable in terms of feature selection for classification of BRB faults.

Chapter 5

In this chapter, a new manuscript is attached and is ready for submission. A new method is proposed for diagnosing fault severity by calculating slope of two reference side lobes. It is observed that the motor with two neighbouring BRBs have a smaller slope than that of spaced BRBs. Slope differential for both cases shows that neighbouring BRB faults produce side lobes harmonic peak with certain close proximity. By simply finding the slope of the harmonic due to BRB faults, one can determine the severity of faults. It is proposed that slopes differential can serve as a criterion for identifying neighbouring and Spaced BRB faults.

Chapter 6

In this chapter, the research work is summarized by discussing weakness and strength of the proposed methods. Future work is discussed in brevity.

References

- [1] Ion B. and Syed A. Nasar. "The induction machines design handbook" second edition, Taylor and Francis group Boca Raton London New York. 2010.
- [2] IAS Motor Reliability Working Group. Report of large motor reliability survey of industrial and commercial installations, Part 1. IEEE T Ind Appl 1985; 21: 853–864.
- [3] F. C. Trutt, J. Sottile, and J. L. Kohler, "Online condition monitoring of induction motors", IEEE Trans. Industry Applications, vol. 38, no. 6, pp. 1627 - 1632, 2002.
- [4] Mehrjou, M.R., Mariun, N., Hamiruce M. M & Misron, N. "Rotor fault condition monitoring techniques for squirrel-cage induction machine-a review" Mech. Syst. & Signal Proc. Vol.25 (8), pp.2827-2848, 2011.
- [5] M. Schwartz, Principle of electrodynamics, Dower Publ. Inc, New York, 1972, pp. 180.
- [6] Hussain, S, N. and Zaidi, S, H. "Modeling and analysis of three phase induction motor with broken rotor bar" 17th IEEE Int. Multi Topic Conf., Dec. 2014, pp.488-493.
- [7] Ben S.S., Bacha, K., Chaari, A. "Support vector machine based decision for mechanical fault condition monitoring in induction motor using an advanced Hilbert-Park transform" ISA Trans. Vol.51 (5), pp.566-572, Sept. 2012.

- [8] Tandon, N., Yadava, G.S. & Ramakrishna, K.M. "A comparison of some condition monitoring techniques for the detection of defect in induction motor ball bearings" *Mech. Syst. & Signal Proc.*, Vol.21(1), pp.244-256 2007.

Chapter 2: Literature Review

Chapter 2 comprises of two sections. In the first section, various fault diagnosis techniques including artificial intelligence (AI) for induction motors are reviewed. Although various signal techniques are categorised into parametric and non-parametric method for easy distinction, more focus is placed on the review of artificial intelligence (AI) in the first section of this literature review. In the second section, a published conference paper is attached, and the paper is a literature review as well. The combination of the two sections provides a comprehensive literature review of the various techniques in this field.

Fault analysis is a vital procedure in condition monitoring of induction motors. It serves as a guide to identify the immediate cause of a motor's dysfunction. An early diagnosis helps to prevent motor deterioration beyond repair. This review explores various fault analysis methods reported in the literature for fault diagnosis purpose.

In this thesis, the focus is the fault diagnosis for squirrel-cage induction motors. The squirrel-cage induction motor is a reliable machine widely used in industry due to ruggedness, compactness and the least maintenance culture in comparison with other machines. However, like any type of electromechanical device, it is susceptible to different faults, such as BRB and bearing faults. BRB faults are the focus in this review. BRB faults are said to account for about 9% of induction motor failures [1]-[2].

The real-time condition monitoring technique maintains the unique feature of discovering fault condition at the very onset, thus preventing the fault aggravation. A fault undetected at an early stage could cause sudden motor failure and financial loss due to the

process downtime. Various signal techniques have since been deployed for BRB fault diagnosis, however, only a limited number of these techniques guarantees excellent accuracy and reliability. The MCSA is one of the most popular signal techniques. It comprises both parametric and non-parametric methods, but researchers have mostly employed non-parametric approaches due to characteristic simplicity and relative statistical property. However, non-parametric approaches suffer the setback of leakage and poor stability [1].

The non-parametric approach for signal analysis does not make any assumptions in the processing of the signal data. This method is a two-step procedure. The first step involves the estimation of autocorrelation sequence and the second step performs the transformation to obtain signal estimates. The objective of this thesis is to review spectral analysis techniques that can provide features capable of classification of induction motor faults using machine learning.

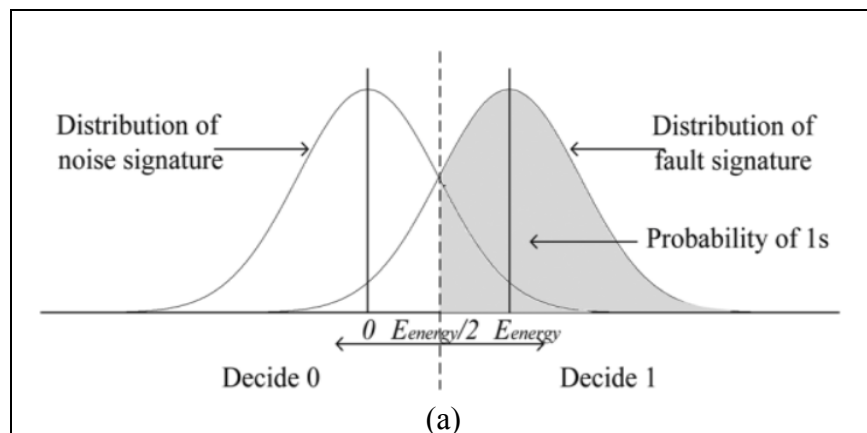
2.1 Non-Parametric Approach

FFT is a traditional non-parametric method that uses motor current signal data and most commonly used for BRB faults detection. A single BRB fault can be detected from monitoring frequency sidebands of the motor current signal that emerge close to the fundamental frequency through the FFT algorithm. These sidebands are most visible under full load condition of the motor. Therefore, the limitation of the traditional FFT technique is exposed under no load condition, as the FFT is incapable of distinguishing a healthy motor condition from faulted conditions under no load. Another worrying issue with the traditional FFT application is its total reliance on amplitude and sideband frequency as criteria for fault

detection. It's been observed that under unbalance voltage, motor current analysis exhibit spectrum behavior close to that of BRB fault current spectrum, making it difficult to clearly identify fault. FFT is also ineffective when considering motor under transient state [1][2].

Power spectral density (PSD) estimates have different deployment methodology, such as traditional periodogram which uses Discrete Fourier Transform (DFT) or Welch's PSD estimate, which is an enhancement of traditional periodogram. This technique partitions the signal into K segments and performs an average of different segments, applies a window to the different segment and then eliminates the window effect by a certain factor [1]-[2].

A robust method based on statistics and MCSA is proposed in [3]-[4] for eccentricity fault detection. This approach is centered on inspecting the motor current frequency spectrum for the noise signal frequency and fundamental harmonic signal frequency. The output of probabilistic and iterative approaches is represented in Fig. 2.1. Results show great potential, nevertheless technique dependability on prior knowledge of motor current harmonics places a limitation for real-time implementation.



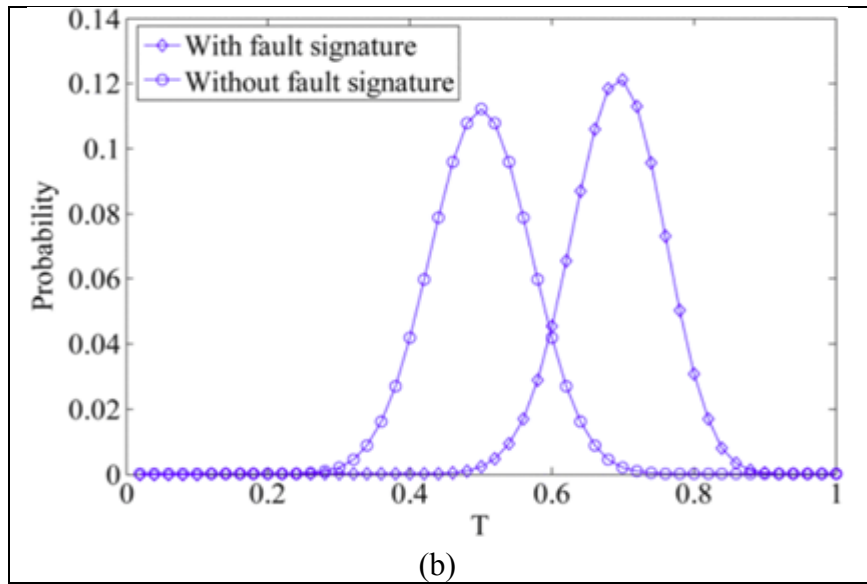


Figure 0.1: Probability distributions: (a) of 1 and 0 s in Det_mat. (b) of T, SNR=-65 dB (normalized) [3].

In [5], the fault diagnosis is proposed through the application of FFT and PSD methods on the collected signal in the order shown in Fig. 2.2. The FFT of the signal is used to produce complex conjugates of the signal i.e. real and imaginary constituents. These constituents are then processed further to obtain the PSD of the signal. Varying harmonics for different motor conditions, specifically from 1st to 19th harmonics were obtained through PSD application. These harmonics which serve as features for different fault conditions, such as BRBs, unbalance voltages, stator winding faults, and eccentricity faults, are fed into Fuzzy min-max (FMM) neural network and classification and regression tree (CART) for fault detection. Achieving a 96% average accuracy, results obtained from the proposed technique shows potentiality of the method. For BRB fault detection, the most notable feature differences for the motor with BRB faults and a healthy motor condition is that 5th harmonics amplitudes highlights dissimilarity. This feature is said to be a good tip for detecting the presence of

BRB faults in [6]. Inference drawn from [6] addresses the fault indicator for BRB faults, however, features for fault detection remain limited to amplitudes of the harmonic spectrum.

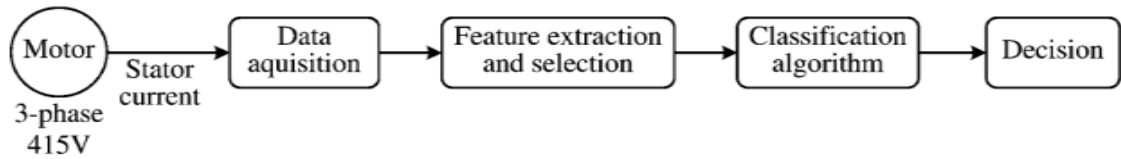


Figure 0.2: Overview of the proposed method for fault detection and diagnosis [5].

In [7], a new approach capable of detecting BRB faults under no load condition is proposed. The amplitude of side lobes, which serves as a fault indicator, is computed through the sliding DFT application. This method proves to be effective for steady-state condition as DFT retains the drawback of the fixed window that makes it effective for transient motor conditions. A novel counter current braking method (CCB) was demonstrated as an effective technique capable of detecting the BRB fault in [8]. The CCB method is used to induce a uniform frequency in the stator component, which allows the diagnosis of BRB faults. The method using STFT of the signal is obtained and figures depicting different motor conditions are shown in Fig. 2.3. Based on this figure, it is clear that the single BRB fault introduces a new component and distorts the asymmetry of the motor. The worthy feature to note of the PSD technique is that a further dimension is added to the signal that allows for feature extraction for classification purposes.

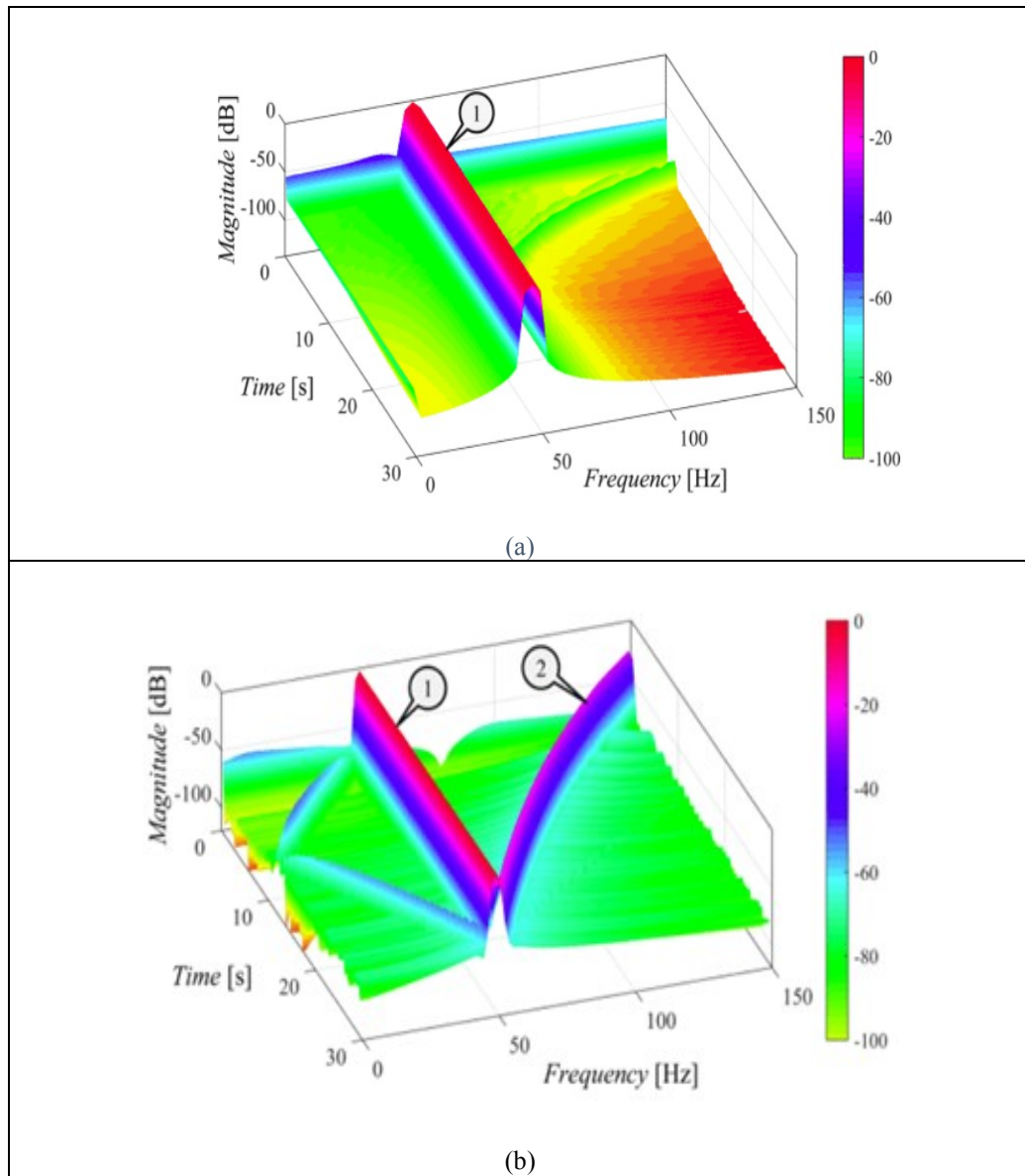


Figure 0.3: STFT current spectrogram (a) Healthy motor (b) Motor with 1BRB [8].

The Multitaper method (MTM) is presented in [9] [10]. This method does not segment the signal to obtain estimates like PSD, although they both have similar enhanced resolution as opposed to the classical periodogram. It simply applies orthogonal tapers to fit the signal. As typical of the non-parametric method, MTM is a two-step approach. Firstly, a suitable window has to be chosen; and secondly, a resolution level is selected. From the

electroencephalogram (EEG) analyses in anesthesia and sleep in [8], the issue of MTM capability to address the bias common in spectral analysis is presented. The argument that MTM remains an effective signal analysis tool is indisputable as evident in Fig. 2.4. It promises a better resolution and exhibits consistent variance within the signal estimates through the taper estimation effect, a typical setback of classical periodogram. This technique is often used for the signal analysis in biomedical engineering but is scarcely used in electrical engineering.

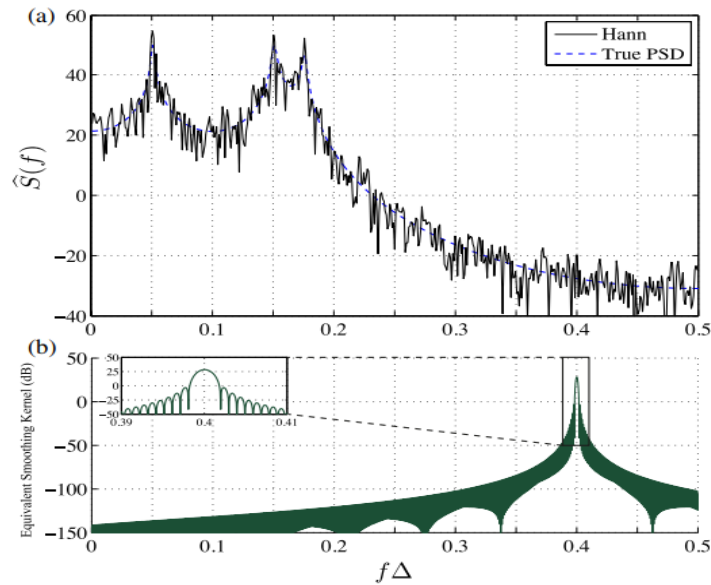


Figure 0.4: Tapered estimate of the PSD of the AR (6) process. (a) Tapered estimate using the Hann taper. (b) Equivalent smoothing kernel $\frac{1}{\Delta} |H(f)|^2$ centered at $f\Delta=0.4$. The zoomed-in view of the main lobe is shown on the top left [9] (AR depicts Auto regressive).

2.2 Artificial Intelligence Methodology

Machine learning methods can be applied to fault diagnosis of induction motors. The SVM classification is proposed in [11]. The SVM is a supervised machine learning algorithm

that uses the optimization algorithm to distinguish features for classification. Using 80 samples from the maximum of spectral amplitudes for different motor conditions, SVM classifies faults by finding the mean between various data points for dissimilar motor conditions. The 92.87% accuracy using the SVM proves its successful application. A dual SVM procedure is employed to detect BRB faults in [12]. The first phase of this approach involves a single class SVM used to train only the healthy motor. The selected features in this case are the number of poles and actual speed of the motor. With sufficient training, the SVM model shows a deviation from the trend when the data from a faulty motor is supplied. The second phase of this approach scrutinizes harmonics to locate faulty rotor bars that show notable discrepancy between healthy and faulty motor conditions. Although the methodology is good, results do not show utter reliability for online fault detection.

In [13], an automated detection technique is suggested for BRB faults detection. The technique relies on the extraction from wavelet decomposition, which is then processed and represented in two dimensions (2D) and denoted as scaled transform (ST), the processed extraction can then serve as features as shown in Fig. 2.5. This method requires too much computation, and the expert interpretation of the extraction following the decomposition of the signal.

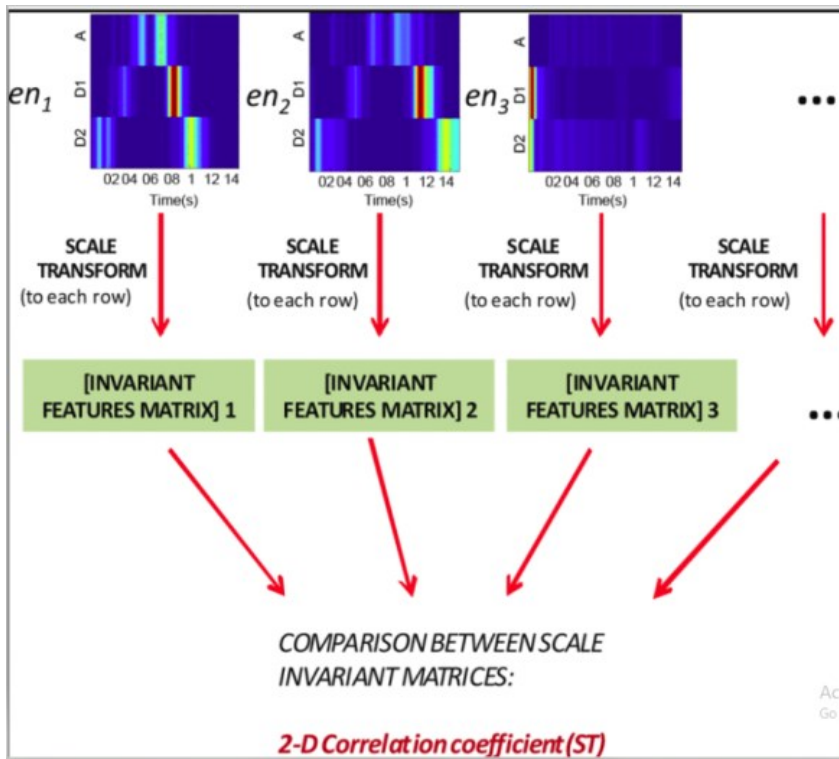


Figure 0.5: Schematic representation of the pattern standardization and comparison [13].

A survey of various techniques is deliberated in [14]. ANN is highlighted as having advantages over other diagnostic techniques due to its accuracy and reliability. However, its utter dependence on sufficient training time is noted as the drawback associated with adopting this approach. Conversely, identifying features that can best distinguish various conditions will reduce training and computation time since the training time is a function of number of features. The higher the features the higher the training time [11]. The vibration signal has been employed for BRB fault detection in [15], the principal component analysis (PCA) is first deployed to trim down irrelevant features, and the linear discriminant analysis (LDA) technique is then used for classification. The PCA process involves screening data to create orthogonal features, by reducing dimensionality from 16-3-2 as shown in Fig. 2.6. The

result shows that method has the potential of correctly classifying faults. However, an overlap can be seen between faults and healthy motors, and the fault severity cannot be clearly classified using this method.

A supervised ANN approach was presented in [16]. A multi-layer feed-forward neural network with the back-propagation algorithm is designed to accommodate a number of features to prevent high computation time. Fig. 2.7 displays the algorithm for harnessing features for training and fault detection using ANN. About 16 neural network modules comprising of 67 input factors are used to identify the machine condition. A unique feature of this method is the synchronization of ANN with a fuzzy logic. Developing a generic ANN model is cumbersome, because doing that will require a humongous data set that will impact adversely on computation time when trying to achieve convergence through finding mean square error for data set. According to [17], integrating ANN with fuzzy network creates a hybrid neural network that has generic property. This is possible because fuzzy logic is able to interpret empirical information as numerical value by some functions [18]. The issues of lack of memory space and high computation time is taken care of by this method. The different module had different input in relation to fault condition under survey and results show that technique can be relied on.

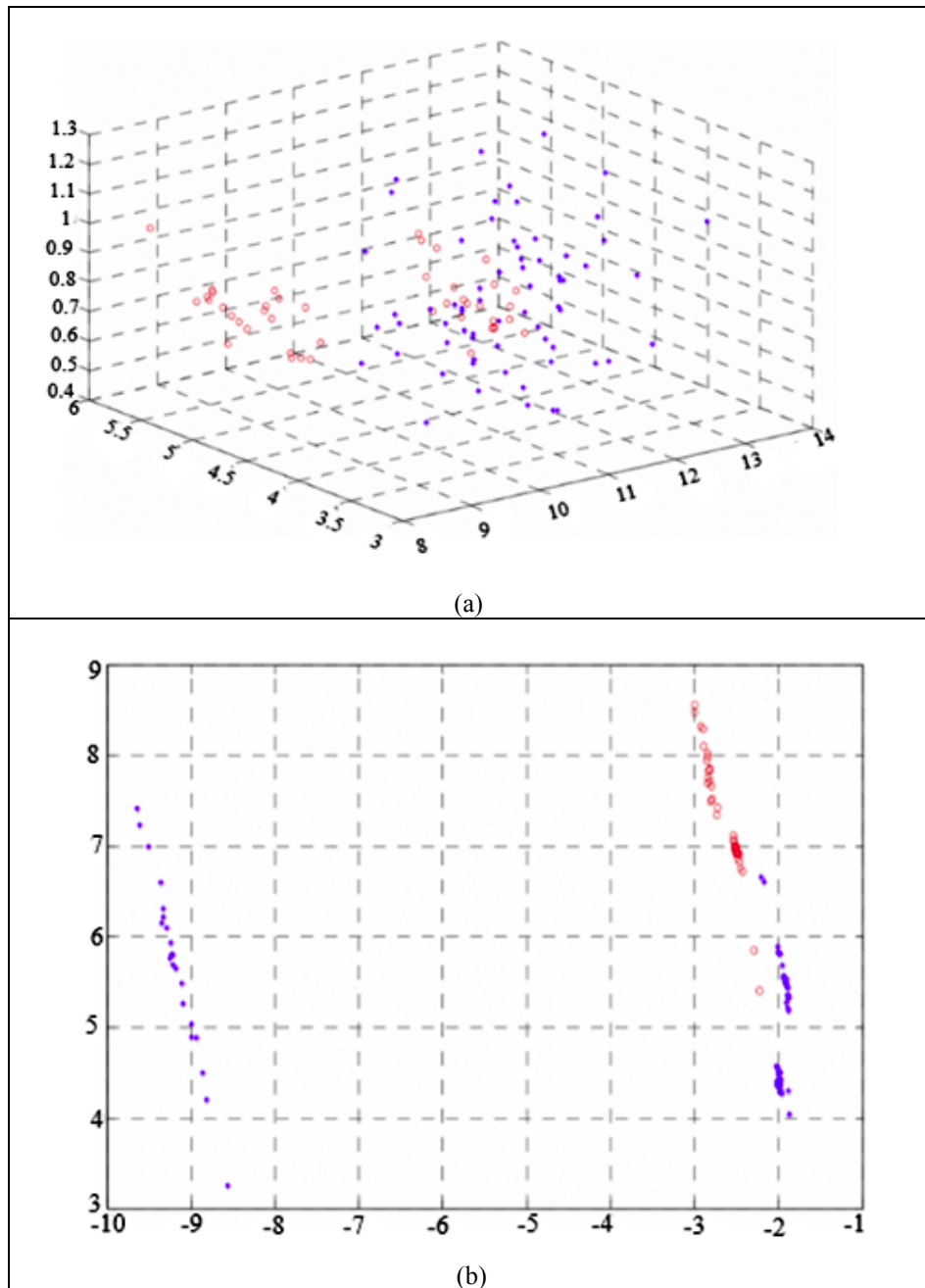


Figure 0.6: Training data set for 3-dimensional problem after applying PCA (cross-validation 1): red - healthy bars, blue - broken bars (b) Training data set for 2-dimensional problem after applying PCA (cross-validation 1): red - healthy bars, blue - broken bars [15]

Artificial Ant System (AAS) unsupervised machine learning approach differs from the supervised approach in that the former does not require any expert knowledge. An unsupervised AAS approach is presented in [19] for detection of induction motor faults, such as BRBs and bearing failure diagnosis. A BRB fault is treated as an electrical fault, while the bearing fault is a mechanical fault. The classification is done using the Ant clustering technique. The proposed methodology can identify faults with limited information.

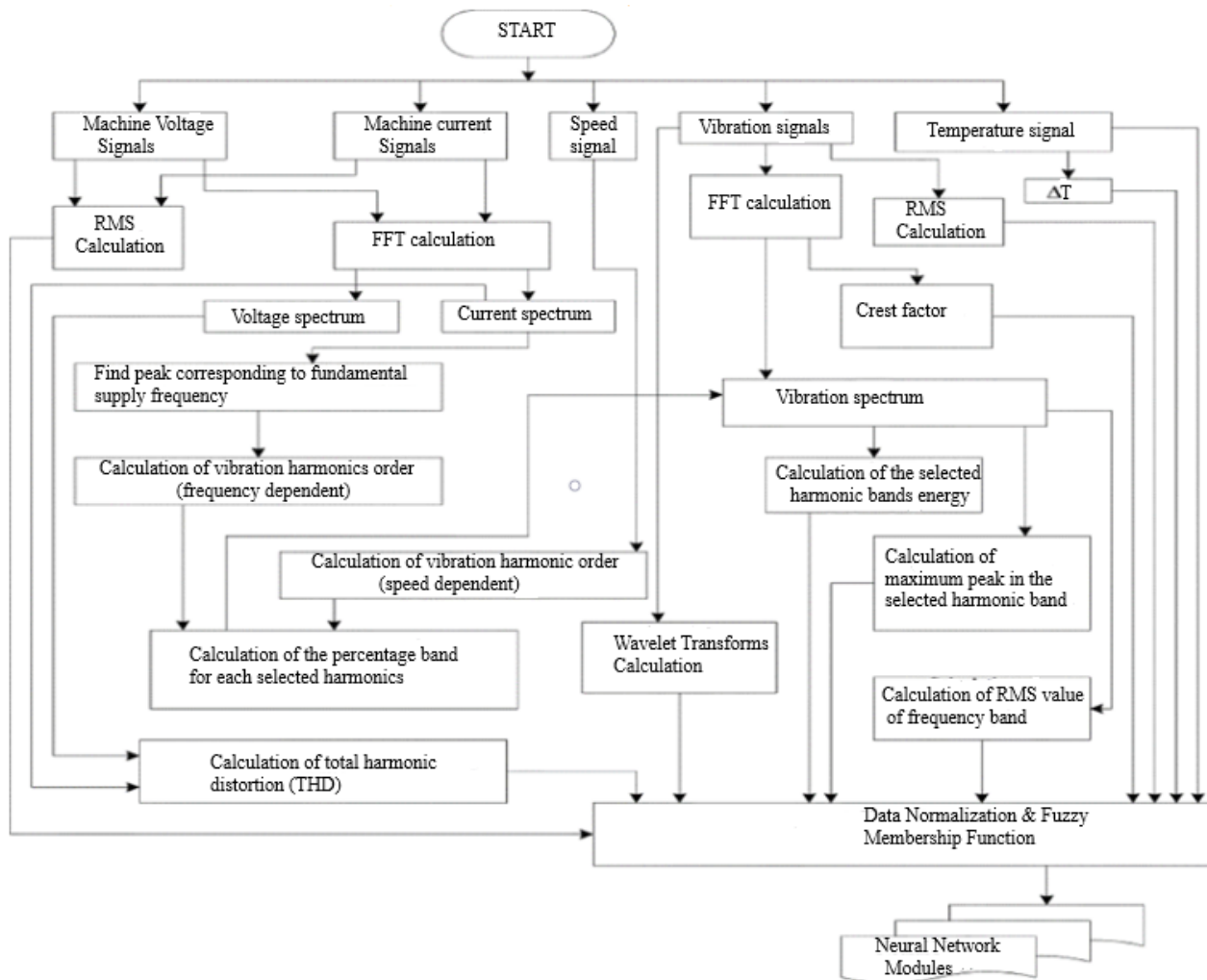


Figure 0.7: Training and testing data production algorithm [15].

Feature screening is carried out and three different machine learning techniques, Artificial Ant Clustering (AAC), Adaptive-Network-based Fuzzy Inference System (ANFIS), and the Multi-Layer Feed-Forward network (MLFF), are deployed for training and classification of induction motor faults in [19]. Classification results in Table 2.1 for all three techniques shows that the AAC boosts the best accuracy with a 1.33% error rate. The final classification result is presented in Fig. 2.8. AAC proves to be the most effective of AI techniques reviewed.

Table 0.1: Performance Comparison of the AAC, MLFF, and the ANFIS [18]

Algorithm	Best System Parameters	Classification error rate
AAC	$e=0.5$ $f=0.8$ $\zeta=1$ $\alpha=0.01$	1.33 %
Multi-Layer Feed-Forward network (MLFF)	Hidden neurones $n=10$	2 %
Mountain clustering/ANFIS	Cluster radius: $R=0.8, 0.9, 1.0$	2.67 %

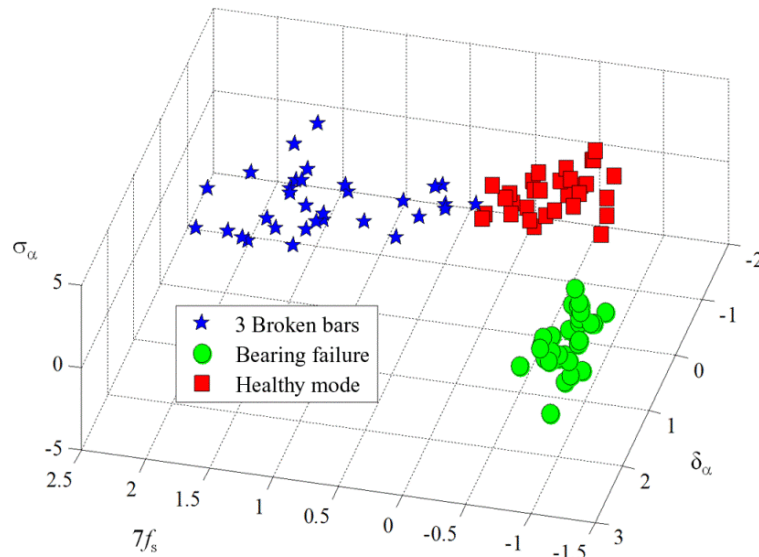


Figure 0.8: Test set in the three-dimensional feature space (Fop) after standardization.

Healthy machine $\langle\langle \blacksquare \rangle\rangle$, defective machine $\langle\langle \star \rangle\rangle$, bearing failure $\langle\langle \bullet \rangle\rangle$ [19].

Condition Monitoring Techniques for Induction Motor

Comparative review of various techniques

One of the quests of this thesis is to find the most reliable method for condition monitoring and fault diagnosis of BRB fault of induction motors. The literature review of implemented techniques could provide insight to a reliable and effective technique.

Extensive review of previous work on the subject of interest can set a good precedence for an exciting thesis program. The following published manuscript will show a more comprehensive review.

This manuscript has already been published in the Proceedings of 2017 IEEE Industry Applications Society (IAS) Annual Meeting, pp. 1-10, Cincinnati, OH, USA, October 1- 5, 2017. This paper was presented in the conference by Dr. Xiaodong Liang. The co-author Kenneth Edomwandekhoe conducted the literature review, wrote part of the paper under the supervision of Dr. Liang. Dr. Liang wrote part of the paper and modify the whole paper.

A few adjustments were done on the figures, tables and referencing in the manuscript in order to conform to Memorial University manuscript standard format.

Condition Monitoring Techniques for Induction Motor

Xiaodong Liang, *Senior Member IEEE*, Kenneth Edomwandekhoe. *Student Member*

IEEE

Faculty of Engineering and Applied Science, Memorial University of Newfoundland,

St. John's, Newfoundland, Canada

***Abstract-* Induction motors are used in various work environment and critical industrial processes; operating conditions and well-being of these machines need to be monitored to avoid potential failures. In this paper, an extensive literature review is conducted for condition monitoring techniques for induction motors. Various state-of-art techniques are presented and summarized under three categories: 1) signature extraction-based approach, 2) model-based approach, and 3) knowledge-based approach. Advantages and drawbacks of several commonly used methods are demonstrated. Although research has been conducted in this area for several decades, condition monitoring and fault diagnosis of induction motors remains an active research area, especially recent emerging transition from traditional techniques to knowledge-based approach using artificial intelligent, which opens a pathway to an exciting new research direction.**

Index Terms — Artificial intelligent, condition monitoring, induction motors, machine learning, signal processing.

I. INTRODUCTION

Induction motors are most widely used electric machines in various industrial sectors and home appliances due to their compactness, ruggedness, and reliability features. Compare to other types of motors, induction motors require the least maintenance. Although relatively robust, faults still occur in induction motors, which can interrupt critical processes and production [20] [21][22].

The maintenance of an induction motor can be classified into three types: 1) scheduled maintenance; 2) breakdown maintenance; and 3) condition-based maintenance. The scheduled maintenance involves the planned scrutiny and repair of machines at a given time, which usually requires an expert to effectively overhaul and pinpoint motor defects, so that repair can be done before the machine resumes work. The breakdown maintenance employs the process of allowing the machine to run until it eventually wears out. This maintenance methodology is more costly, due to having to replace the entire machine rather than repair or replace parts. The condition-based maintenance includes observing and getting periodic update about the condition of a machine during operation and taking proactive step when a fault is at the incipient stage, to avoid severe damage and unplanned process down-time [20]. Therefore, it has become necessary to develop a condition-based maintenance culture, which will prevent untimely interruption of work process, reduce process downtime and maintenance costs [20] [21][22]. The principal objective of condition monitoring techniques is to construct a reliable mechanism for fault detection at the incipient stage, so that the machine can be shut down in a controlled manner for checking and repairing, thus avoiding excess outage time imposed by sudden breakdown [21].

Industrial survey has revealed that a large percentage of faults occur at stators, rotors, and bearings [21]-[24]. The statistical percentages of fault occurrence and fault types are shown in Fig. 2.9 [20]-[24]. Similar survey results for medium-size induction motors conducted by IEEE industrial application society (IAS) and Electric Power Research Institute (EPRI) are provided in Table 2.2 [25].

Faults in machines usually occur in a cascade sequence, a certain fault occurrence at a point in the machine could deteriorate and cause a more severe fault occurrence at other location in the machine. For example, a fault stimulated by unbalance voltage supply initially provokes an inter-turn fault through stator winding insulation degradation, which could further deteriorate to a single line fault and a line-to-line fault [20]-[22]. The cascade fault sequence phenomenon makes it imperative to detect faults at the incipient stage [22].

The fault detection can be divided into three fundamental categories: 1) signature extraction based approach; 2) model-based approach; 3) knowledge-based approach [26][27]. Condition monitoring techniques can also be classified into two broad types: invasive and non-invasive. Table 2.3 highlights advantages and disadvantages under the two types.

In this paper, an extensive literature review is conducted for state-of-the-art condition monitoring techniques for induction motors. The three fundamental categories are discussed in detail serving as the backbone of the paper. These approaches are applied to detect several critical conditions of induction motors including broken rotor bars, stator winding inter-turn fault and insulation deterioration, and bearing fault. The objective of this review is to strike

a balance between accuracy of methodology and implementation constraint with economic advantage in view.

The paper is organized as follows: in Sections II, III and IV, the signature extraction-based approach, the model-based approach, and the knowledge-based approach are explained, respectively, several techniques related to each approach are demonstrated; conclusion are drawn in Section IV.

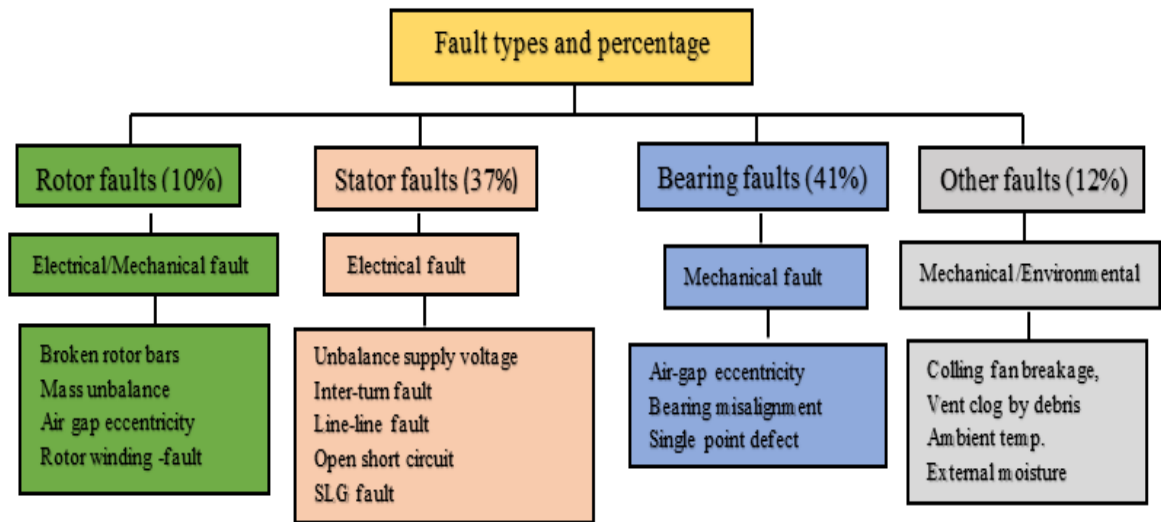


Figure 0.9: Fault types and percentage of occurrence in induction motors [20]-[24]

Table 0.2: Fault Survey Results for Induction Motors from IEEE-IAS and EPRI [25]

Major Components	IEEE-IAS % of failures	EPRI % of failures
Bearing related	44	41
Stator related	26	36
Rotor related	8	9
Others	22	14

Table 0.3: Stator end winding insulation failure due to broken rotor bar fragment in a 6.6-kV 500-kW induction motor [28]:

Invasive Methods		Non-Invasive Methods	
Advantages	Disadvantages	Advantages	Disadvantages
Provide accurate and reliable results through the use of sensors	Installation of special sensors are required	Does not require installation of special sensors.	An indirect approach
A more direct approach	Complex installation process	Relatively easy implementation procedure.	It might require expert's opinion.
It might not require much expertise to understand result.	A more expensive technique	More economical approach	It does require a more analytical approach
	It might interference with motor normal operation during application.	No interference with normal motor operation during application.	

II. THE SIGNATURE EXTRACTION BASED APPROACH

The signature extraction-based approach is utilized by surveying fault signatures in time and/or frequency domain. Signatures extracted from recorded signals are employed to diagnose faults. Significant amount of research has been done in this area [27]. Among various condition monitoring techniques, monitoring signals can be current, voltage, power, vibration, temperature, and acoustic emission.

When considering condition monitoring, the investigation usually involves steady-state and transient-state modes. Prior to the innovation in signal processing, researchers concentrated on fault detection techniques in steady-state mode, which includes techniques such as Fast Fourier Transform (FFT). With the innovation in signal processing, techniques that study transient mode have attracted more research interests [21].

A. Broken Rotor Bars (Steady-state Analysis)

It has been proven that faults of induction motors introduce additional frequency components in the stator current signal, therefore, stator currents as input data are widely used in condition monitoring, and the frequency spectrum of the stator current is analyzed for condition monitoring purpose [21]-[14], [28]-[34]. The classical approach used in an industrial environment for the detection of broken rotor bars in induction motors is based on the analysis of the stator current in steady state [34].

Among various spectral analysis methods, Motor Current Signature Analysis (MCSA) is one of the most popular techniques for online monitoring induction motors in an industrial environment. It has remote monitoring capability using the stator current as monitoring signal, which can be conveniently measured at the motor control center. This remote monitoring capability is an advantage of MCSA over vibration, speed, or flux spectrum analysis. MCSA has been most successful in detecting broken rotor bars or end rings [28].

The frequency of the motor current spectrum for a faulty motor with broken rotor bars is characterized by a certain upper and lower band frequencies, otherwise known as sideband frequencies [21]-[24], [28]-[34]. Most research on broken rotor bar fault have mainly focused on steady-state condition. Nonetheless, some research investigation has shown that steady-state study cannot be relied on under certain conditions [34].

For a healthy motor, there is symmetry of cage winding, and only forward rotating field exist, thus, the rotor frequency equation is shown in Equation (1). However, with the presence of a broken rotor bar fault, asymmetry exists and a resultant backward rotating field

relative to forward rotating rotor generates additional frequency in the motor current harmonic spectrum [32]-[34]. The frequency is known as a lower side band rotor frequency expressed in Equation (2). An upper sideband current constituent is prompted by the stator winding, which is due to rotor oscillation as shown in Equation 3 [29]-[35].

$$f_2 = sf_1 \quad (1)$$

$$f_{b_lower} = f_1(1 - 2s) \quad (2)$$

$$f_{b_upper} = f_1(1 + 2s) \quad (3)$$

From Equations (1)-(3), the broken rotor bar fault generates a resultant current constituent of frequencies expressed in Equation (4) [23] [24], [29]-[35].

$$f_b = f_1(1 \pm 2s) \quad (4)$$

Where, f_b represents broken bars frequency, f_1 is the supply frequency, and s is the rotor slip.

References [28]-[29] provide a general formula for multiple frequency bands related to a broken rotor bar as follows:

$$f_b = f_1(1 \pm 2ks), k = 1, 2, 3 \dots n \quad (5)$$

It is reported in [29] that additional frequency components related a broken rotor bar exist, which can be observed from the stator current harmonic spectrum as follows:

$$f_b = \left[\left(\frac{k}{p} \right) (1 - s) \pm s \right] f_1 \quad (6)$$

Where, p is the number of pole pairs, and $k/p = 1, 2, 3 \dots n$

A single broken rotor bar could not instantaneously cause induction motor failure. However, a multiple broken rotor bars could cause motor start-up failure due to insufficient accelerating torque during start-up procedure [29]. MCSA provides sensitive detection of broken rotor bars, the criterion for fault threshold is well established between -50 dB and -35 dB with respect to the fundamental component [28].

Although MCSA has been successful in the field, false fault indication is a common issue using this technology. A false positive (FP) indication (false alarm) refers to the case where a fault alarm is given for a healthy rotor, which can result in unnecessary inspection of the motor and interruption of the process. A false negative (FN) indication refers to the case where MCSA fails to detect a fault condition. The consequence can be very serious. For example, protrusion of a broken bar or a bar fragment into the air gap or stator end winding can lead to a forced outage of the motor and the entire process that it drives. Fig. 2.10 shows a broken bar fragment causing stator end winding insulation failure of a 6.6-kV 500-kW induction motor. Typical causes of FP and FN are shown in Table 2.4 (III) [28].

As an example, the rotor axial air duct causing FP as listed in Table 2.4 (III) is demonstrated in [36]. Rotor axial air ducts are used in large motors for cooling and reducing weight and material. Axial air ducts cause the reluctance of the magnetizing flux path to vary depending on the relative position between rotor ducts and the rotating magnetic field. The magnetic asymmetry produced by air ducts can result in the modulation of the magnetizing current proportional to twice the slip frequency, i.e., $2sf_1$. The ducts produce $2sf_1$ current sidebands if the pole number of poles and the number of air ducts of the motor are equal. In

this case, the modulation of stator current causes torque pulsation and motor vibration at $2sf1$, which can be misinterpreted as rotor faults, when current- or vibration-based spectrum analysis is performed. A direct example of this from the field is a 6.6-kV 2400-kW eight-pole motor at a power plant in USA that was diagnosed with a rotor damage. The broken-bar frequency component measured with MCSA was between -32 dB and -37 dB, which exceeded the alarm level and indicated a broken rotor bar. The vibration spectrum analysis indicated a broken bar as well. However, when the motor was examined, it turned out to be a false positive indication due to equal number of axial kidney holes and poles in this motor [36].



Figure 0.10: Stator end winding insulation failure due to broken rotor bar fragment in a 6.6-kV 500-kW induction motor [28]

Table 0.4: FSC values: (a) FSC vs. the number of BRBs, (b) FSC vs. sample number using TLS ESPRIT [37].

		Diagnosis of MCSA	
		Healthy	Faulty
Actual rotor condition	Healthy	<u>True Negative</u>	<p style="text-align: center;"><u>False Positive</u></p> <ul style="list-style-type: none"> • Low frequency load oscillations • Axial air duct • Magnetic anisotropy • Rotor ovality • Porosity (<i>Al</i> die cast rotor)
	Faulty	<p style="text-align: center;"><u>False Negative</u></p> <ul style="list-style-type: none"> • Outer cage fault in double cage rotor • Nonadjacent broken bars • Load variation • Incorrect speed estimate 	<u>True Positive</u>

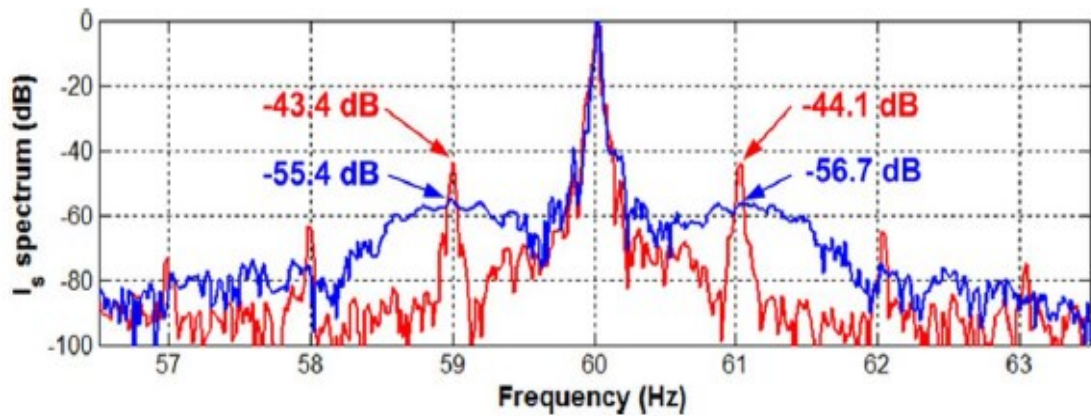


Figure 0.11: MCSA results for the same motor with a broken rotor bar under a constant load and a gradual varying load condition [28].

Another issue with MCSA is that MCSA is intended for steady-state operation, so it becomes ineffective for cases where the load level varies with time. MCSA results for the

same motor with a broken rotor bar under a constant load (1785 r/min) and a gradual varying load (1775–1795 r/min) condition are shown in Fig. 2.11. It is found that the fb component exceeds -45 dB for the case of a constant load, which can lead to a correct fault detection, but for the case a gradual varying load, the fb component is measured below -55 dB although the machine does have a broken rotor bar [28].

In addition to the MCSA, a subspace spectral estimation technique, also known as high-resolution spectral analysis, is proposed in [37] to detect broken rotor bars and bearing faults. Stator current measurements serve as the signal. The advantage of this technique is that it can detect the faults and also determine their severity. Frequency components including frequencies close to the fundamental frequency are separated based on high-resolution spectral analysis. Once fault sensitive frequencies are estimated, their corresponding amplitudes are obtained by using the least squares estimator, and a fault severity criterion is derived from the amplitude estimates [37].

The fault severity is represented by Fault Severity Criterion (FSC) values, a higher FSC value means a more severe fault. Fig. 2.12(a) shows the FSC values for an induction motor vs. the number of broken rotor bars (BRBs), where 0 corresponds to a healthy induction motor without a broken rotor bar, and other values correspond to the number of broken rotor bars. The two methods, Root-MUSIC and TLS-ESPRIT are used and show comparable results in Fig. 2.12(a). Fig. 2.12(a) indicates that the FSC value increases with the number of broken rotor bars. Fig. 2.12(b) shows the FSC values vs. sample number using the TLS ESPRIT method. This figure indicates that the FSC values also increase with sample number [37].

B. Broken Rotor Bars (Transient Analysis)

Although widely used, the spectral analysis of the stator current in steady state for broken rotor bar detection has two major issues: 1) load dependence; 2) exterior influences.

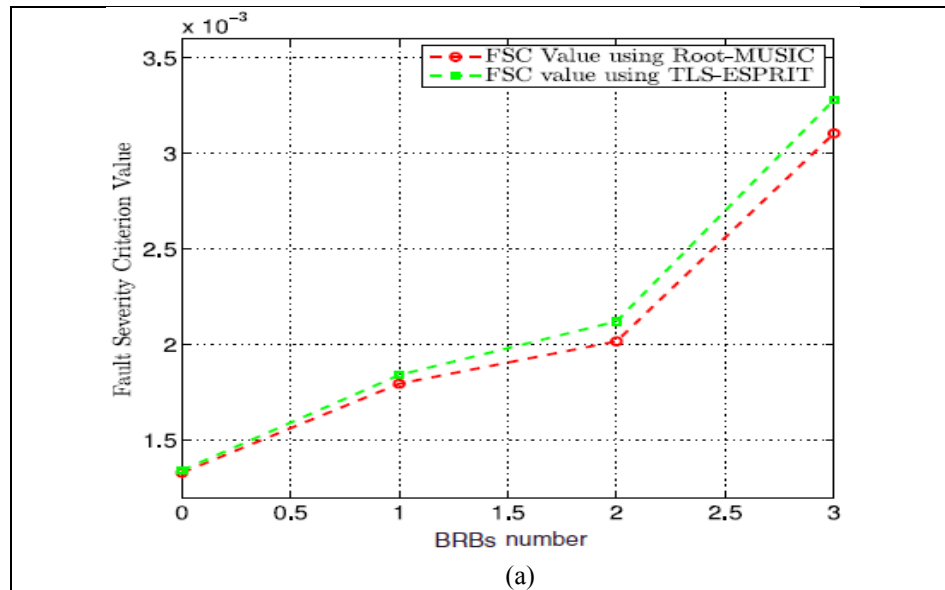
Regarding load dependence, the separation of the frequency associated with broken rotor bars and the main frequency is dependent on motor inertia, and thus, as load increases, the separation increases. With a lower load, the separation could decrease until both spectral lines cannot be distinguished, making it difficult to detect the fault. Under the aforementioned condition the steady state investigation technique cannot be termed reliably [34]. Also, continuous fluctuations of motor load give rise to changes in frequency associated with the broken rotor bar, thus, making it difficult to automatically detect the rotor fault [34].

Regarding external influences, frequencies similar to those used for rotor bar breakage detection can be generated by other causes, such as low-frequency oscillating torque loads, voltage fluctuations, bearing faults, voltage fluctuations etc, which reduces reliable fault detection [34].

To overcome these problems, the analysis of the current and/or other magnitudes during transient processes of induction machines have been recently investigated [33] [34][38].

In References [33] [34], an algorithm to detect broken rotor bars based on the Discrete Wavelet Transform (DWT) application on the start-up current transient is proposed. A phenomenon known as single mean-square computation determines a weighing function, and from its value, the motor condition is monitored online.

The Field Gateway Programmable Array (FGPA) is used for the implementation of the algorithm. The method uses time-scale decomposition of the original signal to detect the frequency associated with broken rotor bar fault and determine its severity. The amplitude of frequency associated with broken rotor bars increases when there is increase in load and the number of broken rotor bars. When the load on a motor is near a name-plate value, the speed of the motor is far below the speed under no load. In this state, the motor fault frequency related to broken rotor bars is more alienated from the main operating frequency, thus making it easy to detect. However, when the motor load is close to no-load, the fault frequency associated with broken rotor bars becomes difficult to identify because it's close to the motor operating frequency [33] [34].



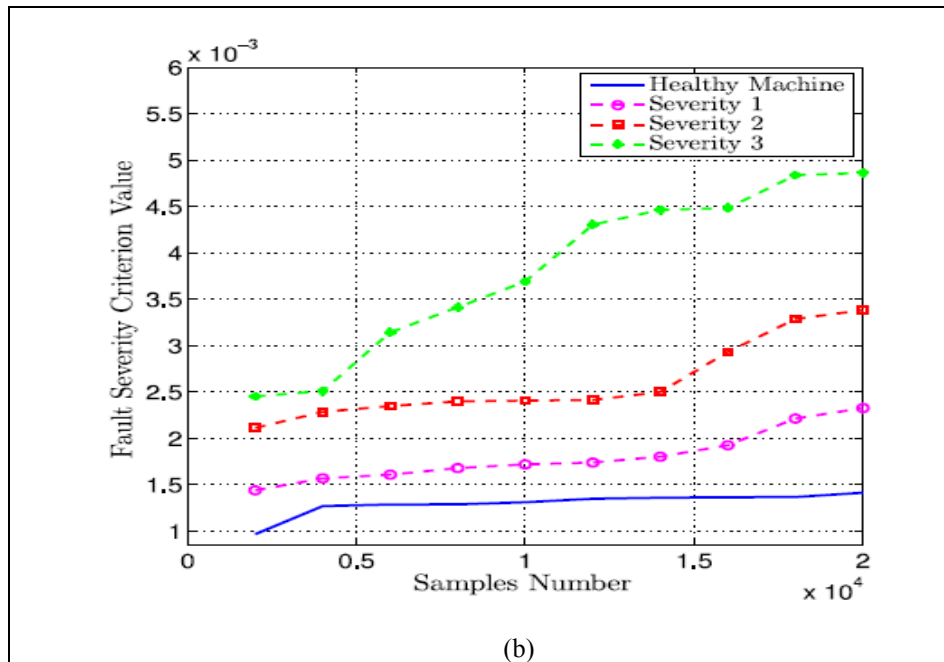


Figure 0.12: FSC values: (a) FSC vs. the number of BRBs, (b) FSC vs. sample number using TLS ESPRIT [37].

The Wavelet theory has proven to be a powerful tool for the analysis of transient processes. The DWT decomposes the motor start-up transient current into a set of low frequency signals. Each signal contains the information of the original signal within a certain frequency band. When a broken rotor bar occurs, a characteristic harmonic with a particular frequency variation appears during the motor start-up process. The evolution of this harmonic is reflected clearly in the low-frequency wavelet signals, which allows the detection of broken rotor bars because the same healthy machine will not have such a particular frequency variation. The proposed approach in [34] focuses on low frequency high-order wavelet signals, the frequency bands for these signals are shown in Table IV. Fig. 2.13 shows the Wavelet analysis of a start-up current and the FFT analysis of a steady-state current for a loaded machine with two broken rotor bars [34].

Table 0.5: Frequency Bands for High Order Wavelet Signals [34]

Level	Frequency band
$d7$	19.53 – 39.06 Hz
$d8$	9.76 – 19.53 Hz
$a8$	0 – 9.76 Hz

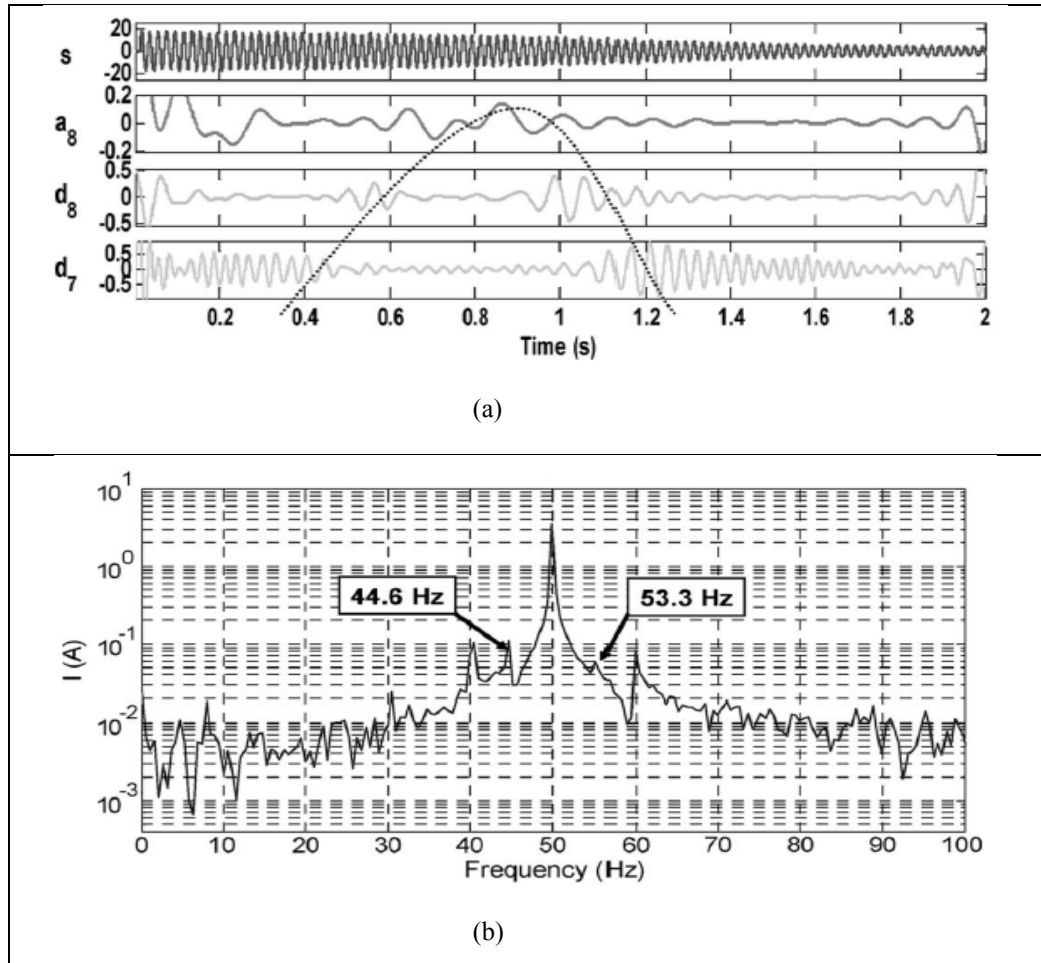


Figure 0.13: Loaded machine with two broken rotor bars. (a) Wavelet analysis of start-up current, (b) FFT analysis of the current in steady state [34].

To apply the proposed method in [34], the guideline is that the start-up time of an induction motor should be longer than 0.5 s. One drawback of this method is that it is not suitable for induction motors supplied power by variable frequency drives. Luckily, the

broken rotor bar detection for variable speed drive-fed induction motors at start-up can be achieved by high-resolution spectral analysis proposed in [39], where the time–frequency spectrum is able to graphically show a different pattern for healthy and faulty conditions of the motor [37] [39].

Reference [38] proposes an automated method for the detection of the number of broken rotor bars of an induction motor. It is based on transient analysis of the start-up current using wavelet approximation signal, which isolates a characteristic component that emerges once a rotor bar is broken. After the isolation of this component, a number of stages are applied that transform the continuous-valued signal into a discrete one [38].

C. Stator Winding Inter-turn Faults and Winding Insulation Monitoring

Stator faults such as a single line to ground fault are often a result of winding insulation degradation. The inter-turn defect is considered to be the source of insulation deterioration resulted from the cumulative damage from the dielectric stresses of over voltages, high temperature, and other adverse conditions. If undetected, these defects can increase in size until a catastrophic fault occurs, thus damaging the machine. The early detection of stator winding insulation deterioration prior to a complete failure provides an opportunity for a scheduled maintenance to be performed without the loss of production time [21]-[24] [29][40][41]. Several techniques are proposed: effective negative-sequence impedance [41], voltage mismatch [40] [42], short term averaging of forwards and backwards rotating stator current phasors [43], air-gap flux [44], and three-phase currents [32] etc. When the three-phase currents monitoring method is used, a harmonics analysis is required. Ideally, only a

single space harmonic exists in the rotor magnetic field of an induction motor, but in actual machines, owing to rotor slotting; the rotor magnetic field does have additional harmonics [32].

It has been reported in [29] that axial leakage flux can help detect inter-turn fault. Voltage induced in a search coil placed in the centre of the machine shaft is a function of the flux component [30]. Equation (7) is the voltage spectral component used for detecting this fault type known as rotor slot harmonics [24] [32].

$$f_i = \left[k \pm \left(\frac{n}{p} \right) (1-s) \right] f \quad (7)$$

Where $k = 1, 3$, $n = 1, 2, 3$ and p is number of pole pairs, and s is the slip. The rotor slot harmonics frequency depends on the number of rotor slots, supply frequency, slip and machine pole pairs. Rotor slot harmonic order can be calculated as follows [29] [32]:

$$H_{RSH} = k \frac{N_r}{p} \pm 1 \quad (8)$$

Where N_r represents number of rotor slots, and p is the number of pole pairs, $k=1, 2, 3 \dots$

D. Bearing Faults - Vibration and Acoustic Monitoring

The bearing is an indispensable component of any electrical motor. Main duty of bearings is to provide slipping of the rotor inside the stator, maintaining a uniform air gap. Generally, there are two kinds of bearings, sleeve and rolling-element bearing. More often, rolling element (ball and roller) bearings have been used in many electrical machines while sleeve bearings are a good fit for large electrical machines. In general, a bearing has three

main components that can typically experience damage: inner race, outer race and rollers or balls [46]. Because bearing fault accounts for most fault in induction machines, thus it is of almost importance to monitor bearing condition [47].

Vibration signal analysis is the most industrial accepted approach. Motor vibration data contains substantial analytical information about stator and rotor winding and core condition, air gap eccentricity, voltage or current unbalance etc. Most research on detecting bearing failure is based on vibration analysis [48] [49].

A motor current spectral method for bearing fault detection is proposed in [47] [50]. Their findings recommend that fault frequencies property that are present in motor vibration as a result of bearing faults can also be detected in the motor current. However, bearing defect in motor current is more tedious to detect than bearing defect in motor vibration. There are two types of bearing faults. Single point defects and generalized roughness. Fig.2.14 represents a flow chart of the types of fault and their characteristics effects [50]. Every bearing fault has characteristic frequencies, which are expressed as follows [51]:

$$F_{CF} = \frac{1}{2} F_R \left(1 - \frac{D_B \cos(\theta)}{D_p} \right) \quad (9)$$

$$F_{ORF} = \frac{N_B}{2} F_R \left(1 - \frac{D_B \cos(\theta)}{D_p} \right) \quad (10)$$

$$F_{IRF} = \frac{N_B}{2} F_R \left(1 + \frac{D_B \cos(\theta)}{D_p} \right) \quad (11)$$

$$F_{BF} = \frac{D_p}{2D_B} F_R \left(1 - \frac{D_B^2 \cos^2(\theta)}{D_p^2} \right) \quad (12)$$

Where, D_p represents ball pitch diameter, F_R represents speed of rotor, θ is ball contact angle, N_B is number of balls, and D_B is ball diameter [51].

This method uses the peak amplitude signal as the indices for bearing fault detection. Amplitude signal for healthy and faulty bearings for no load and full load were obtained. It was discovered that amplitude peak increases when the size of outer race of bearing defect increases. For a varying load there was a varying amplitude peak, large enough to detect fault condition [49] [51].

The advantage of acoustic emission (AE) monitoring over vibration monitoring is that the former can detect the growth of subsurface cracks, whereas the latter can detect defects only when they appear on the surface. It is also important to note that the energy released by neighboring components in the vibrational frequency range (up to 50 kHz), which often masks the vibrational energy released from a defective rolling element bearing, do not affect the AE signal released in the very high frequency range.

Nevertheless, the direct vibration spectrum from a defective bearing may not indicate the defect at the early stage [46] [51]. Figs. 2.15 and 2.16 shows vibration velocity signal output for a healthy and a faulty motor condition [51].

E. Signal Injection Techniques

The signal injection-based temperature estimation technique is an invasive method that requires injecting either a DC or an AC signal into the system [52]-[62]. The dc current injection technique was first introduced in 1980 by Derek A. Paice [52]. The idea is to let a small dc current (3% of the rated ac current) to flow through the motor winding in one phase

by means of a series asymmetric resistance. From the measurements of the dc current and dc voltage, the stator winding resistance and the temperature can be evaluated.

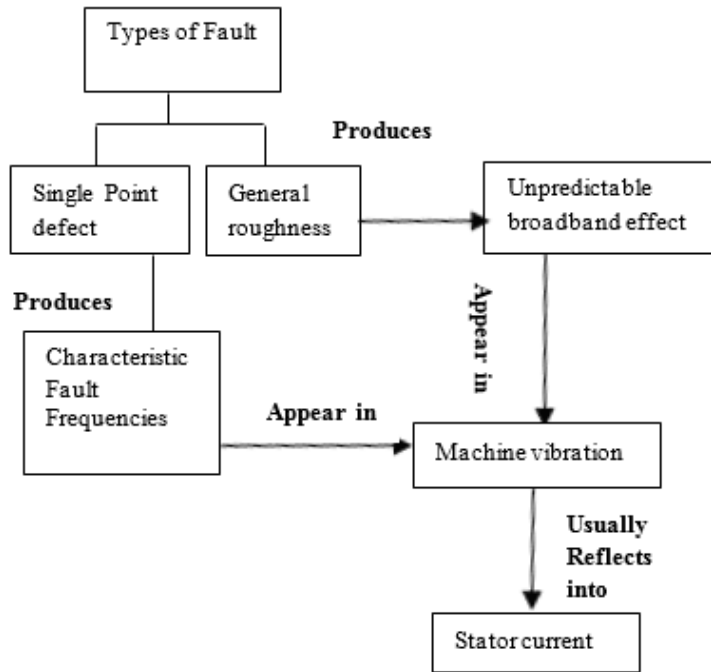


Figure 0.14: Flowchart showing effects of two categories of bearing faults [51].

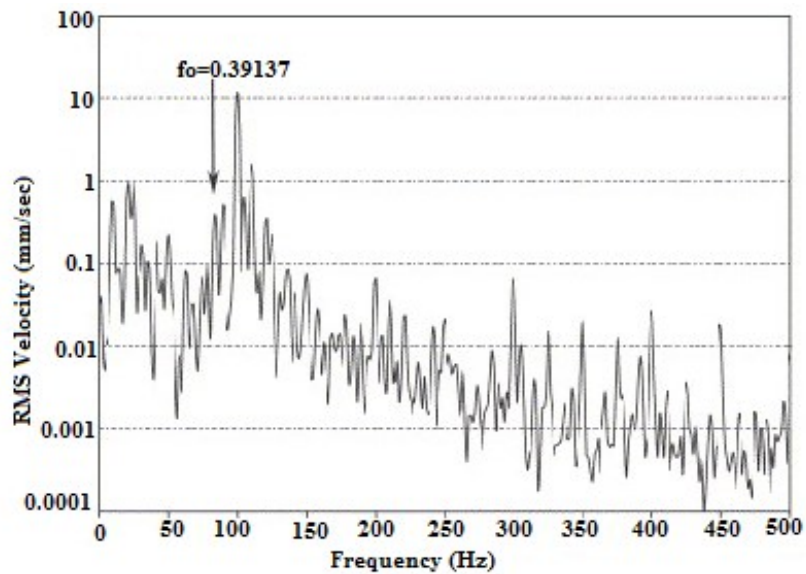


Figure 0.15: Spectrum of vibration velocity of a motor with a healthy bearing [51].

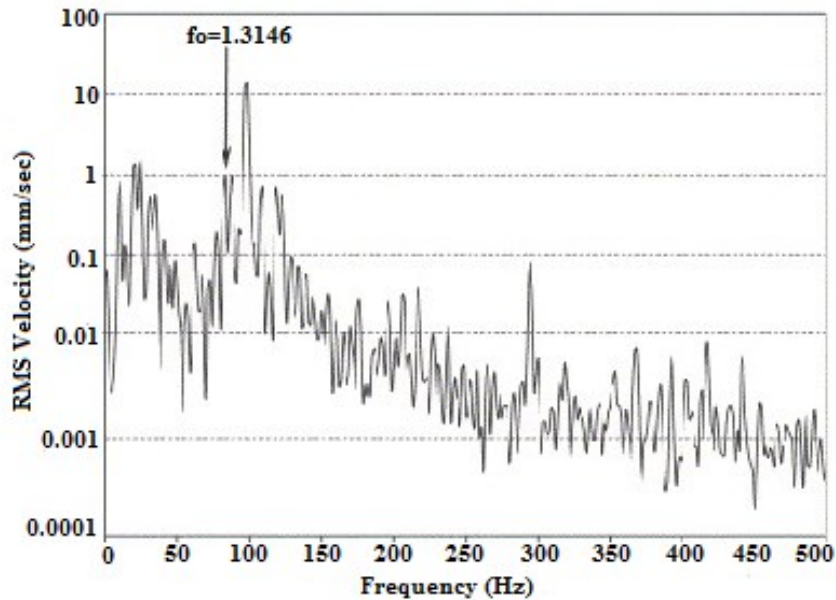


Figure 0.16: Spectrum of vibration velocity for a motor with 1500µm bearing defect [51].

The disadvantages of the DC signal injection approach include: 1) additional hardware is required to realize the signal injection, 2) the estimated temperatures are average quantities so local hotspots in electrical circuits cannot be identified, and 3) the continuous injected dc current could cause torque pulsation and magnetic saturation.

Reference [41] proposes an improved DC signal injection technique for stator-resistance (R_s)–based thermal monitoring of small line-connected induction machines. A simple device is developed for injecting a small dc signal into line-connected induction machines for stator resistance estimation. The proposed scheme intermittently injects a controllable dc bias into the motor with very low power dissipation, which reduce the influence of torque pulsation caused by continuous injected dc current in [52]. Fig. 2.17 shows this DC signal injection approach [60]. The obtained varying dc resistance can be used to perform temperature estimation and determine thermal time constant. This procedure is

independent on parameters of the machine, nor model. It's relatively simpler method than the thermal model [54]. Based on the linear relationship of resistivity with temperature of the stator winding, the stator winding temperature is estimated as follows [57] [60][62]:

$$T = T_0 + \frac{R - R_0}{\alpha R_0} \quad (13)$$

$$R = R_0[1 + \alpha (T - 25)] \quad (14)$$

Where, R_0 represents winding resistance at 25oC, α is a constant and a property of winding element, R_0 and R are the resistance at T_0 and T , respectively.

The AC signal injection monitoring techniques are proposed in [53]-[57]. Both high frequency and low frequency signal can be used for this technique. Stator resistance - rotor resistance ($R_s - R_r$) based induction machine temperature estimation is proposed in [58]-[62]. Based on the estimated stator resistance and rotor resistance, stator and rotor temperature are estimated correspondingly [59].

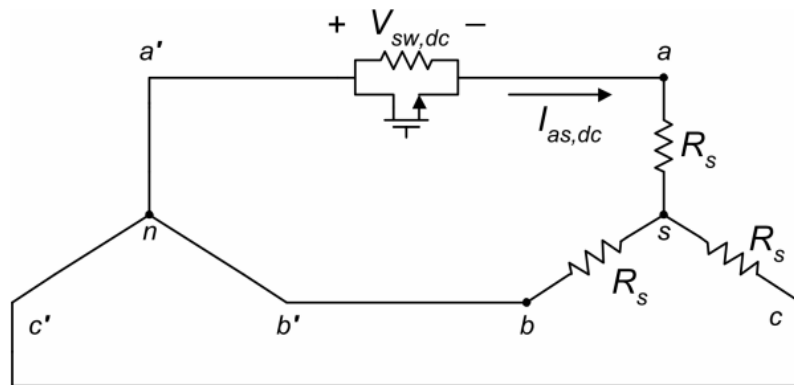


Figure 0.17: DC equivalent circuit of source, motor and DC injection circuit [60].

III. THE MODEL-BASED APPROACH

The model-based approach relies on machine's mathematical modeling. Various approaches have been proposed to model the behavior of the induction motor under fault conditions [27].

In Reference [63], an algorithm shown in Fig. 2.18 was developed for modeling and simulation of transient state of induction motor. The unbalanced voltage problems can be simulated using the created direct mathematical model of the induction motor.

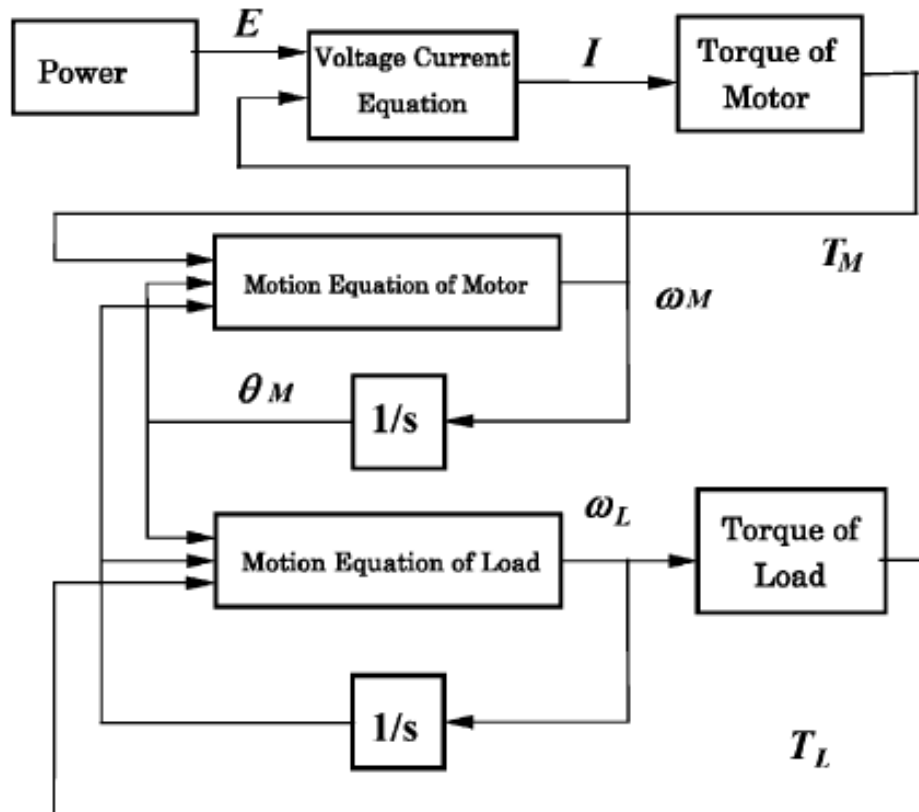


Figure 0.18: Block diagram of mathematical model for induction motors [63].

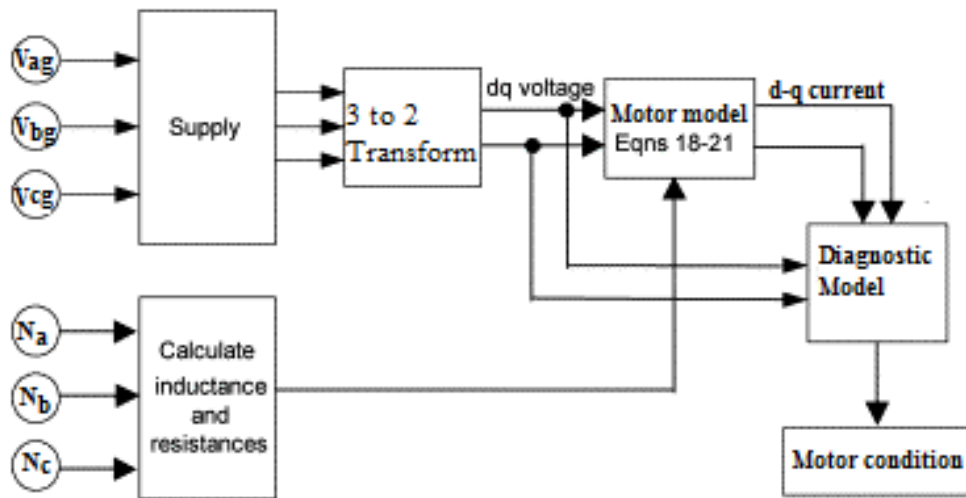


Figure 0.19: Simulation of an asymmetrical induction motor model [66]

In References [64]-[66], MATLAB/Simulink model of induction motor was implemented, and simulated results were analyzed for different faults conditions. The d-q model transform was employed for modeling of induction motor. Both healthy condition and asymmetry condition modeling for stator inter-turn fault was carried out. Fig. 2.19 shows simulation model for an asymmetric induction motor [66].

IV. THE KNOWLEDGE-BASED APPROACH

Artificial intelligent techniques have been applied in fault diagnosis of very complex time-varying and non-linear systems. However, their application in condition monitoring and fault diagnosis of induction motors is new.

A comparison of various artificial intelligent methods including Naive Bayes, k-Nearest Neighbor (KNN), Support Vector Machine (Sequential Minimal Optimization) (SVM/SMO), Artificial Neural Network (Multilayer Perceptron) (ANN/MLP), Repeated

Incremental Pruning to Produce Error Reduction, and C4.5 Decision Tree is provided in [67], it is found that for stator faults, the KNN, and ANN/MLP methods show better performance with 100% accuracy; for broken rotor bars faults, both ANN/MLP and KNN methods have accuracy rates over 99.7%; for bearings faults, the KNN, ANN/MLP, and C4.5 methods present promising results; for multi-classification, the ANN/MLP and KNN methods exceeds 92.5% accuracy; for robustness tests with defective bearings, the SVM/SMO method shows the best performance in terms of accuracy and processing time [67]. Based on the comparison, it shows ANN has the best performance for various fault detection. In addition to ANN, the SVM started gaining attention recently in this research area, SVM has excellent performance in generalization, so it can produce high accuracy in classification of machine condition monitoring [49].

The implementation of ANN models for Fault prediction hinges in the fact that they can be used to infer a function from observations. This technique comes handy in applications when it's practically impossible for computation to be done manually due to complexity of the data. Back-Propagation (BP) neural network is the most common type of ANN employed for solving fault diagnosis and prognosis problems.

A unique advantage besides a few others that makes BP application stand out, is because it does not require the knowledge of the exact form of analytical function on which the model should be built. For a BP model to operate, certain precision application order such as function type, number and position of parameters are not required. Moreover, it is compatible with various conditional operation, for example it has capacity for a multi-input, multi-output, quantitative or qualitative, complex system with very good abilities of data

fusion, self-adaptation and parallel processing. Thus, it is best suited for fault diagnosis selection [68].

BP is a multilayer feed-forward network usually containing the input layer, hidden layer, and output layer which employs the training methodology of error back propagation algorithm. Fig. 2.20 shows the BP neural network with a single hidden layer. BP network utilizes the steepest decent method by varying the weights and limits of the network to minimize the sum of squared errors [68] [69].

The aim of ANN training is to attain the proper fit that meets the input and the target of training data. Following training of BP network, calculations for final output of the updated weight are carried out for each set of test data. For a given fault diagnosis type, the features collected after training can be utilized as database by BP network for prediction and classification of fault conditions of induction machines [68].

Before application of ANN technique for broken rotor bar detection, the following were considered: 1) appropriate input variables selection, 2) number of output variables, and 3) layers and neurons in each layer. Pilot test were carried out on the networks. The selected network is composed of two input variables. The first input variable represents harmonic amplitude associated with the broken rotor bar, the second input variable is the slip s , used for reliability improvement of the desired classification. Fig. 2.20 shows multilayer neural network construction for the broken rotor bar fault detection

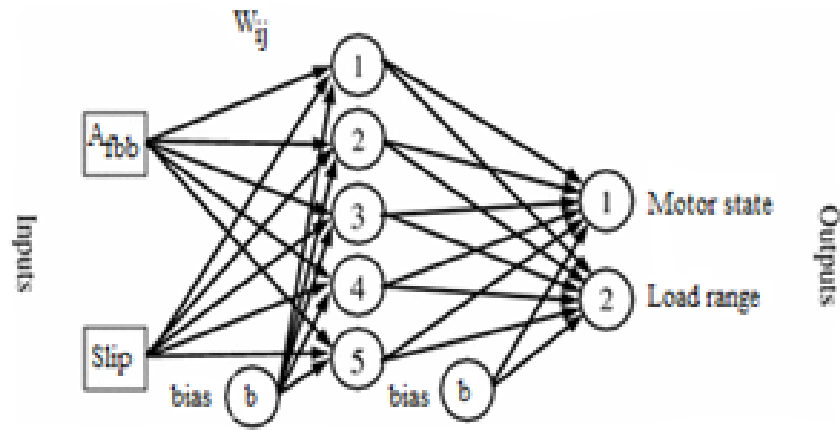


Figure 0.20: Neural network architecture [69]

The network is configured such that, there are two inputs neurons, one hidden layer of five neurons and two outputs neurons. The motor state neuron output corresponds to zero for the healthy machine, 0.5 corresponds to the case of one broken bar and 1 for the case of two broken bar. For the second neuron, which characterizes the load range. In this case, 0 corresponds to the case of low loads, 0.5 corresponds to half loads and 1 corresponds to the full loads. All activations functions of neurons are sigmoid. The training algorithm used is the BP gradient. With the chosen inputs, the results are acceptable after a few tens of iterations. Fig. 2.21 shows the broken rotor bars detection under different loads [69].

Reference [70] demonstrated the application of ANN for detection of four types of bearing faults. Fig. 2.22 shows the learning curve of neural network (NN) with eight input features. The training stops when the Mean Square Error (MSE) reaches zero or a predefined maximum number of epochs is reached. Fig. 2.22 confirms that the training with average 75 epochs, (defined limit for this case) satisfy the MSE stopping condition.

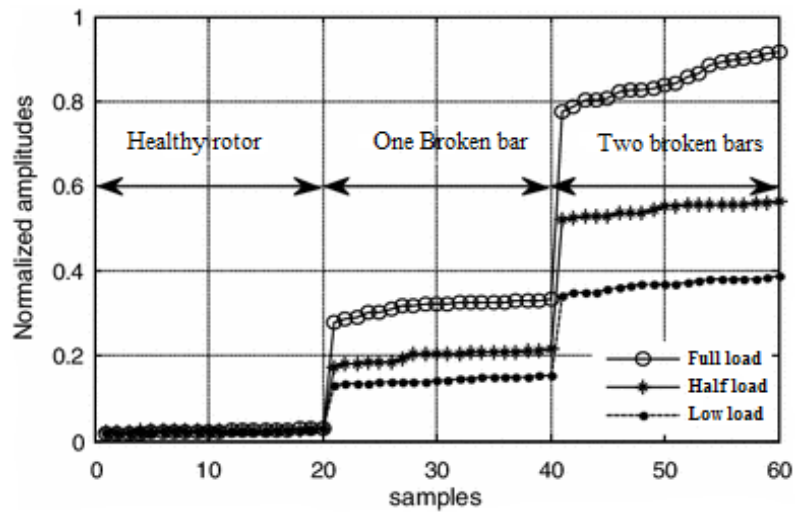


Figure 0.21: Normalized amplitudes of broken rotor bar components at different loads and motor states (the motor is 1.1 kW) [69].

ANN can also be used for insulation degradation fault detection. A specialist model procedure of ANN was employed in [71] [72]. The K-means algorithm operates condition-based monitoring by separating the data in individual classes, but unable to give interpretation motor condition, thus expert knowledge is required.

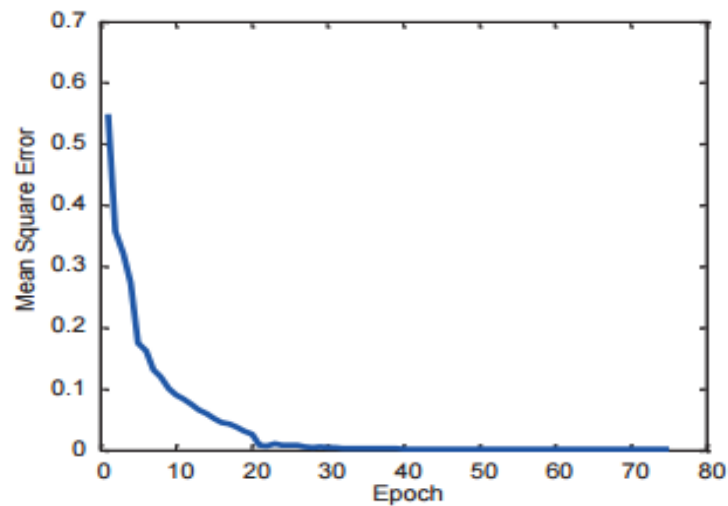


Figure 0.22: The learning curve of NN with eight input feature [70].

V. CONCLUSIONS

Various condition monitoring approaches for induction motors have been discussed in this paper under the three categories: 1) signature extraction-based approach, 2) model-based approach, and 3) knowledge-based approach. The strengths and drawbacks for several commonly used methods are analyzed comparatively.

Due to non-invasive nature of knowledge-based approach using artificial intelligent and machine learning and its excellent performance, it can be concluded that this method: 1) is a more reliable methodology; 2) can be employed for real-time condition monitoring; and 3) has high accuracy. The reliability and accuracy of this technique can compensate for the relative time constrain associated with data training required prior to the fault classification, which is usually perceived as a drawback. Therefore, the knowledge-based approach using artificial intelligent and machine learning opens a pathway to an exciting new research direction in condition monitoring and fault diagnosis of induction motors.

REFERENCES

- [1] Ayhan, B. ; Mo-Yuen Chow, H.J. ; Trussell, H.J. ; Myung-Hyun Song, H.J. "A case study on the comparison of non-parametric spectrum methods for broken rotor bar fault detection", IECON'03 2003, Vol.3, pp.2835-2840.
- [2] J. Cusid, L. Romeral, J. A. Ortega, J. A. Rosero, A. G. Espinosa, "Fault detection in induction machines using power spectral density in wavelet decomposition", IEEE Trans. Ind. Electron, vol. 55, no. 2, pp. 633-643, Feb. 2008.
- [3] S. Choi, E. Pazouki, J. Baek, H. R. Bahrami, "Iterative condition monitoring and fault diagnosis scheme of electric motor for harsh industrial application", IEEE Trans. Ind. Electron. vol. 62, no. 3, pp. 1760-1769, Mar. 2015.
- [4] A. Picot et al., "Statistic-based spectral indicator for bearing fault detection in Permanent-magnet synchronous machines using the stator current", J. Mech. Syst. Signal Process. vol. 46, no. 2, pp. 424-441, Jun. 2014.
- [5] Seera, M., Lim, CP., Ishak, D and Singh, H. "Fault Detection and Diagnosis of Induction Motors Using Motor Current Signature Analysis and a Hybrid FMM-CART Model" IEEE Trans On Neural Networks & Learning Sys, Vol.23(1), pp.97-108, Jan. 2012.
- [6] J. Faiz, B. M. Ebrahimi, H. A. Toliyat, W. S. Abu-Elhaija, "Mixed-fault diagnosis in induction motors considering varying load and broken bars location", Energy Conv. Manage., vol. 51, no. 7, pp. 1432-1441, Jul. 2010.

- [7] Moussa, Mohamed Amine., Boucherma, Mohamed and Khezzar, Abdelmalek “A Detection Method for Induction Motor Bar Fault Using Sidelobes Leakage Phenomenon of the Sliding Discrete Fourier Transform” IEEE Transactions on Power Electronics, Vol.32(7), pp.5560-5572, July 2017.
- [8] Jerkan, Dejan G., Reljic, Dejan D. and Marcetic, Darko P. “Broken Rotor Bar Fault Detection of IM Based on the Counter-Current Braking Method” IEEE Transactions on Energy Conversion, Dec. 2017, Vol.32(4), pp.1356-1366.
- [9] Babadi, Behtash and Brown, Emery N. “A Review of Multitaper Spectral Analysis” IEEE Transactions on Biomedical Engineering, Vol.61 (5), pp.1555-1564, May 2014.
- [10] Das, P and Babadi, B. “Dynamic Bayesian Multitaper Spectral Analysis” IEEE Transactions on Signal Processing, Vol.66 (6), pp.1394-1409, Mar., 2018.
- [11] Amel, B., Laatra, Y., Sami, S. and Nourreddine, D. “Classification and diagnosis of broken rotor bar faults in induction motor using spectral analysis and SVM” 2013 Eighth International Conference and Exhibition on Ecological Vehicles and Renewable Energies, March 2013, pp.1-5.
- [12] U. Krebel, "Pairwise classification and support vector machines", in Advances in Kernel Methods Support Vector Learning, Eds. Cambridge, MA: MIT Press, pp. 255-268, 1999.
- [13] J. Antonino-Daviu, S. Aviyente, E. G. Strangas and M. Riera-Guasp “Scale invariant feature extraction algorithm for the automatic diagnosis of rotor asymmetries in induction motors” IEEE Trans. Ind. Informat., vol. 9, no. 1, pp. 100-108, 2013.

- [14] Xiaodong Liang, and Kenneth Ik Edomwandekhoe, "Condition Monitoring Techniques for Induction Motors", Proceedings of 2017 IEEE Industry Applications Society (IAS) Annual Meeting, pp. 1-10, Cincinnati, OH, USA, October 1- 5, 2017.
- [15] Jakovljevic, B. B., Kanovic, Z. S. and Jelicic, Z. D. "Induction motor broken bar detection using vibration signal analysis, principal component analysis and linear discriminant analysis" 2012 IEEE International Conference on Control Applications, Oct. 2012, pp.1686-1690.
- [16] G. K. Singh, S. A. S. A. Kazzaz, "Development of an intelligent diagnostic system for induction machine health monitoring", IEEE Syst. J., vol. 2, no. 1, pp. 273-288, Jun. 2008.
- [17] W. Xu, D. Wang, Z. Zhou, H. Chen, "Fault diagnosis of power transformers: Application of fuzzy set theory expert systems and artificial neural networks", Proc. IEE Sci. Meas. Technol., vol. 144, no. 1, pp. 39-44, 1997-Jan.
- [18] J. M. Keller, J. H. Douglas, "Incorporating fuzzy membership functions into the perception algorithm", IEEE Trans. Pattern Anal. Mach. Intell., vol. PAMI-7, no. 6, pp. 693-699, Nov. 1985.
- [19] A. Soualhi, G. Clerc, H. Razik, "Detection and diagnosis of faults in induction motor using an improved artificial ant clustering technique", IEEE Trans. Ind. Electron., vol. 60, no. 9, pp. 4053-4062, Sep. 2013.

- [20] J. Karmakar, S. Chattopadhyay, M. Mitra, and S. Sengupta, "Induction Motor Fault Diagnosis Approach through Current Signature Analysis" Springer eBooks [online] available: <http://www.springer.com/978-981-10-0623-4>.
- [21] S.A. Taher, M. Malekpour, and W. Hong, "A Novel Technique for Rotor Bar Failure Detection in Single-Cage Induction Motor Using FEM and MATLAB/SIMULINK" *Mathematical Problems in Eng.*, Vol.2011, pp.1-14, 2011.
- [22] M. Ojaghi, M. Sabouri, and J. Faiz, "Diagnosis methods for stator winding faults in three-phase squirrel-cage induction motors" *International Transactions on Electrical Energy Systems*, Vol.24 (6), pp.891-912, June 2014.
- [23] S. Chandra, G. Ayyappan, K. Srinivas, and D. Ganesh, "Simulation and testing of induction motor faults in MATLAB for online condition monitoring", *IUP Journal of Elec. & Electron. Eng.*, Vol. 9(2), pp.7-18 Apr. 2016.
- [24] V.F. Pires, M. Kadivonga, J.F. Martins, and A.J. Pires, "Motor square current signature analysis for induction motor rotor diagnosis" *Measurement*, Vol.46 (2), pp.942-948, Feb. 2013.
- [25] P. Zhang, Y. Du, T. G. Habetler, and B. Lu, "A survey of condition monitoring and protection methods for medium-voltage induction motors", *IEEE Trans. Ind. Appl.*, vol. 47, no. 1, pp. 34-46, 2011.
- [26] A. Berzoy, A. A. S. Mohamed, and O. Mohammed, "Complex-vector model of interturn failure in induction machines for fault detection and identification", *IEEE Trans. Industry Applications*, vol. 53, no. 3, pp. 2667 – 2678, 2017

- [27] F. Duan, and R. Živanović, “Condition Monitoring of an Induction Motor Stator Windings Via Global Optimization Based on the Hyperbolic Cross Points”, IEEE Trans. Industrial Electronics, vol. 62, no. 3, pp. 1826-1834, 2015.
- [28] S. B. Lee, D. Hyun, T. Kang, C. Yang, S. Shin, H. Kim, S. Park, T. Kong, and H. Kim, “Identification of false rotor fault Indications produced by online MCSA for medium-voltage induction machines”, IEEE Trans. Industry Applications, vol. 52, no. 1, pp. 729 – 739, 2016.
- [29] M. Seera, C. P. Lim, H. Ishak, and H. Singh, “Fault Detection and Diagnosis of Induction Motors Using Motor Current Signature Analysis and a Hybrid FMM–CART Model”, IEEE Trans. Neural Networks & Learning Syst., Vol.23 (1), pp.97-108, Jan. 2012.
- [30] X. Wang, and Z. Zhao, “Research on Broken rotor bar Fault Diagnosis of Induction Motor Based on LabVIEW”, Procedia Engineering, Vol.15, pp.2550-2554, 2011.
- [31] G. Didier, H. Razik, A. Rezzoug, R. Belmans, and J. Melkebeek, “An induction motor model including the first space harmonics for broken rotor bar diagnosis”, European Transactions on Electrical Power, Vol.15 (3), pp.229-243, May 2005.
- [32] R. Sharifi, and M. Ebrahimi, “Detection of stator winding faults in induction motors using three-phase current monitoring”, ISA Transactions, Vol.50 (1), pp.14-20, 2011.
- [33] A. Ordaz-Moreno, R.D. Romero-Troncoso, J. Vite-Frias, J. Rivera-Gillen, and A. Garcia-Perez, “Automatic online diagnosis algorithm for broken-bar detection on induction motors based on discrete wavelet transform for FPGA implementation”, IEEE Trans. Ind. Electron., Vol.55 (5), pp.2193-2202, May 2008.

- [34] J. Antonino, M. Riera, J. Roger-Folch, M. P. Molina, "Validation of a new method for the diagnosis of rotor bar failures via wavelet transform in industrial induction machines", *IEEE Trans. Ind. Appl.*, vol. 42, no. 4, pp. 990- 996, Jul./Aug. 2006.
- [35] M.R. Mehrjou, N. Mariun, M.M. Hamiruce, and N. Misron, "Rotor fault condition monitoring techniques for squirrel-cage induction machine □ a review", *Mech. Syst. & Signal Proc.*, Vol.25 (8), pp.2827-2848, 2011.
- [36] S. Lee, J. Hong, S. B. Lee, E. J. Wiedenbrug, M. Teska, and H. Kim, "Evaluation of the influence of rotor axial air ducts on condition monitoring of induction motors", *IEEE Trans. Industry Applications*, vol. 49, no. 5, pp. 2024 – 2033, 2013.
- [37] Y. Trachi, E. Elbouchikhi, V. Choqueuse, and M. E. H. Benbouzid, "Induction machines fault detection based on subspace spectral estimation", *IEEE Trans. Industrial Electronics*, vol. 63, no. 9, pp. 5641-5651, 2016.
- [38] P. Karvelis, G. Georgoulas, I. P. Tsoumas, J. A. Antonino-Daviu, V. Climente-Alarcón, and C. D. Stylios, "A symbolic representation approach for the diagnosis of broken rotor bars in induction motors", *IEEE Trans. Industrial Informatics*, vol. 11, no. 5, pp. 1028 – 1037, 2015.
- [39] R. Romero-Troncoso, D. Morinigo-Sotelo, O. Duque-Perez, R. Osornio-Rios, M. Ibarra-Manzano, and A. Garcia-Perez, "Broken rotor bar detection in VSD-fed induction motors at startup by high-resolution spectral analysis," in *Proc. Int. Conf. Elect. Mach.*, pp. 1848–1854, Sep. 2014.

- [40] F. C. Trutt, J. Sottile, and J. L. Kohler, "Online condition monitoring of induction motors", IEEE Trans. Industry Applications, vol. 38, no. 6, pp. 1627 – 1632, 2002.
- [41] J. L. Kohler, J. Sottile, and F. C. Trutt, "Condition monitoring of stator windings in induction motors: part I - experimental investigation of the effective negative-sequence impedance detector", IEEE Trans. Industry Applications, vol. 38, no. 5, pp. 1447 – 1453, 2002.
- [42] J. Sottile, F. C. Trutt, and J. L. Kohler "Condition monitoring of stator windings in induction motors: part II - experimental investigation of voltage mismatch detector", IEEE Trans. Industry Applications, vol. 38, no. 5, pp. 1454 – 1459, 2002.
- [43] D. G. Dorrell, and K. Makhoba, "Detection of inter-turn stator faults in induction motors using short term averaging of forwards and backwards rotating stator current phasors for fast prognostics", DOI 10.1109/TMAG.2017.2710181, IEEE Trans. Magnetics.
- [44] G. Mirzaeva, K. I. Saad, and M. G. Jahromi, "Comprehensive diagnostics of induction motor faults based on measurement of space and time dependencies of air gap flux", IEEE Trans. Industry Applications, vol. 53, no. 3, pp. 2657-2666, 2017.
- [45] M. Malekpour, B.T. Phung and E. Ambikairajah, "Online technique for insulation assessment of induction motor stator windings under different load conditions", IEEE Trans. Dielectrics and Electrical Insulation, Vol. 24, No. 1, pp. 349-358, 2017.
- [46] H. Su, K. Chong, and R. Kumar, "Vibration signal analysis for electrical fault detection of induction machine using neural networks", Neural Computing and Applications, Vol.20 (2), pp.183-194, 2011.

- [47] N. Tandon, G.S. Yadava, and K.M. Ramakrishna, "A comparison of some condition monitoring techniques for the detection of defect in induction motor ball bearings", *Mech. Syst.& Signal Proc.*, Vol.21(1), pp.244-256 2007.
- [48] Mikhail Tsyarkin, "The Origin of the Electromagnetic Vibration of Induction Motors Operating in Modern Industry: Practical Experience - Analysis and Diagnosis", DOI 10.1109/TIA.2016.2633946, *IEEE Trans. Industry Applications*.
- [49] Shrinathan Esakimuthu Pandarakone, Yukio Mizuno, and Hisahide Nakamura, "Distinct Fault Analysis of Induction Motor Bearing using Frequency Spectrum Determination and Support Vector Machine", DOI 10.1109/TIA.2016.2639453, *IEEE Trans. Industry Applications*.
- [50] S. Wadhvani, S. Gupta, and V. Kumar, "Fault classification for rolling element bearing in electric machines", *IETE Journal of Research*, Vol.54 (4), p.264-275, 2008.
- [51] J.R. Stack, T.G. Habetler, and R.G. Harley, "Fault classification and fault signature production for rolling element bearings in electric machines", *IEEE Trans., Ind., Applications*, Vol.40 (3), pp.735-739, June 2004.
- [52] D. A. Paice, "Motor thermal protection by continuous monitoring of winding resistance", *IEEE Transactions on Industrial Electronics and Control Instrumentation*, Vol. IECI-27, No. 3, pp. 137 – 141, 1980.
- [53] J. Cusidó, L. Romeral, J. A. Ortega, A. Garcia and J. Riba, "Signal injection as a fault detection technique", *Sensors*, pp. 3356-338, Mar. 2011.

- [54] M.O. Sonnaillon, G. Bisheimer, C. De. Angelo, G.O Garcia. “Online sensor-less induction motor temperature monitoring”. IEEE Trans Ind. Appl., Vol 25, pp.273-280, June 2010.
- [55] P. Zhang, Y. Du, T.G. Habetler, and B. Lu, “Magnetic Effects of DC Signal Injection on Induction Motors for Thermal Evaluation of Stator Windings”, IEEE Trans., Ind. Electron., Vol.58 (5), pp.1479-1489, May 2011.
- [56] C. Kral, T. G. Habetler, R. G. Harley, F. Pirker, G. Pascoli, H. Oberguggenberger, and M. F. Claus-Jurgen “Rotor temperature estimation of squirrel-cage induction motors by means of a combined scheme of parameter estimation and a thermal equivalent model,” IEEE Trans. Ind. Appl., vol. 40, no. 4, pp. 1049–1057, Aug. 2004.
- [57] L. Sang-Bin, T.G. Habetler and R. G. Harley. “An evaluation of model-based stator resistance estimation for induction motor stator winding temperature monitoring”, IEEE Trans. Energy Convers., Vol. 28, pp. 702-709, Aug. 2012.
- [58] T.G. Habetler, “Current-based motor conditioning monitoring: complete protection of induction and PM machines”, Aegean Int. Conf., Elect. Machines and Power Electronic, pp. 378-384, 2007.
- [59] P. Zhang, B. Lu, and T. G. Habetler, “A remote and sensor-le stator winding resistance estimation method for thermal protection of soft-starter-connected induction machines”, IEEE Trans. Ind. Elec., Vol. 55, No. 10, pp. 3611-3618, Oct 2008

- [60] S. Lee, and T.G. Habetler, “An online stator winding resistance estimation technique for temperature monitoring of line-connected induction machines”, IEEE Trans. Ind. Appl., Vol.39 (3), pp.685-694, June 2003.
- [61] Y. Wu, and H. Gao, “Induction-motor stator and rotor winding temperature estimation using signal injection method,”, IEEE Trans. Ind. Appl., vol. 4, pp. 1038–1044, Jul./Aug. 2006.
- [62] Z. Gao, T.G. Habelter, R.G. Harley, and R.S. Colby. “A sensor-less rotor temperature estimator for induction machines, based on a current harmonic spectral estimation scheme”, IEEE Trans. Ind. Appl., Vol 55, pp.407-416, Jan 2008.
- [63] M. Ikeda, and T. Hiyama, “Simulation studies of the transients of squirrel-cage induction motors”, IEEE Trans. Energy Conv., Vol.22 (2), pp.233-239 June 2007.
- [64] H. Arabaci, and O. Bilgin, “Squirrel cage of induction motors simulation via SIMULINK”, International J. Modeling and Optimization, Vol.2 (3), pp.324, Jun 2012.
- [65] M. Sahraoui, A. Ghoggal, S.E. Zouzou, and M.E. Benbouzid, “Dynamic eccentricity in squirrel cage induction motors – Simulation and analytical study of its spectral signatures on stator currents”, Simulation Modelling Practice and Theory, Vol.16 (9), pp.1503-1513, 2008.
- [66] M. Arkan, D. Kostic-Perovic, and P.J. Unsworth. “Modelling and simulation of induction motors with inter-turn faults for diagnostics”, Elect. Power Syst. Research Fuel & Energy abstracts, Vol.47 (2), pp.57-66, 2006.

- [67] R. H. C. Paláciosa, I. N. d. Silva, A. Goedel, W. F. Godoy, “A Comprehensive Evaluation of Intelligent Classifiers for Fault Identification in Three-Phase Induction Motors”, *Electric Power Systems Research*, 127, pp. 249–258, 2015.
- [68] Z. Zhang, Y. Wang, and K. Wang, “Fault diagnosis and prognosis using wavelet packet decomposition, Fourier transform and artificial neural network”, *Journal of Intelligent Manufacturing*, Vol.24 (6), pp.1213-1227, 2013.
- [69] S. Guedidi, S. Zouzou, W. Laala, K. Yahia, and M. Sahraoui, “Induction motors broken rotor bars detection using MCSA and neural network: experimental research”, *Int. J. Syst. Assurance Eng. and Management*, Vol.4 (2), pp.173-181, 2013.
- [70] A. Chandel, and R. Patel, “Bearing fault classification based on wavelet transform and artificial neural network”, *IETE Journal of Research*, Vol.59 (3), pp.219-225, Jun. 2013.
- [71] A. S. Guedes, S. M. Silva, F. Cardoso, and C. A. Conceição, “Evaluation of electrical insulation in three-phase induction motors and classification of failures using neural networks”, *Elec. Power Syst. Research*, Vol.140, pp.263-273, 2016.
- [72] H. Su, and K. T. Chong, "Induction Machine Condition Monitoring Using Neural Network Modeling", *IEEE Trans. Ind., Electron*, Vol.54 (1), pp.241-249, Feb. 2007.

Chapter 3 : Current Spectral Analysis of Broken Rotor Bar

Faults for Induction Motors

A version of this manuscript has been published in the Proceedings of 31st Annual IEEE Canadian Conference on Electrical and Computer Engineering (CCECE 2018), Québec City, Québec, Canada, May 13-16, 2018.

The research work is done under the supervision of Dr. Xiaodong Liang. Kenneth Edomwandekhoe conducted research, created models, and wrote the paper. Dr. Liang suggested necessary further research steps and modified the whole paper.

A few adjustments were done on the figures, tables and referencing in the manuscript in order to conform to Memorial University manuscript standard format.

Current Spectral Analysis of Broken Rotor Bar Faults for Induction Motors

Kenneth Edomwandekhoe, *Student Member IEEE*, Xiaodong Liang, *Senior Member IEEE*,

Faculty of Engineering and Applied Science, Memorial University of Newfoundland,
St. John's, Newfoundland, Canada.

***Abstract-* Traditional fast Fourier transform (FFT) has gained enormous recognition for broken rotor bar (BRB) fault detection in induction motors using the sideband features as fault indices, however, the false alarm from inaccurate diagnosis remains a major setback associated with the technique. This paper presents two reliable spectral analysis approaches for BRB fault detection and analysis for induction motors: Thompson Multitaper (MTM) power spectral density (PSD) estimate, and Welch PSD estimate. The two methods are implemented using the simulated stator current signal of an induction motor obtained by the finite element method. The Finite Element analysis software, ANSYS, is used to design and simulate different motor conditions: a healthy motor, a motor with one, two and three BRBs. It is verified that the proposed methods provide robust and reliable BRB fault detection for induction motors.**

Index Terms- Induction motor, Spectral analysis, Thompson Multilayer power spectral density estimate, Welch power spectral density estimate.

I. INTRODUCTION

Induction motors are the corner stone for industrial machinery operation today. Up to 80% of energy conversion in the industry involves induction motors because of their ruggedness, reliability, and fairly cheap maintenance practice. Due to their applications in critical industrial processes, incipient detection of various faults, such as mechanical, electrical, and thermal, during operation are very important.

Current spectral analysis diagnostic method has been reported in a number of literatures for induction motors fault detection. The most popular technique is the motor current signature analysis (MCSA). In [1], the traditional MCSA is used to detect the presence of one broken rotor bar (BRB) fault in induction motors, and the fault identification is based on the presence of additional side bands amid the fundamental motor current frequency. The sidebands that emerge as a result of broken rotor bars are caused by distorted symmetry in the rotor circuit. Upper and lower sidebands can be obtained by decomposition of the asymmetry condition into positive and negative phase sequence components. Sidebands induced by BRBs can be validated by the equation, $(1 \pm 2s)f$ where s is the slip of the motor, and f is the excitation current frequency [2].

However, the traditional MCSA has drawbacks, such as inability to manage varying time condition, and inaccurate or false diagnostic. The severity of BRB faults is associated with the amplitude increase of sidebands. For an increased number of broken rotor bars, there is a consequent increase in the peak of sidebands measured in db. However, unbalanced

voltage supply can also introduce asymmetry and additional sidebands. This similarity can present conflict in deciphering the source of the fault [3].

Considering that the traditional fast Fourier transform (FFT) cannot process non-stationary signals, the short time Fourier transform (STFT) is employed for the motor transient condition with the time-frequency representation in [4]. However, the STFT also has its limitation with characteristics of applying a fixed window to all signals, which introduces the loophole of data loss due to approximation and low resolution. To eliminate the drawback of STFT, this paper presents two techniques that resolve unreliability common with the aforementioned methods. The proposed two spectral analysis techniques, Thompson Multitaper PSD estimation, and Welch PSD estimation, cater for the loss of data information by performing a gross average of the segmented signals with application of suitable widow property, and thus, eliminate inaccuracies. The paper is structured as follows: In Section II, the modeling and analysis of induction motors using the finite element method are discussed; In Section III, the two proposed spectral techniques are presented, and the simulation data are analyzed using the two techniques; conclusions are drawn in Section IV.

II. FINITE ELEMENT ANALYSIS

A. Induction Motor Used in Finite Element Analysis

Finite Element (FE) analysis is a numerical approach for solving parameters represented in differential equations in electromagnetic devices, which allows geometrical shape representation, nonlinear effect analysis, material properties and boundary conditions in different regions of the machine. The Finite Element analysis software ANSYS is used in

this paper. The design data entered into the software include: machine type, dimensions of the stator and rotor of the machine, number of poles, control type, specifications of windings, slots, wires, conductors, and insulation [5].

There are four fundamental steps involved in modeling an induction motor using ANSYS: 1) Description of geometrical parameters, and construction of a two-dimensional (2D) model; 2) Definition of physical parameters such as regions and materials; 3) Construction of an electric circuit model; and 4) Meshing of the study domain and solving problem. Fig. 1 shows the complete geometrical 2D models of the induction motor under investigation in this paper for four different scenarios: 1) a healthy motor; 2) the motor with one BRB; 3) the motor with 2 BRBs; 4) the motor with 3 BRBs. All four scenarios consider 75% loading of the motor. The highlight rotor bar in Fig. 3.1 represent a broken rotor bar. Parameters of the machine used in the simulation are detailed in Table 3.1 (I).

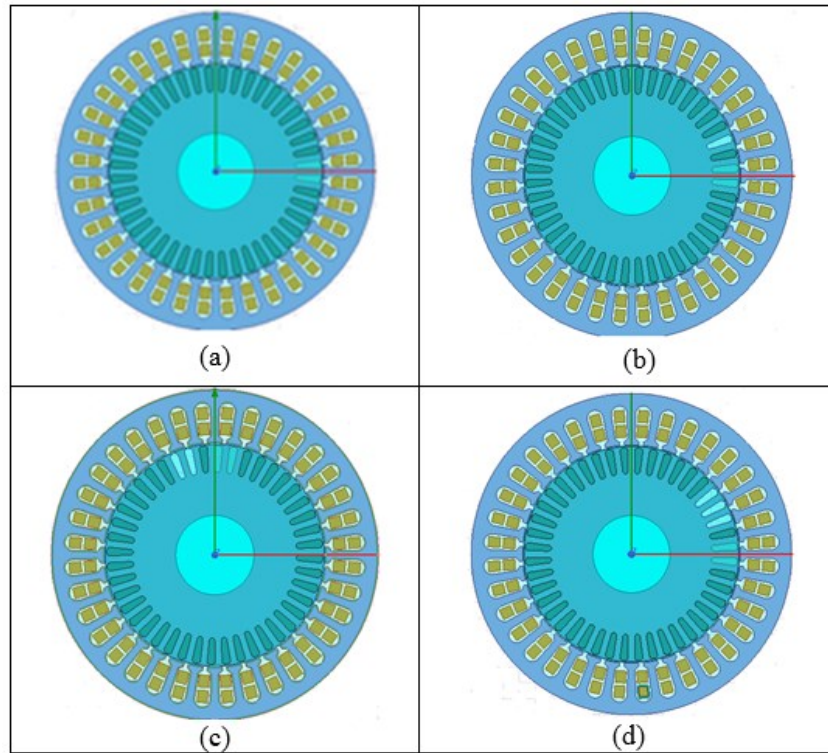


Figure 0.1: Induction motor FE analysis model at 75% loading: (a) a healthy motor, (b) a motor with 1BRB, (c) a motor with 2BRBs, and (d) a motor with 3 BRBs.

Table 0.1: Specifications of Induction Motor Used in the Simulation

General data		Stator		Rotor	75% loading	
P_{out} , kW	3	Number of Slots	44	36	Stator resistance, Ohms	0.806
Line Voltage, V	240				Rotor resistance, Ohms	0.778
Number of Poles	4	Inner diameter, mm	136	48	Inductance, Henry	0.0006
Speed, rpm	1724				Torque, N-m	10
Frequency, Hz	60	Type of steel	M19_24G			
		Length of bar, mm	4.5	1.75		

B. Simulation Signals

The simulated motor phase currents for the four scenarios, a healthy motor and the same motor with different number of broken rotor bars, are shown in Fig. 3.2. These

simulated current signals can be further screened and used for BRB fault diagnosis for induction motors. Figs. 3.3 and 3.4 show the corresponding speed and torque characteristics for the four scenarios. It can be clearly visualized that BRB faults have direct impact on speed and torque of induction motors.

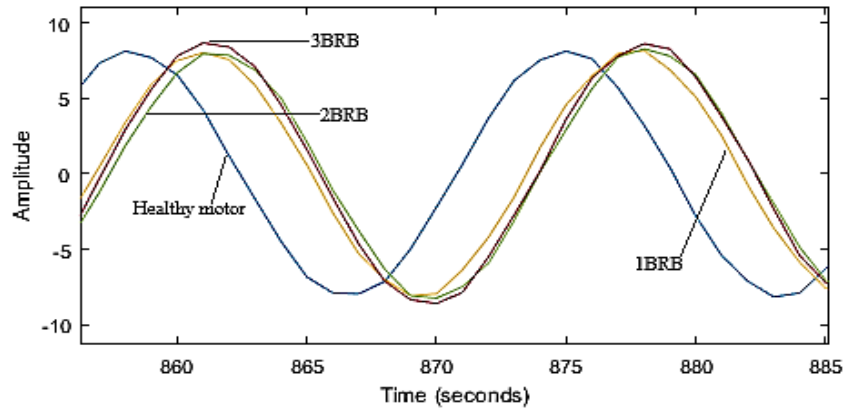


Figure 0.2: Simulated induction motor stator current at 75% loading using ANSYS for the four scenarios defined in Fig. 3.1.

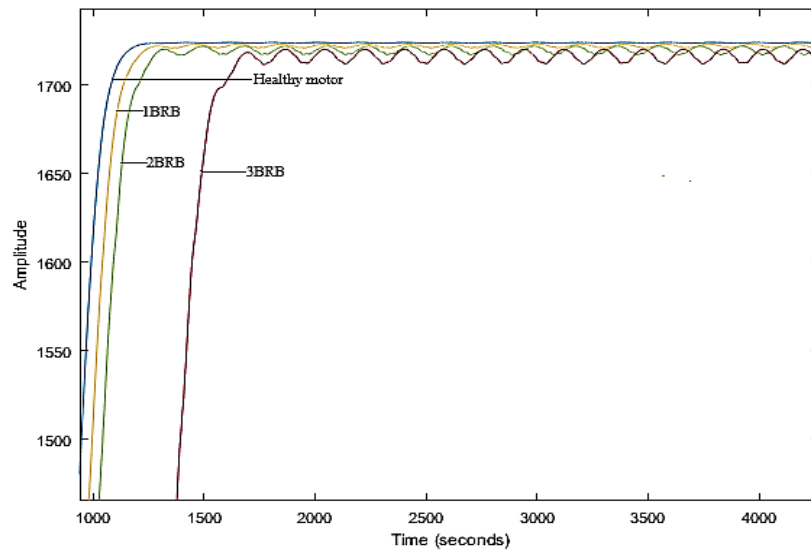


Figure 0.3: Simulated induction motor speed signal at 75% loading using ANSYS for the four scenarios defined in Fig. 3.1.

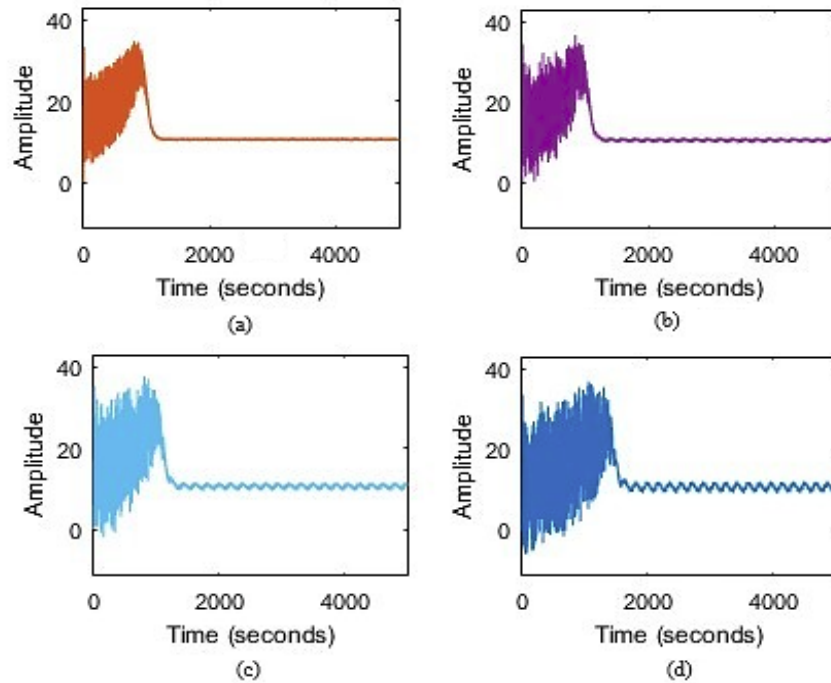


Figure 0.4: Simulated induction motor torque signal at 75% loading using ANSYS: (a) a healthy motor, (b) a motor with 1BRB, (c) a motor with 2BRBs, and (d) a motor with 3BRBs.

III. THE PROPOSED SPECTRAL ANALYSIS METHODS

A. The Multitaper Method

The Thomson Multitaper estimator has been successfully applied in many areas for spectral analysis. In this method, the data are multiplied with special windows (tapers) before the frequency decomposition. The windows often used are the Discrete Prolate Spheroidal Sequences (DPSS), developed by Slepian and Pollack. A Fourier Transform is performed after multiplying data with DPSS windows, and the absolute square of the resulting signal is calculated. The procedure is repeated with K different orthogonal windows, K statistically uncorrelated estimates of the spectra are generated. The number $K = 2TW - 1$, where T is

the window size, and W is the bandwidth. The DPSS windows are selected for favorable spectral leakage properties. Both orthogonality and time-frequency concentration of the windows are vital to the success of this method [6], [7].

For a given stationary discrete-time random process, $x(n)$, the spectrum $S(MT)(f)$ can be estimated from N samples $x = [x(0), x(1), \dots, x(N-1)]^T$ of the process by using Thomson Multitaper estimator as follows [6]:

$$S^{(MT)}(f) = \frac{1}{K} \sum_{k=0}^{K-1} S_k(f) \quad (1)$$

$$S_k(f) = \Delta t \left| \sum_{n=0}^{N-1} g_{k,n} x_n e^{-i2\pi f n \Delta t} \right|^2 \quad (2)$$

Where, $S^{(MT)}(f)$ is the multitaper estimate, $S_k(f)$ is a windowed periodogram obtained by using the data window $hk = [hk(0) \dots hk(N-1)]^T$, and N is the number of data samples. In a simple form, the multitaper method simply averages the K modified periodograms to produce the multitaper PSD estimate. K represents partitioned signal segment. In this paper, in order to analyze frequency characteristics, the raw data of the simulated stator currents of the healthy motor and the motor with BRBs in Fig. 3.2 are processed using Thomson Multitaper method.

The results of the two-sided PSD estimation of the current input is shown in Fig. 3.5. Table 3.2 (II) summarizes critical sidebands' amplitudes and frequencies. It was observed in Fig. 3.5 and Table 3.2 (II) that, for every BRB fault, both amplitude and frequency are affected. There is a concomitant increase in amplitude (measured in db) for additional BRB. This assertion is verified by carefully observing the amplitude of the sample bands separated

by the widow feature application of the MTM technique. It is easy to identify immediate consequence of an additional BRB by monitoring different frequency bands and amplitude. The reference line indicates the instantaneous influence for each additional BRB. The results obtained in this paper agree with that based on the experimental approach in [8].

B. Welch Power Spectral Density

The Welch PSD estimation involves separating the signal into multiple segments, screening modified periodograms of these sections and averaging these modified periodograms. Each segment is associated with a Hanning window. The modified periodograms are averaged to obtain the PSD estimate. When it's difficult to divide the length of input signal exactly into an integer number of segments with 50% overlap, the input signal can be condensed consequently [9]. The procedure implementing the Welch PSD estimation is listed as follows [10]:

- 1) The input signal is divided into overlapping segments.
- 2) The specified window is applied to each segment.
- 3) FFT is applied to the windowed data.
- 4) The periodogram of each windowed fragment is calculated.
- 5) The resultant average fragments of the signal form the spectral estimate.

The MATLAB tool box is employed for implementation of the Welch PSD estimation technique. The purpose of the hanning window function is to reduce the side-lobe level in the spectral density estimate. For the nonrectangular method of window analysis for a signal

(n), the window hop size R is specified within the average signal range to prevent non-uniformity introduced to the signal. In this case, a rectangular Hanning window is chosen, and thus, R is set as $\frac{1}{2}$ of M , where M represents the length of a signal. The window is applied, and the overlap parameter adopted in MATLAB tool box is $M - R$. In this paper, the simulated stator current signals from ANSYS in Fig. 3.2 are used to obtain Welch PSD estimate, and the results are a one-sided PSD estimate as shown in Fig. 3.6. Table 3.3 (III) also shows tabulated sideband frequency and amplitude for the four scenarios. It is found that for increased BRBs, there is an observable increase in amplitude, which is evident in the reference line indicating the effect of fault severity.

Thomson Multitaper estimator and Welch PSD estimation method can reduce variability in the periodogram by averaging over approximately uncorrelated PSD estimates. However, the two methods differ in how uncorrelated PSD estimations are produced. The Thomson Multitaper technique is a non-parametric method, it uses the full signal in each modified periodogram, and the orthogonality of the Slepian tapers decorrelates different modified periodograms. On the other hand, Welch's method is a parametric method, it uses overlapped segment averaging approach of the signal in each modified periodogram, and the segmenting decorrelates different modified periodograms.

Tables 3.2 (II) and 3.3 (III) indicate that both techniques follow the similar trend of maintaining the amplitude increase as the spectrum of selected segment changes with an increased number of BRBs. The amplitude for the two techniques increases in the order of -17.47 db, -36.57 db, -40 db, -42.45 db, and -28.24 db, -40 db, -52.24 db and -57.63 db. The numerical difference between the two techniques can be attributed to the halving of signal

window employed by Welch PSD technique whereas the full signal is applied for Thompson PSD. This approach results in an exaggerated average in higher values as shown in Table 3.3 (III). However, the wide acclaimed and expected amplitude db value for a single BRB fault (being between -35 db and -50 db), is well represented in Figs. 3.5 and 3.6 with Fig. 3.5 showing -36.57 db and Fig. 3.6 showing -40 db.

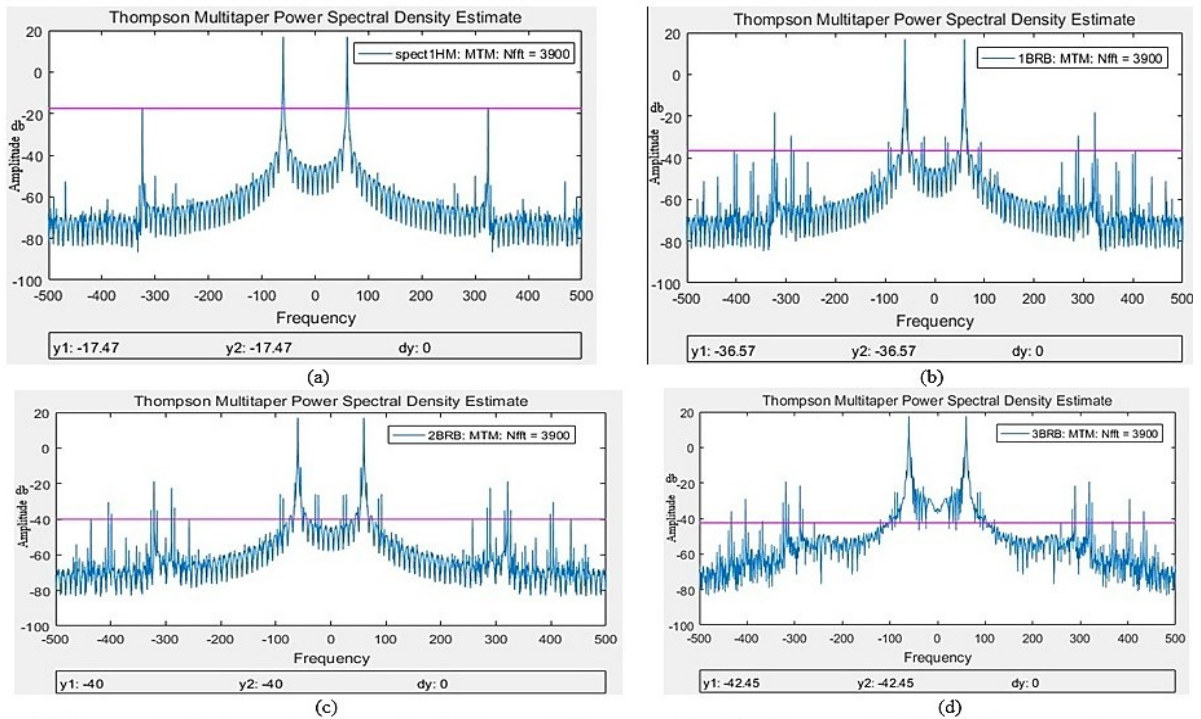


Figure 0.5: Thompson Multitaper estimation for current spectrum: (a) a healthy motor; (b) a motor with 1BRB; (c) a motor with 2BRBs; (d) a motor with 3BRBs

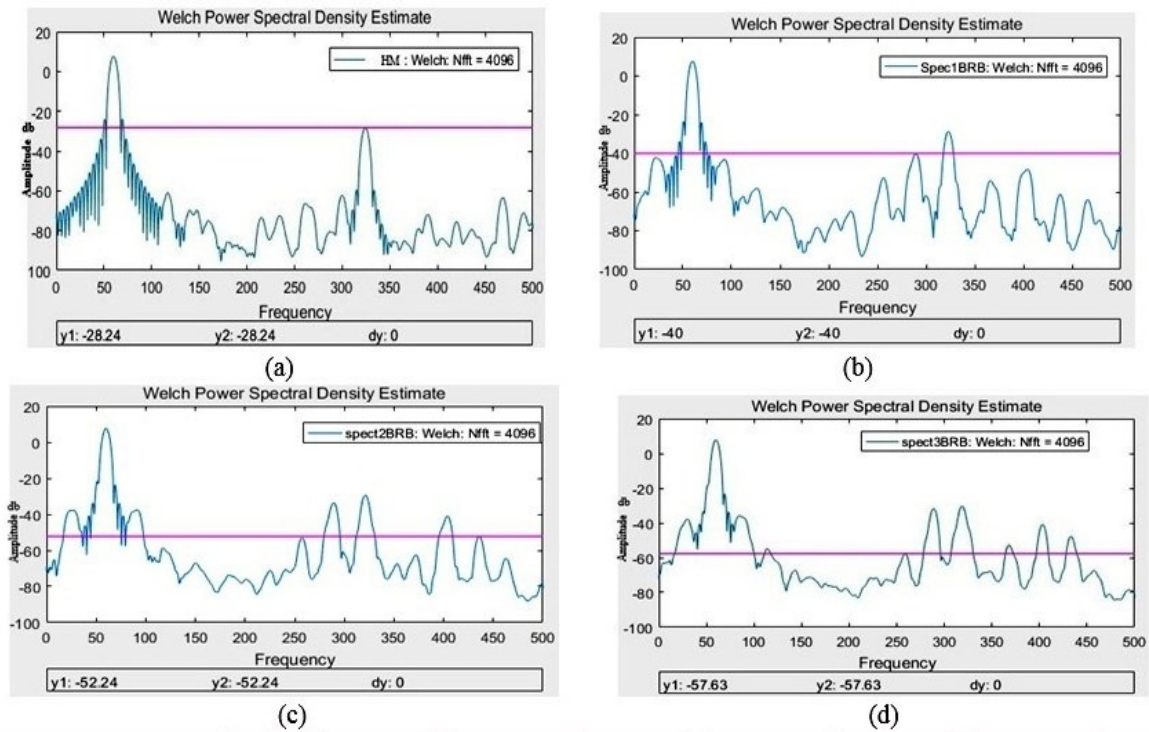


Figure 0.6: Welch PSD estimation for current spectrum: (a) a healthy motor; (b) a motor with 1BRB; (c) a motor with 2BRBs; (d) a motor with 3BRBs.

Table 0.2: AMPLITUDES FOR DIFFERENT BRB FAULTS USING THOMSON MULTITAPER ESTIMATOR

A healthy motor		A motor with 1BRB		A motor with 2BRBs		A motor with 3BRBs	
Frequency (Hz) X-axis	Amplitude (db)Y- axis	Frequency (Hz) X-axis	Amplitude (db)Y-axis	Frequency (Hz)X-axis	Amplitude (db)Y- axis	Frequency (Hz)X-axis	Amplitude (db)Y-axis
324.87	-17.47	284.36	-36.57	258.097	-40	260.12	-42.45

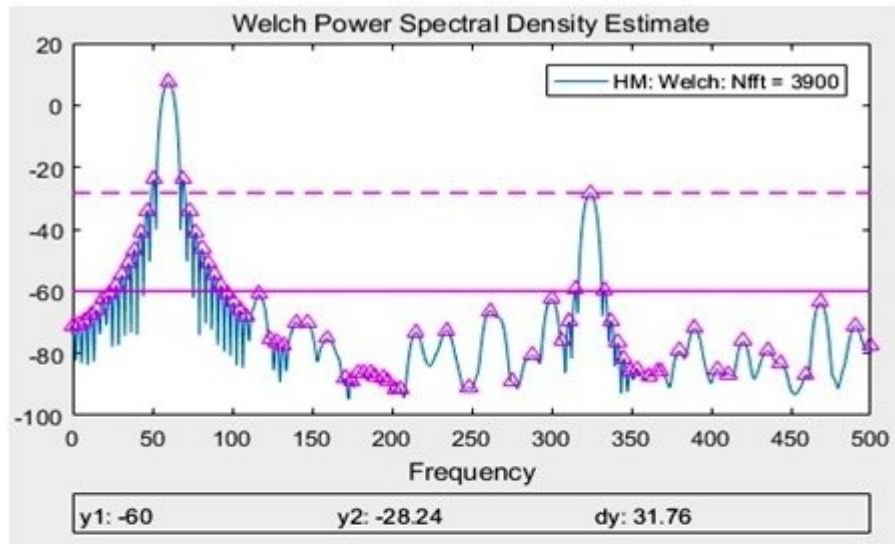
Table 0.3: Amplitudes for Different BRB Faults Using Welch PSD Estimation

A healthy motor		A motor with 1BRB		A motor with 2BRBs		A motor with 3BRBs	
Frequency (Hz) X-axis	Amplitude (db)Y- axis	Frequency (Hz) X axis	Amplitude (db)Y- axis	Frequency (Hz)X axis	Amplitude (db)Y- axis	Frequency(Hz) X axis	Amplitude (db)Y- axis
324.87	-28.24	289.98	-40	257.59	-52.24	258.60	-57.63

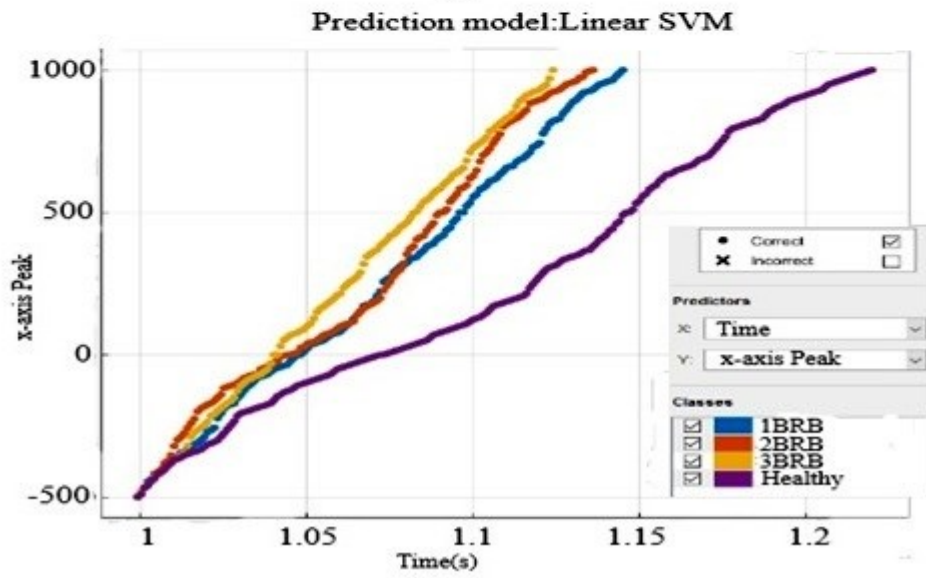
C. BRB Faults Detection Using Welch PSD Estimation

In this section, the Welch PSD estimation results are used for BRB faults detection through machine learning. The peaks of the spectrum unveil a clear cut evident of the three faults (i.e 1BRB, 2BRB and 3BRB). In order to enable training and selection of best features, the peaks of the spectrum are selected as sub-condition for classification. Table IV shows an excerpt of features used for classification, which includes the highlighted peaks of both x-axis and y-axis, electrical power, mechanical power and time. These features are obtained from ANSYS simulation of the motor. The highlighted peaks in Fig. 3.7(a) can serve as part of the features because the standard yardstick for differentiating healthy motor from BRB faulted motor and the severity of BRB faults usually increases in sideband amplitudes, which correspond to x- and y-axis peaks. Thomson Multitaper estimator does not offer these features, so it is not considered.

The linear support vector machine (SVM) classifier is used for training and classification in this paper. The linear SVM model is designed to find the most optimal hyperplane within the feature space with a high accuracy. It is a supervised SVM training model, in that each row has a label, an element and a class that allows classes to be identified after training [11]. The linear SVM model is trained using features in Table 3.4 (IV). The output results are shown in Fig. 3.7. Fig. 3.7 indicates that a 3BRB motor attains the highest peak quicker than a 2BRB motor, a 2BRB motor attains the highest peak quicker than a 1BRB motor, and a 1BRB motor attains the highest peak quicker than a healthy motor.



(a)



(b)

Figure 0.7: Welch PSD estimation for power spectrum of x and y peaks; (b) SVM classification model for BRB faults for the induction motor.

Table 0.4: Feature Selected Using Welch PSD Estimation Technique for SVM Classification

Labels	Electrical Power	Mechanical Power	Time	x-axis Peak	y-axis Peak
Healthy motor	4376.42	3914	0.999	-499.75	-77
1BRB	4805	3459	1.031	-465.9	-63.9
2BRB	5246	3883	1.032	-474.25	-.51
3BRB	5528	1967	1.119	-433	-48

IV. CONCLUSION

In this paper, two current spectral analysis techniques for broken rotor bar faults of induction motors based on Finite Element analysis, Thompson Multitaper estimator and Welch PSD Estimate, are proposed. It is found the two methods can effectively detect one broken rotor bar fault in induction motors. The Welch PSD estimation can realize multiple BRBs fault detection through machine learning successfully.

The finite element analysis provides an accurate way for obtaining the stator current of an induction motor, which can be further used for the current spectral analysis. Through the FEM modeling, it is found that BRB faults have direct impact on the speed and torque of induction motors.

V. REFERENCES

- [1] P. Zhang, Y. Du, T. G. Habetler, and B. Lu, "A survey of condition monitoring and protection methods for medium-voltage induction motors", *IEEE Trans. Ind. Appl.*, vol. 47, no. 1, pp. 34-46, 2011.
- [2] Naha, A., Samanta, A.K., Routray, A. and Deb, A. K. "A Method for Detecting Half-Broken Rotor Bar in Lightly Loaded Induction Motors Using Current", *IEEE Trans. Instrumentation and Measurement*, Vol.65 (7), pp.1614-1625, July 2016.
- [3] S. Nandi, H. A. Toliyat, and X. Li, "Condition monitoring and fault diagnosis of electrical motors-A review", *IEEE Trans. Energy Conversion*, Dec. 2005, Vol.20 (4), pp.719-729.
- [4] Arabaci, Hayri and Bilgin, Osman "The Detection of Rotor Faults By Using Short Time Fourier Transform", 2007 *IEEE 15th Signal Processing and Communications Applications*, pp.1-4, 2007.
- [5] Mohammed, O.A., Abed, N.Y. and Ganu, S. "Modeling and Characterization of Induction Motor Internal Faults Using Finite-Element and Discrete Wavelet Transforms", *IEEE Trans. Magnetics*, Vol.42 (10), pp.3434-3436, Oct. 2006.
- [6] M. Hansson-Sandsten, "A Welch method approximation of the Thomson multitaper spectrum estimator", *Proceedings of the 20th European Signal Processing Conference (EUSIPCO)*, pp. 440 – 444, 2012.
- [7] M. K. v. Vugt, P. B. Sederberg, and M. J. Kahanac, "Comparison of spectral analysis methods for characterizing brain oscillations", *National Center for Biotechnology*

Information, U.S. National Library of Medicine, <https://www.ncbi.nlm.nih.gov/pmc/articles/PMC2839452/>

[8] J. Cusidó, L. Romeral, J. A. Ortega, J. A. Rosero, and A. G. Espinosa, "Fault detection in induction machines using power spectral density in wavelet decomposition", IEEE Trans. Ind. Electron., vol. 55, no. 2, pp. 633-643, Feb. 2008

[9] Parhi, Keshab K and Ayinala, Manohar. "Low-Complexity Welch Power Spectral Density Computation", IEEE Trans. Circuits and Systems I: Regular Papers, Jan. 2014, Vol.61 (1), pp.172-182

[10] Percival, D. B., and A. T. Walden, Spectral Analysis for Physical Applications: Multitaper and Conventional Univariate Techniques. Cambridge, UK: Cambridge University Press, 1993

[11] Ferreira, L.V., Kaszkurewicz, E. and Bhaya, A. "Solving systems of linear equations via gradient systems with discontinuous right-hand sides: application to LS-SVM", IEEE Trans. Neural Networks, Vol.16 (2), pp.501-505 Mar. 2005

Chapter 4: Advanced Feature Selection for Broken Rotor Bar Faults in Induction Motors

A version of this manuscript has been published in the Proceeding of IEEE 54th Industrial and Commercial Power Systems (I&CPS) Conference, Niagara Falls, ON, Canada, May 7 - 10, 2018. This paper has been presented in the conference by Dr. Xiaodong Liang. The research is done under the supervision of Dr. Liang. Kenneth Edomwandekhoe conducted research, created models, and wrote the paper. Dr. Liang revised the manuscript, and ensured principles were observed and followed strictly, and that results agreed with stipulated theories.

Figure and table numbers were modified in accordance with master's manuscript prescription by faculty of electrical engineering and computer science of Memorial University of Newfoundland.

Advanced Feature Selection for Broken Rotor Bar Faults in Induction Motors

Kenneth Edomwandekhoe, *Student Member, IEEE*, Xiaodong Liang, *Senior Member,*

IEEE

Faculty of Engineering and Applied Science, Memorial University of Newfoundland,

St. John's, Newfoundland, Canada.

Abstract—This paper presents an effective fault detection approach for broken rotor bar (BRB) faults in induction motors using machine learning. Three methods, Fast Fourier Transform (FFT), Yule Walker Estimate by Auto Regression (YUL-AR), and Matching Pursuit (MP), are considered for feature selection purpose. These methods are implemented on stator current signals of an induction motor under healthy and different number of broken rotor bars (BRBs) conditions simulated by the finite element analysis software ANSYS. It is found that the proposed MP method offers the most effective feature selection among the three methods and is able to classify BRB faults accurately through support vector machine (SVM) and artificial neural network (ANN).

Index Terms— Broken rotor bar, Fast Fourier Transform, feature selection, induction motor, Matching Pursuit.

I. INTRODUCTION

Online real-time monitoring can identify faults at early stage and mitigate the likelihood of machine unprecedented failure. Accurate detection of incipient faults can improve workflow, reduce maintenance costs and process downtime, and prevent disruptive failures and machine damage [1]. It is reported by IEEE and Electric Power Research Institute (EPRI) that the broken rotor bar (BRB) fault of induction motors results in 8-9% machine failures in industry [2]. A BRB fault is an electrical fault, which can be the result of high temperature, vibration, uneven magnetic pull caused by non-linearity or transient condition during motor start-up [2]. If left unchecked, the incipient stage of one BRB fault can deteriorate to several BRBs and can hinder the machine's start-up performance. A BRB fault leads to asymmetry condition inside the motor. The asymmetry is induced by back electromotive force (EMF) of lower sideband harmonics, which can be observed in frequency spectrum of the motor stator current through a spectral analysis. Therefore, online monitoring and spectral analysis of the motor stator current have proved effective for a BRB fault detection.

The most successfully deployed method for the BRB fault detection is Motor Current Signature Analysis (MSCA) [3]-[11] because of its non-invasive, easy to implement, lower cost, reliable and effective nature [9]-[11]. Although different signal processing techniques using vibration signal [11], supply voltage [12], magnetic flux [13], active and reactive power [14][15] have been deployed for BRB fault diagnosis, some of these techniques require sensors and probes, so they can be expensive and not as easy to implement as MSCA. However, MSCA has its own limitations and is only suitable to: 1) motor operating under

steady-state condition (stationary signal); and 2) motor with symmetric sinusoidal voltage supply.

Traditional MSCA approach involves scrutiny of the double slip frequency amplitude of the stator current spectrum by Fast Fourier Transform (FFT), where distinctive sidebands close to the motor current fundamental harmonic frequency appear. However, there are several issues associated with the BRB fault detection using FFT technique: 1) FFT becomes ineffective under no load or light load conditions, usually sideband frequency associated with a BRB fault becomes more distinct under a heavy load condition [12]; 2) Similar sideband frequency components for healthy motors do appear due to the motor's asymmetry condition and uneven resistance associated with rotor bars [3]-[5],[16], although asymmetry induced by voltage supply has amplitude lower than that associated with a BRB fault [16];

3) The severity of the fault has a relation with amplitude of sidebands (a higher amplitude is observed with increased numbers of BRBs), but sideband amplitudes are also related to motor loading (a higher loading factor leads to an increased sideband amplitude) [16]; 4) For variable frequency drive (VFD) fed induction motors, FFT is ineffective because it cannot filter lower band harmonics from the VFD; 5) FFT cannot provide accurate and reliable diagnosis of BRB fault for motor transient condition (nonstationary signal) [5]. For transient states, other spectral analysis techniques, such as discrete wavelet transform (DWT), Wavelet Packet analysis (WPA) and Hilbert transform (HT), are being deployed [6]-[8].

To overcome issues of existing methods, fault diagnosis using machine learning attracts more research interests lately. Feature selection is an important part of online fault

diagnosis using machine learning [17]-[20]. In this paper, the BRB fault detection for induction motors is investigated using three different techniques, FFT, Yule Walker Estimate by Auto Regression (YUL-AR), and Matching Pursuit (MP), for feature selection purpose. Through the application of MP methodology, distinct contrasting features emerge from different motor BRB fault conditions. These features are then trained and tested for fault detection. Using the proposed MP technique, the fault classification can be achieved in a unique pattern, and severity of fault can be identified from notification of the numbers of BRBs present. This Paper offers a new contribution that helps in automatic detection of a BRB fault with great accuracy.

The paper is organized as follows: In Section II, the stator current signal preparation through the finite element analysis software ANSYS is demonstrated; Feature selection for BRB fault detection using three different methods, FFT, YUL-AR, and MP, are investigated in Section III; In Section IV, the classification results using two machine learning methods, support vector machine (SVM) and artificial neural network (ANN), are presented using the features selected through the MP method; conclusions are drawn in Section V.

II. STATOR CURRENT SIGNAL FROM FINITE ELEMENT ANALYSIS

Main issues of the BRB fault detection for induction motors include: 1) how to accurately represent the motor model under fault conditions, and 2) how to derive clear-cut features that can be used to distinguish between healthy and faulted motors. Complicated asymmetry or deviation from normal settings due to an induction motor internal fault make

such fault modeling challenging and cumbersome. To minimize uncertainties, assumptions are usually made for analytical procedures of an internal fault modeling. Several reported research results have been focused on analytical methods in modeling of induction motors with impractical assumptions, such as neglecting saturation effect and assuming linearity of the core [21]-[25]. The finite-element (FE) analysis, on the other hand, can model induction motors for different types of internal faults with great accuracy [26] [27].

In this paper, the FE analysis is used to model BRB faults of an induction motor. The motor used in the model is a three phase, 60 Hz, 3 kW, 240 V, 4-pole squirrel-cage induction motor. The simulation is carried out for the motor under a healthy state, and for the same motor under one, two and three BRBs states, all with 75% loading factor.

The model is developed in 2D Maxwell RMxprt of ANSYS software. Fig. 1 (a) shows a complete model of a healthy motor developed in RMxprt. The BRB fault is implemented by deleting rotor bars from the healthy motor model in the software. Once a rotor bar is deleted, it becomes a highlighted bar in the model. Fig. 4.1 (b), (c), and (d) show a model with highlighted one, two, and three rotor bars, respectively. Since each highlighted bar represents a broken rotor bar, these models represent 1BRB, 2BRBs and 3BRBs faults of the motor.

The simulated stator current signals using the FE analysis for the healthy motor and the motor with one, two, and three BRBs are shown in Fig. 4.2. The corresponding torque characteristics are represented in Fig. 4. 3. Perturbation is observed in the torque characteristic for the motor with BRB defects. The magnitude of perturbation tends to increase with the increased number of BRBs. Fig. 4.3 reveals that the impact of BRB fault

increases as the number of BRBs increases. At incipient stage of the fault, the motor might not be affected significantly, but when the number of BRBs increases from one to three, the condition deteriorates. The smooth operation of the motor will be altered, signs of wear and tear due to vibration and overheating will appear. Although the torque signal possesses good features for the BRB fault diagnosis, it's rarely used due to inaccessibility of the parameter in real time.

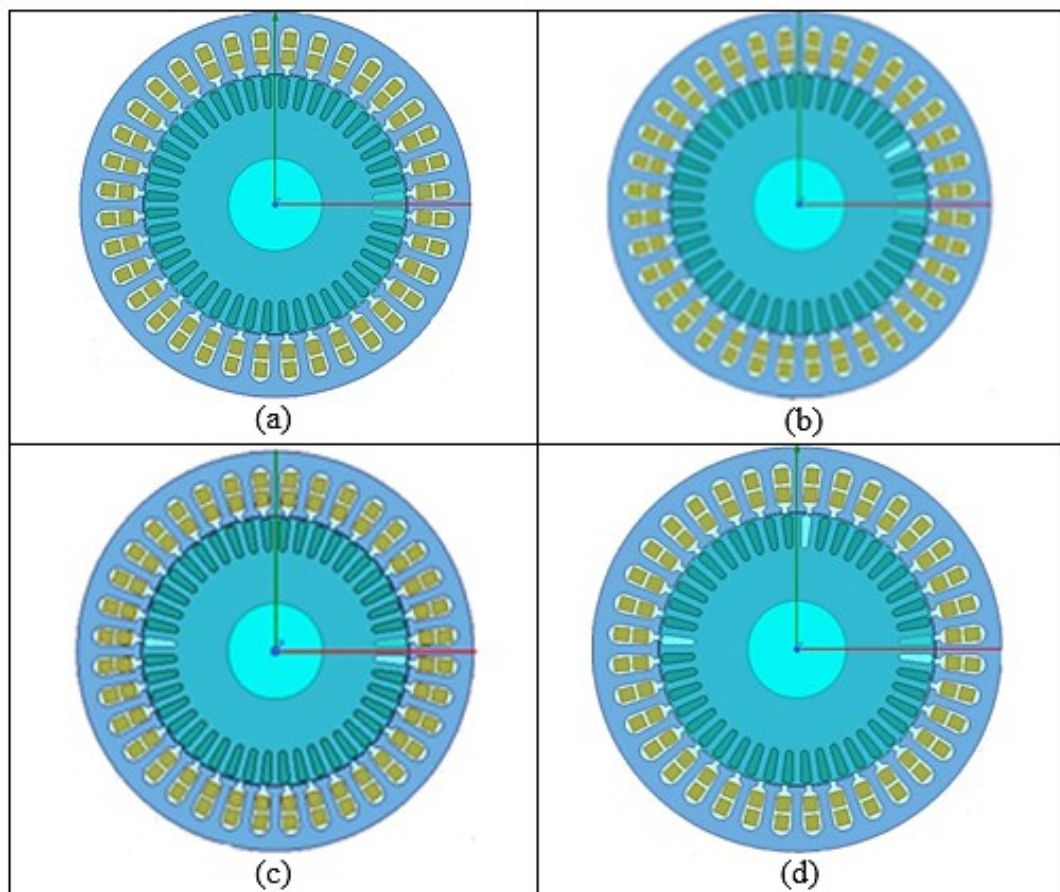


Figure 0.1: Induction motor model at 75% loading: (a) a healthy motor, (b) a motor with one BRB, (c) a motor with two BRBs, and (d) a motor with three BRBs.

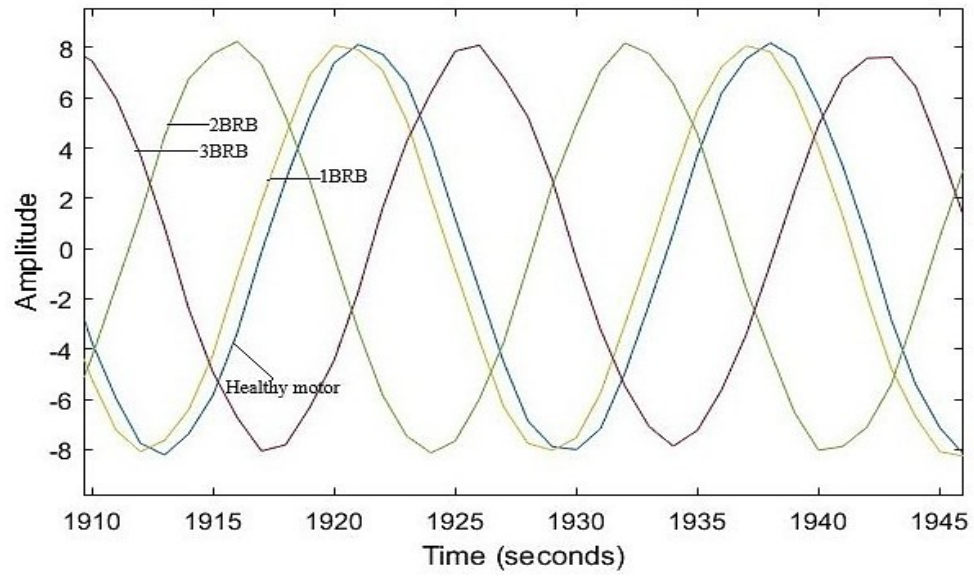


Figure 0.2: Induction motor stator current at 75% loading.

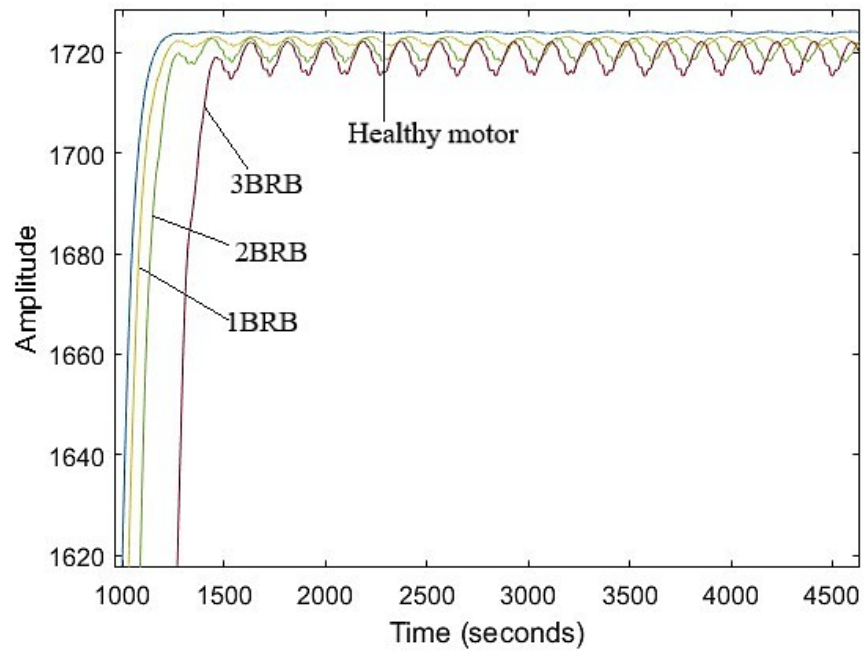


Figure 0.3: Torques calculated by ANSYS at 75% loading for a healthy motor and motor with one, two and three BRBs.

III. FEATURE SELECTION TECHNIQUES

Various signal processing techniques, such as Short Time Fourier Transform [28], Hilbert Transform [8][9], Wavelet Transform [7][18][26][29][30], and Empirical mode decom-position (EMD) [31], are being used for BRB fault diagnosis of induction motors. The wavelet transform provides a localized explicit representation of nonstationary signals by variable window feature and is suitable for a signal analysis that requires time and frequency resolution. As an adaptive multi-scale signal decomposition technique, the EMD can decompose a complex signal into bands of extracted intrinsic mode functions, which reveal physical meaning of the signal, based on local characteristic time scale of the signal [31].

Because the stator current signal of induction motors during BRB faults is non-stationary, frequency or time domain spectral analysis of stator current may not be adequate for effective derivation of necessary features for fault classification using machine learning techniques, the time-frequency domain approach appears to be more suitable.

This paper focuses on a comparative approach for best feature selection for classification. Three different spectral analysis techniques, FFT, YUL-AR, and MP, are deployed in the paper. FFT is a frequency domain technique, YUL-AR is a time domain technique, while MP is a technique effective in techniques is shown in Table 4.1 (I). Based on research results, the technique with most suitable features will be used for classification. Artificial intelligence methods have been successfully applied for classification of induction motor faults [32] [33]. In this paper, ANN and SVM will be used for BRB faults classification using the selected features.

A. Fast Fourier Transform

The FFT technique is firstly applied on the simulated stator current signals of the induction motor from FE analysis shown in Fig. 4.2 for both healthy and faulted motor cases. Fig. 4.4 shows the motor stator current spectra obtained using FFT for a healthy motor, a motor with one, two and three BRBs. It can be clearly visualized with the aid of the markers that both amplitude and frequency in the spectra change with the increased number of broken rotor bars.

Different BRBs create different sample frequency sidebands in the stator current. Points with higher amplitudes, at which faults are indicative, can be used as reference in relation to the amplitude of fundamental frequency for different BRB fault conditions. The solid horizontal line on top of Fig. 4.4 (b) (c) (d) serves as the fundamental frequency reference base line for measuring the amplitude of the signal, and the dashed horizontal line in the middle of these graphs serves as the measurement reference line representing emergence of a fault. It is observed that, for an additional BRB, additional sidebands emerge, and an additional BRB has direct impact on the amplitude of the new emerging sidebands. Fig. 4.4 (b) (c) (d) depicts a change in the amplitude between a fault characterized by a BRB frequency sideband and the fundamental frequency.

The sample frequency reference line representing a BRB fault corresponds to the nearest sideband frequency at $(1 \pm 2s)f_s$, where f_s is the supply frequency, and s is the slip of the induction motor. When the number of BRBs increases, the sample frequency reference line is reset to a new emerging sideband frequency, which can serve as a distinguishing feature between fault characteristics for different number of BRBs.

Table 0.1: Comparison of Three Spectral Analysis Techniques (FFT, YUL-AR, AND MP)

Characteristics	FFT	YUL-AR	MP
		Does not apply window to data	Applies window to data
Features	Frequency domain application, Applicable for stationary data only.	Time domain application	Frequency and time domain
Methodology	Assumes fixed rate for signal analysis.	Assumes zero mean for signals.	Uses Singular value decomposition function for signal.
Advantages	1) Can search out dominant frequency in a signal. 2) Can be used to find Power spectral density (PSD) of a signal at a given frequency.	1) Performs as well as other methods for large data records 2) Always produces a stable model.	Multiscale demodulation technique.
Disadvantages	Output phase and magnitude of the signal (complex number). Cannot give any information about time.	1) Performs relatively poorly for short data records. 2) Frequency bias for estimates of sinusoids in noise.	MP requires a large convergence time.

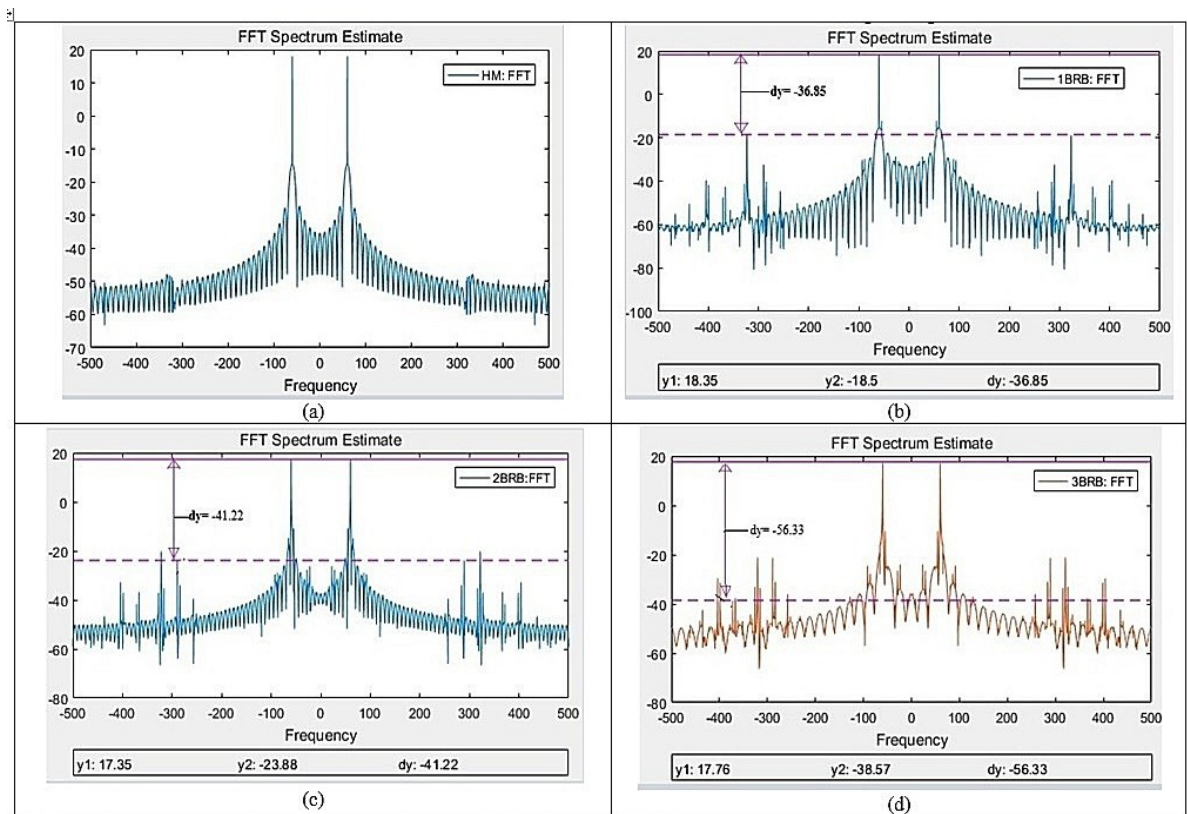


Figure 0.4: Motor stator current spectra obtained by FFT: (a) a healthy motor, (b) with one BRB, (c) with two BRBs, (d) Motor with three BRBs.

Table 0.2: Amplitudes for Different BRB Condition Using FFT

Amplitude (dy)	1BRB		2BRB		3BRB	
	Frequency (X axis)	Amplitude (Y axis)	Frequency (X axis)	Amplitude (Y axis)	Frequency (X axis)	Amplitude (Y axis)
	322.87	-36.85	289.46	-41.22	371.45	-56.33

B. Yule Walker Estimate by Auto Regression

The Yule Walker Estimate by Auto Regression is a parametric statistical approach that estimates covariance sequence for time data series. The Yule-Walker algorithm is used to estimate the spectral content by fitting an autoregressive (AR) linear prediction filter model of a given order to the signal. It is assumed that the mean of the signal is zero. The AR parameters are determined by forming a biased estimate of the signal's autocorrelation function and solving least squared minimization of the forward prediction error.

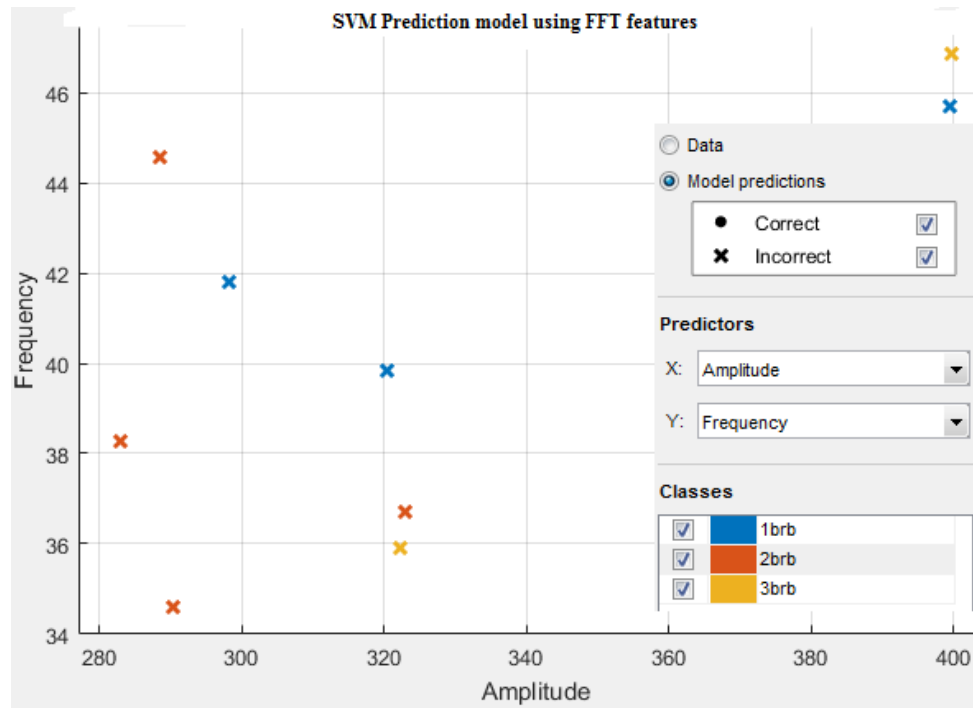


Figure 0.5: SVM 22% failed classifier using FFT features.

Before implementing the YUL-AR technique, the order of the data following AR process must be known. The order of the AR process can be determined by: 1) Akaike information criterion (AIC), 2) Bayesian information criterion (BIC), or 3) Cross-validation. For the cross-validation technique, the given time series data are divided into subsets. The model parameters are estimated using one subset of data, such parameters are then cross-validated with data from the remaining subsets [34].

Yule-Walker estimator can be used to estimate AR coefficients. For a causal AR (p) model,

$$\phi(B)X_t = W_t \quad (1)$$

$$X_t = W_t + \sum_{j=1}^{\infty} \psi_j W_{t-j} \quad (2)$$

Where, X_t is the variance of the AR process, ψ_j is the coefficient, W_t is the model parameter, W_{t-j} is the linear combination of past observations, B is the same as using shift operator, and p is AR model order.

The simulated stator current signals from the FE analysis are analyzed using the YUL-AR technique. Spectral analysis results are shown in Fig. 4.6. The way to measure amplitude and frequency variation for each case is similar to FFT method in Fig. 4.4.

Fig 4.6 shows that YUL-AR technique produces a smoother curve than FFT, and this is due to the all pole model property. YUL-AR has the features of being able to represent spectral with peak limited to a maximum of p/2, where p represents the AR model order. Therefore, choosing the order is crucial to the effectiveness of this method. In this paper, a

model order for the signal is chosen to be 23, and a sampling frequency that follows the Nyquist order is adopted.

The YUL-AR model maintains same limitation as FFT method in terms of lacking variety of features to choose from for classification. Table III shows the amplitude and frequency for the three sidebands that arose as a result of the different BRBs. Results obtained from YUL-AR technique are consistent with FFT, in that it follows same response of increased amplitude with increased number of BRBs. There is also a change in the frequency spectrum.

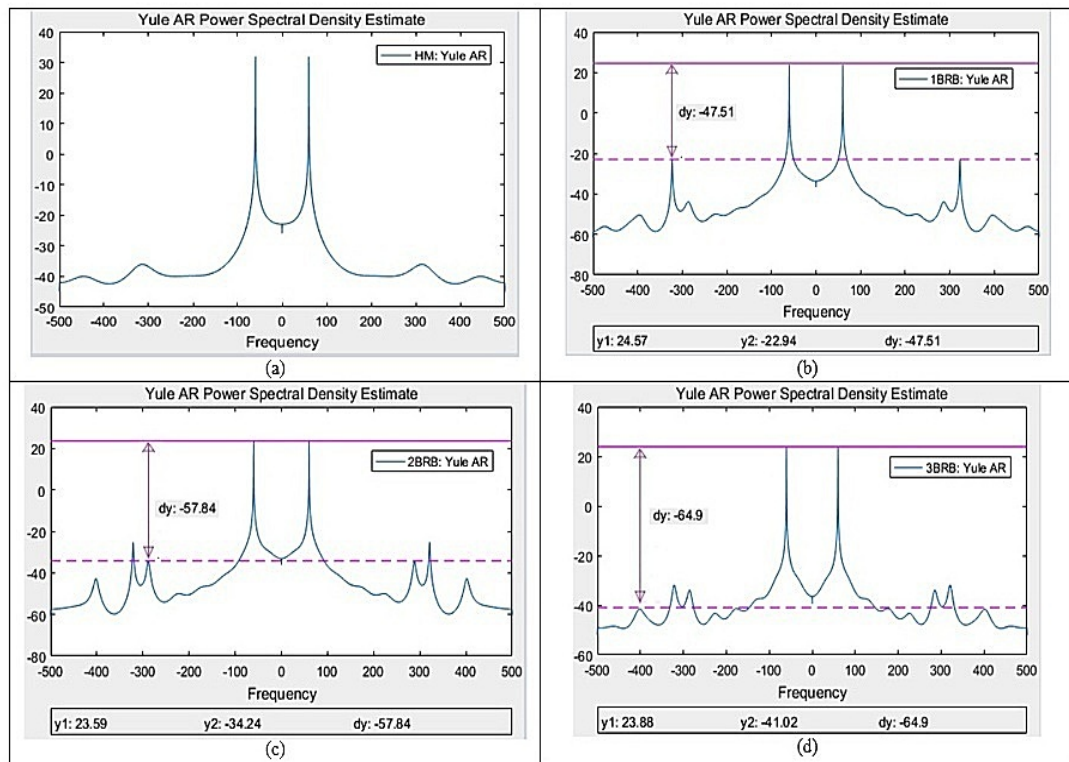


Figure 0.6: Motor stator current spectra obtained by YUL-AR: (a) healthy motor, (b) one BRB, (c) two BRBs, (d) three BRBs.

Table 0.3: Amplitudes for Different BRB Faults Using YUL-AR

		1BRB		2BRB		3BRB	
Amplitude	Frequency (X axis)	Amplitude (Y axis)	Frequency (X axis)	Amplitude (Y axis)	Frequency (X axis)	Amplitude (Y axis)	
		322.87	-47.51	289.80	-57.84	400.01	-64.9

Both FFT and YUL-AR techniques discussed thus far show indications of BRB faults on the evidence of increased amplitude and change in sample frequency spectrum. However, these techniques are ineffective to generate features for fault classification. The next proposed method, MP, is intended to address the drawback so far highlighted.

C. Matching Pursuit

Even with variable windows feature in wavelet transform, their position in the spectrum is fixed with respect to the frequency, and transient at low frequencies or noise at high frequencies are hard to capture. An adaptive spectral analysis approach is needed, which can provide a customized window scheme to represent transient current spectral signals effectively in the time-frequency plane [35].

Matching Pursuit is a greedy algorithm, it is a multiscale decomposition technique based on an over-complete dictionary. It can decompose a signal into a linear arrangement of waveforms, known as atoms, which are confined in time-frequency plane. A dictionary of time-frequency atoms is created by shifting, scaling, and modulating a single atom. This process generates three parameters: u is related to shifting, s is related to scaling, and ξ is related to modulating. A full scale or a redundant dictionary can thus be formed. The signal can be further decomposed using atoms picked iteratively from this redundant dictionary

based on certain selection criteria [36]. An index γ is introduced to represent u , s , and ξ , and the dictionary element can be defined by [36]

$$g_\gamma(t) = \frac{1}{\sqrt{s}} g\left(\frac{t-u}{s}\right) e^{j\xi t} \quad (3)$$

Where $1/\sqrt{s}$ is a normalization constant ensuring the energy of the atom to be unity. The decomposed signal is initialized to be zero. The error after the approximation is known as residue, which is initialized to be the signal itself. For example, the first residue for a signal x is equal to x . In each iteration, the criteria to select an atom from the dictionary is that the inner product of an atom with the residue is maximized. For the n iteration, the atom is chosen by [36]:

$$R^n f = \langle R^n f, g_m \rangle g_m + R^{n+1} f \quad (4)$$

$$g_m = \arg \max_{g_i \in D} |\langle R^n f, g_i \rangle| \quad (5)$$

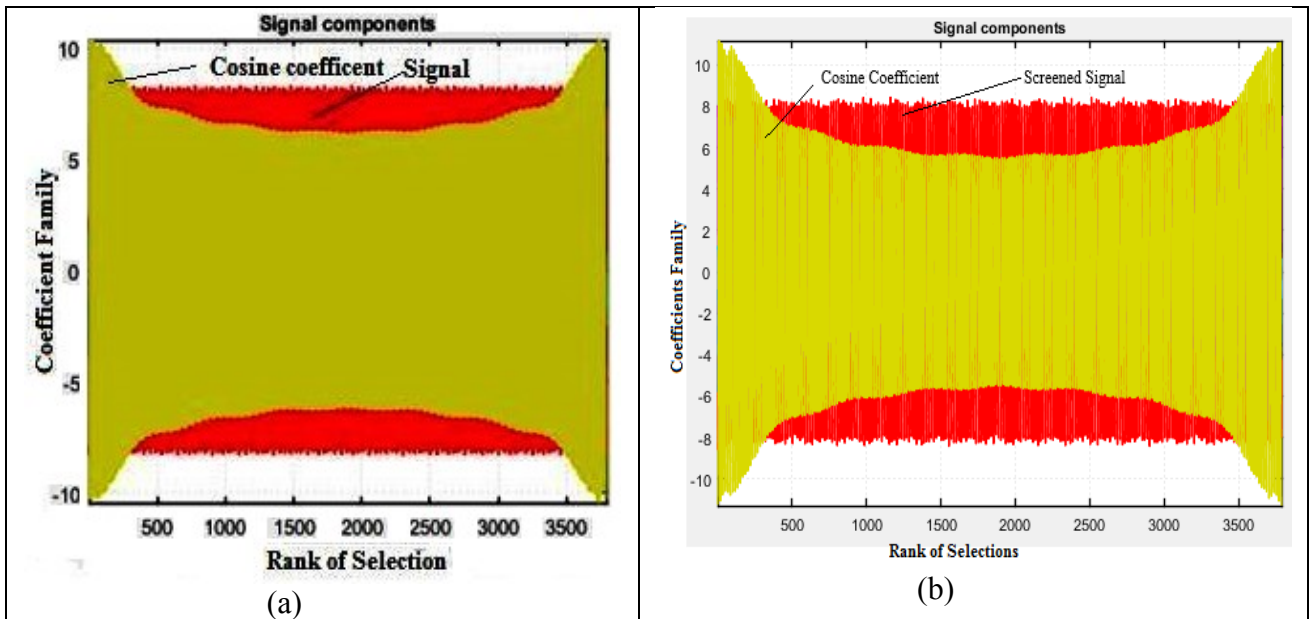
Where, D is the dictionary for MP decomposition. After m th iterations, the signal is approximated by [36]

$$f = \sum_{n=0}^{m-1} \langle R^n f, g_m \rangle g_m + R^m f \quad (6)$$

The motor stator currents obtained by the FE analysis in Fig. 4.2 are analyzed using MP. MATLAB is used to implement the orthogonal matching pursuit (OMP) technique in the wavelet tool box in this paper. The simulated stator current signals are demodulated and fit into predefined dictionary made up of atoms. The approximated signals for different machine model scenarios are represented in Fig. 4.7. Fig. 4.7 represents the most prominent

characteristics of a signal after approximation. There are other sub-dictionary features present within the signal but only the prominent ones are shown in Fig. 4.7. Other non-prominent dictionaries can be seen in residuals.

For healthy, 1BRB, and 2BRBs conditions in Fig. 7 (a), (b) and (c), besides the original signal, the approximated signal has properties corresponding to cosine dictionary from the MP model. There are observable deterioration of the signal and Cosine coefficient from healthy to two BRBs states. For three BRBs condition in Fig. 4.7(d), besides the original signal, two dictionaries (DCT and Cosine) emerge from the approximation due to the increased harmonics. The first stage of approximation is carried out by setting the Level 1 error (L1) equal to 5%.



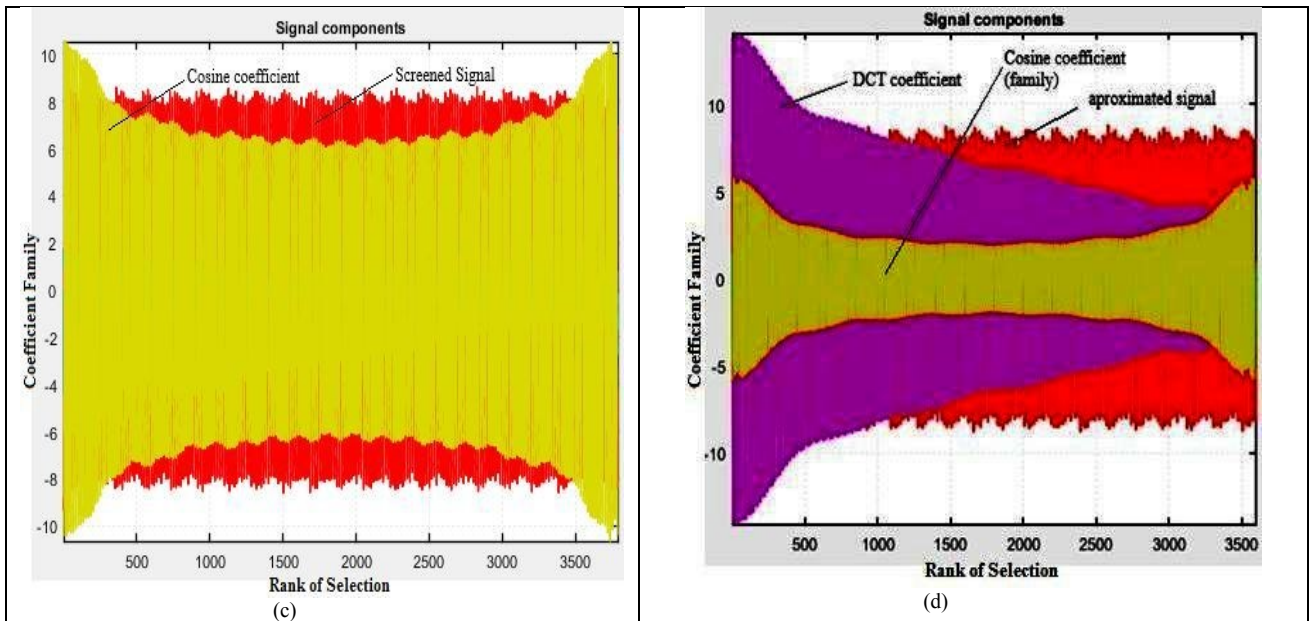


Figure 0.7: Approximated signals obtained by MP: (a) healthy motor, (b) motor with one BRB, (c) motor with two BRBs, (d) motor with three BRBs.

MP has rich resource dictionary that allows for selection of the most appropriate wavelet family, which best suits the stator current signal. This technique is able to separate significant features. The features of the dictionary are usually referred to as atoms. These features are used for training and classification for healthy and faulted motors. The OMP feature indices for the selected coefficients for different motor conditions in this paper are shown in Fig.4.8.

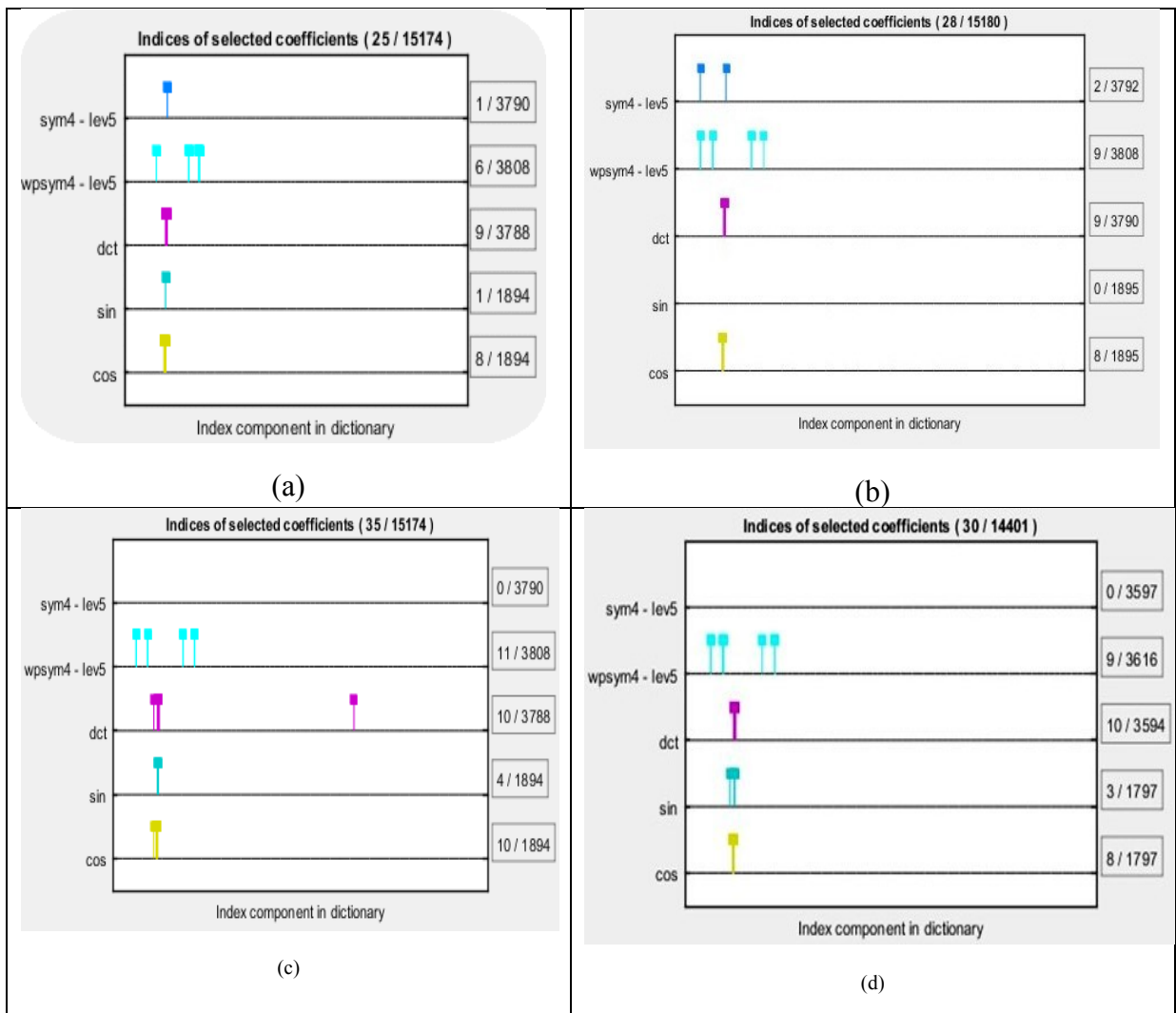


Figure 0.8: The orthogonal MP feature indices for selected coefficients: (a) healthy motor, (b) one BRB, (c) two BRBs, and (d) three BRBs.

As shown in Fig. 4.8, the MP predefined dictionaries are chosen to fit the motor stator current signal, from which features for training and classification are derived: 1) sym4-lev5, which denotes Daubechies least-asymmetric wavelet with 4 vanishing moments at level 5; 2) wpsym4-lev5, which denotes the Daubechies least-asymmetric wavelet packet with 4 vanishing moments at level 5; 3) dct, which depicts discrete cosine; 4) sin, which represents

sine in the MP dictionary; and 5) cos, which represents cosine in the MP dictionary. While performing MP decomposition, it is imperative to consider a signal that is lengthier than the duration of interest. Because no explicit window is used in MP, it is advisable to use a signal at least three times longer than the duration of interest and study only the middle section. This was the approach implemented for this analysis.

MP combines theoretical Fourier-based procedures with an adaptive technique for basic functions selection, and offers good localization capability, flexibility in resolution across the time-frequency plane, and adaptive decomposing of signal. The MP decomposition makes all features clearly definable for selection [36]. These features can then be fed into SVM or ANN for classification and fault prediction.

This study focuses on the most suitable technique for feature selection. MP has clearly shown through the approximation technique that the most contrasting features from the decomposition of the different motor signal can be used for classification.

IV. TRAINING FOR CLASSIFICATION USING MP FEATURES

A. Support Vector Machine

The sub-dictionaries from the MP algorithm have different energy level represented as coefficients. The non-stationary nature of the motor stator current signal results in varying energy. Five symbols are used in this section as defined as follows:

- “RankofSelRank” means the rank of selection rank, which connotes the order for coefficients preference.

- “Coefs” means the coefficients. The coefficients are atoms within the dictionary, and the coefficient with most prominent effect within the sub-dictionary are given the first priority.

- “Familynumber” means the family number, which explains the level in the atoms of the MP dictionary.

- “Ndxinfamily” depicts the index number in family.

- “Ndxindic” depicts the index number in dictionary.

These five elements vary with different conditions and are chosen as features for classification and fault prediction. The above five elements are constituents within the individual atoms in the family. They emerge because of the decomposition of the atoms from different family within MP dictionaries. At the first approximation, the five atoms ranked in the order shown in Fig. 4.8 is produced, and when a further demodulation is done, the outcome is constituents used as features.

The classification results using various selected features through different training are shown in Fig. 4.9. SVM trainer and classification learner from MATLAB tool box was used for training and classification of healthy motor and motor with BRB faults. The SVM quadratic was employed for training and classification. The crux of the classification is painstakingly varying the most suitable features for classification. Different combinations of features were tried before a suitable feature that best classifies different motor conditions can be found. Fig. 4.9 (a) corresponds to RankofSelRank vs. Ndxindic for training and classification. Fig. 4.9 (b) represents Coefs vs. Ndxindic training results. Fig. 4.9 (c) displays output for Ndxinfamily vs. Familynumber training result. Fig. 4.9 (d) represents

RankofSelRank vs. Familynumber training output. It can be seen that Fig 4.9 (d) promises a good classification output using SVM. In Fig. 4.9, the dots with colors depict classifiable data points training output.

The results for SVM is exported and prepared for ANN classification using Python Scripts, which is discussed in the next section of this paper.

Fig. 4.10 represents the Confusion matrix, which indicates the accuracy in percentage of correctly classifying different fault conditions. False alarm are to be avoided during fault classification. This matrix can predict percentage likelihood of false alarms. For RankofselRank vs Familynumber features shown in Fig. 4.9(d), the confusion matrix shows 100% percentage chances of correctly classifying different motor conditions.

B. Artificial Neural Network

Another technique employed for classification in this paper is the feed forward multilayer perceptron technique in artificial neural network. The coefficients used in ANN are obtained from the OMP approximation procedure. The perceptron model is represented in Fig. 4.11, which comprises of two inputs, two hidden layers, and four outputs. The two inputs are RankofselRank and Familynumber (Fig. 4.9(d)). The four outputs represent four conditions, a healthy motor, and a motor with 1BRB, 2BRBs and 3BRB faults. With the aid of a Python script implemented in MATLAB, the training and classification was executed using ANN. Classification outputs are shown in Fig. 4.12.

A 95% of accuracy was achieved using ANN, the performance and target graphical output are displayed in Figs. 4.13 and 4.14. The performance in Fig 4.13 shows similarity of the gradient and mu curves, which connotes momentum update.

The validation check reads zero, underlying the absence of generalization, a phenomenon common with training of neural network model. Fig. 4.14 also supports the accuracy as observed in similarity shapes between network response and targets. The percentage accuracy of SVM and ANN classification proves that features from MP are properly selected and can correctly classify different fault conditions reliably.

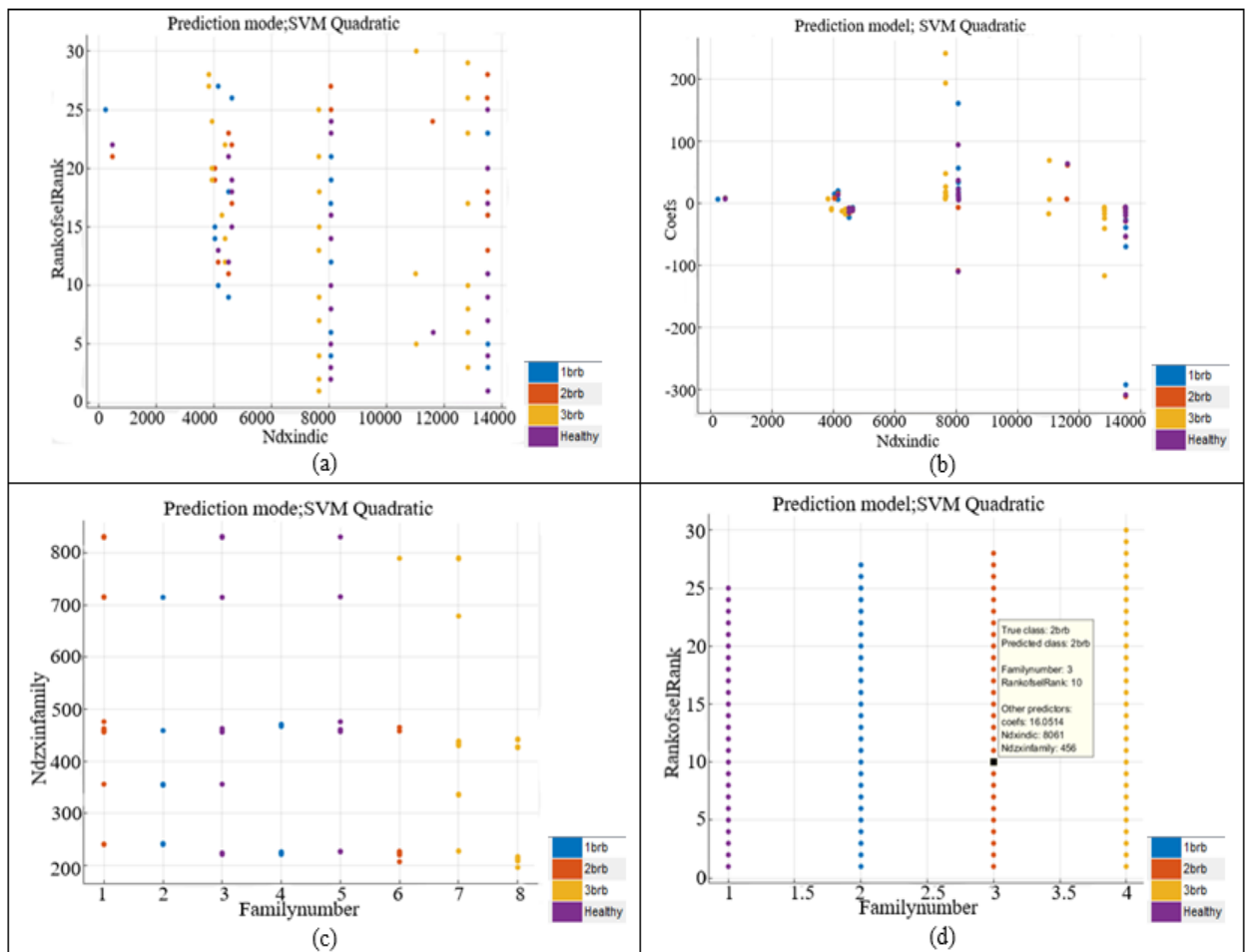


Figure 0.9: SVM quadratic classification by MP features: (a) RankofSelRank vs Ndxindic class, (b) Coefs vs Ndxindic class, (c) Ndzxinfamily vs Familynumber class, d) RankofselRank vs Familynumber.

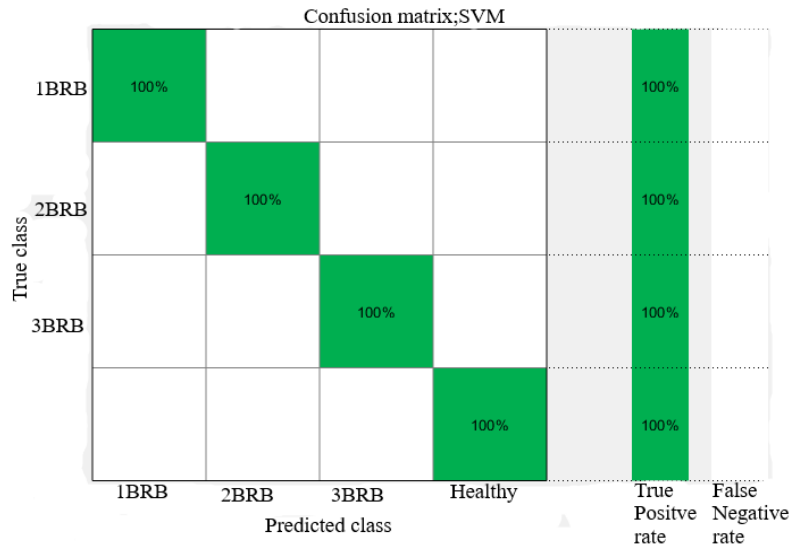


Figure 0.10: SVM quadratic confusion matrix; true positive vs false positive rate.

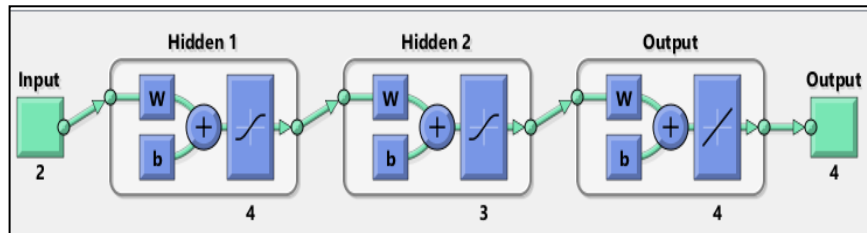


Figure 0.11: ANN model for training and classification output.

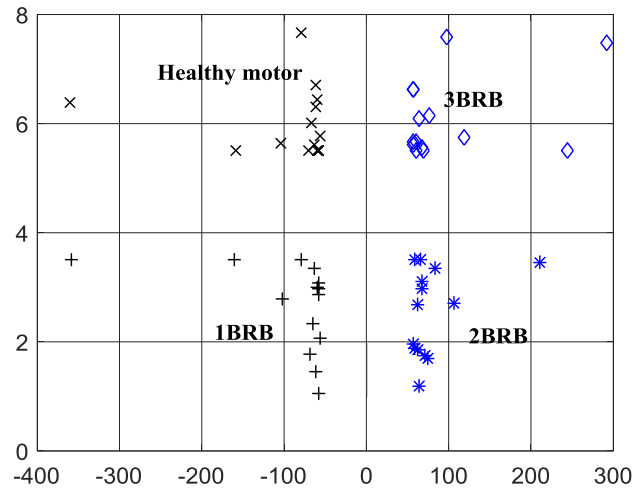


Figure 0.12: ANN training and classification output.

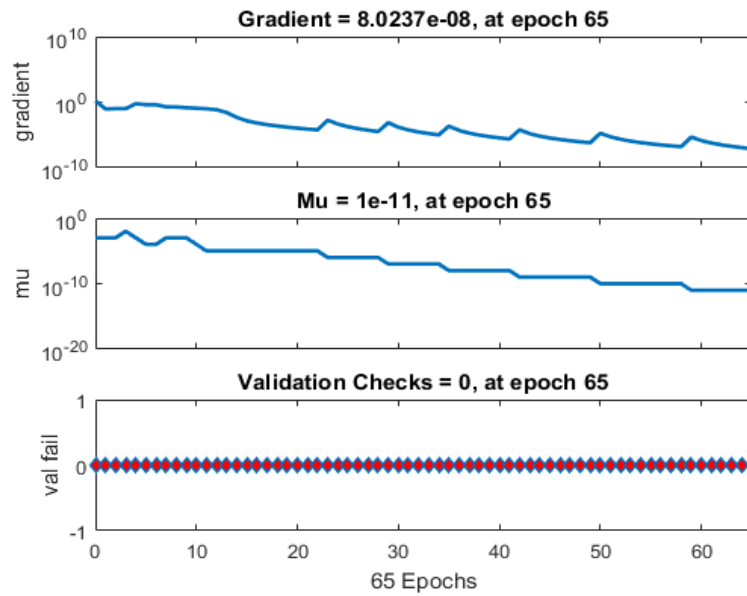


Figure 0.13: Performance for ANN Training

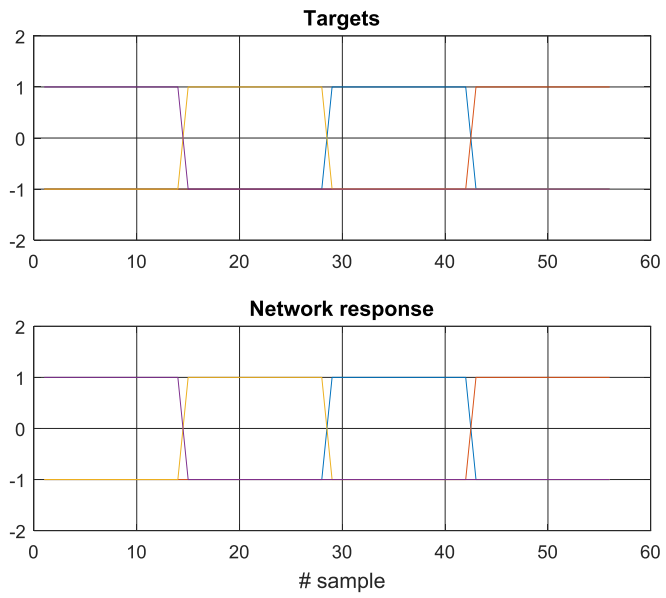


Figure 0.14: Target and response for ANN Training.

V. CONCLUSION

In this paper, three spectral analysis techniques, FFT, YUL-AR, and MP, are investigated to obtain features for classification using machine learning technique for BRB fault diagnosis in induction motors. The techniques are employed on the simulated stator current signal of an induction motor under healthy and BRB fault conditions using FE analysis software ANSYS. It is found that both FFT and YUL-AR are ineffective to generate features for classification purpose.

MP technique appears to be the most effective approach for feature selection in BRB fault diagnosis for induction motors. Features from MP approximation technique are used for training and classification through SVM and ANN. Both SVM and ANN can correctly classify faults with high accuracy.

VI. REFERENCES

- [1] M. Seera, C. P. Lim, H. Ishak, and H. Singh, "Fault Detection and Diagnosis of Induction Motors Using Motor Current Signature Analysis and a Hybrid FMM-CART Model", *IEEE Trans. Neural Networks & Learning Syst.*, Vol.23 (1), pp.97-108, Jan. 2012.
- [2] P. Zhang, Y. Du, T. G. Habetler, and B. Lu, "A survey of condition monitoring and protection methods for medium-voltage induction motors", *IEEE Trans. Ind. Appl.*, vol. 47, no. 1, pp. 34-46, 2011.
- [3] S. Nandi, H. A. Toliyat, and X. Li, "Condition monitoring and fault diagnosis of electrical motors-A review," *IEEE Trans. Energy Convers.*, vol. 20, no. 4, pp. 719-729, Dec. 2005.

- [4] A. Bellini, A. Yazidi, F. Filippetti, C. Rossi, and G.-A. Capolino, "High frequency resolution techniques for rotor fault detection of induction machines," *IEEE Trans. Energy Convers.*, vol. 55, no. 12, pp. 4200-4209, Dec. 2008.
- [5] B. Kim, K. Lee, J. Yang, S. B. Lee, E. J. Wiedenbrug, and M. R. Shah, "Automated detection of rotor faults for inverter-fed induction machines under standstill conditions," *IEEE Trans. Ind. Appl.*, vol. 47, no. 1, pp. 55-64, Jan./Feb. 2011.
- [6] J. Cusidó, L. Romeral, J. A. Ortega, J. A. Rosero, and A. G. Espinosa, "Fault detection in induction machines using power spectral density in wavelet decomposition," *IEEE Trans. Ind. Electron.*, vol. 55, no. 2, pp. 633-643, Feb. 2008.
- [7] Sadeghian, A., Zhongming Ye, A., Bin Wu, A. "Online Detection of Broken Rotor Bars in Induction Motors by Wavelet Packet Decomposition and Artificial Neural Networks," *IEEE Trans. Instru. and Measurement*, Vol.58 (7), pp.2253-2263, July 2009.
- [8] R. Puche-Panadero, M. Pineda-Sanchez, M. Riera-Guasp, J. Roger-Folch, E. Hurtado-Perez, and J. Perez-Cruz, "Improved resolution of the MCSA method via Hilbert transform, enabling the diagnosis of rotor asymmetries at very low slip," *IEEE Trans. Energy Convers.*, vol. 24, no. 1, pp. 52-59, Mar. 2009.
- [9] B. Xu, L., Sun, L. Xu, and G. Xu, "Improvement of the Hilbert method via ESPRIT for detecting rotor fault in induction motors at low slip," *IEEE Trans. Energy Convers.*, vol. 28, no. 1, pp. 225-233, Mar. 2013.
- [10] Z. Zhang, Z. Ren, and W. Huang "A novel detection method of motor broken rotor bars on wavelet ridge," *IEEE Trans. Energy Convers.*, vol. 18, no. 3, pp. 417-423, Sep. 2003.

- [11] J. de Jesus Rangel-Magdaleno, R. de Jesus Romero-Troncoso, R. A. Osornio-Rios, E. Cabal-Yepez, and L. M. Contreras-Medina, "Novel methodology for online half-broken-bar detection on induction motors," *IEEE Trans. Instrum. Meas.*, vol. 58, no. 5, pp. 1690-1698, May 2009.
- [12] M. Nemeč, K. Drobnič, D. Nedeljkovič, R. Fišer, and V. Ambrožič, "Detection of broken bars in induction motor through the analysis of supply voltage modulation," *IEEE Trans. Ind. Electron.*, vol. 57, no. 8, pp. 2879-2888, Aug. 2010.
- [13] M. F. Cabanas et al., "Unambiguous detection of broken bars in asynchronous motors by means of a flux measurement-based procedure," *IEEE Trans. Instrum. Meas.*, vol. 60, no. 3, pp. 891-899, Mar. 2011.
- [14] A. M. Trzynadlowski, E. Ritchie, "Comparative investigation of diagnostic media for induction machine: A case of rotor cage faults", *IEEE Trans. Ind. Electron.*, vol. 47, no. 5, pp. 1092-1099, Oct. 2000.
- [15] M. Drif and A. J. M. Cardoso, "Discriminating the simultaneous occurrence of three-phase induction motor rotor faults and mechanical load oscillations by the instantaneous active and reactive power media signature analyses," *IEEE Trans. Ind. Electron.*, vol. 59, no. 3, pp. 1630-1639, Mar. 2012.
- [16] A. Bellini, F. Filippetti, G. Franceschini, C. Tassoni, and G. B. Kliman, "Quantitative evaluation of induction motor broken bars by means of electrical signature analysis," *IEEE Trans. Ind. Appl.*, vol. 37, no. 5, pp. 1248-1255, Sep./Oct. 2001.

- [17] Dasarathy, B.V. "Feature selection and the concept of immediate neighborhood in the context of clustering techniques," Proceedings of IEEE, Vol.62 (4), pp.529-530, April 1974.
- [18] Ghunem, Refat A., El-Shatshat, R. and Ozgonenel, O. "A Novel Selection Algorithm of a Wavelet-Based Transformer Differential Current Features," IEEE Trans. Power Delivery, Vol.29 (3), pp.1120-1126, June 2014.
- [19] Shivaji, S., Whitehead, E. J., Akella, R. and Sunghun K. "Reducing Features to Improve Code Change-Based Bug Prediction," IEEE Trans. Software Engineering, Vol.39 (4), pp.552-569, April 2013.
- [20] Xiaofei He., Ming Ji., Chiyuan Zhang and Hujun Bao. "A Variance Minimization Criterion to Feature Selection Using Laplacian Regularization" IEEE Trans. Pattern Analysis and Machine Intelligence, Vol.33 (10), pp.2013-2025, Oct. 2011.
- [21] Yuxing Zhang, Mingyuan Zhang, Weiming Ma, Jin Xu, Junyong Lu and Zhaolong Sun. "Modeling of a Double-stator Linear Induction Motor," IEEE Trans. Energy Conversion, Vol.27(3), pp.572-579, Sept. 2012.
- [22] H.A. Toliyat, T.A. Lipo "Transient analysis of cage induction machines under stator, rotor bar and end-ring faults" IEEE Transactions on Energy Conversion, 10 (2) (1995), pp. 241-247
- [23] Degano, M., Zanchetta, P., Empringham, L., Lavopa, E. and Clare, J. "HF induction motor modeling using automated experimental impedance measurement matching," IEEE Trans. Industrial Electronics, Vol.59 (10), pp.3789-3796, Oct. 2012.

- [24] Ayasun, S. and Nwankpa, C.O. "Induction motor tests using MATLAB/Simulink and their integration into undergraduate electric machinery courses," *IEEE Trans. Education*, Vol.48 (1), pp.37-46, Feb. 2005.
- [25] Uddin, M N., Wang, W and Zhi Rui Huang, W. "Modeling and Minimization of Speed Ripple of a Faulty Induction Motor with Broken Rotor Bars," *IEEE Trans. Industry Applications*, Vol.46 (6), pp.2243-2250, Nov.-Dec. 2010.
- [26] Mohammed, O.A., Abed, N.Y. and Ganu, S. "Modeling and Characterization of Induction Motor Internal Faults Using Finite-Element and Discrete Wavelet Transforms," *IEEE Trans. Magnetics*, Vol.42 (10), pp.3434-3436, Oct. 2006.
- [27] J. Faiz, B. M. Ebrahimi, M. B. B. Sharifian, "Finite element transient analysis of an on-load three phase squirrel cage induction motor with static eccentricity", *J. Electromagn.*, vol. 27, pp. 220-227, Oct. 2007.
- [28] Treetrong, Juggrapong "Fault Prediction of Induction Motor Based on Time-Frequency Analysis," *Applied Mechanics and Materials*, Mar 2011, Vol.52-54, p.115.
- [29] M. Riera-Guasp, J. A. Antonino-Daviu, M. Pineda-Sanchez, R. PuchePanadero, and J. Perez-Cruz, "A general approach for the transient detection of slip-dependent fault components based on the discrete wavelet transform," *IEEE Trans. Ind. Electron.*, vol. 55, no. 12, pp. 4167-4180, Dec. 2008.
- [30] M. Riera-Guasp, J. A. Antonino-Daviu, J. Roger-Folch, and M. P. Molina Palomares, "The use of the wavelet approximation signal as a tool for the diagnosis of rotor bar failures," *IEEE Trans. Ind. Appl.*, vol. 44, no. 3, pp. 716-726, May/Jun. 2008.

- [31] R. Valles-Novio, J. J. Rangel-Magdaleno, J. M. Ramirez-Cortes, H. Peregrina-Barreto, R. Morales-Caporal, "Empirical mode decomposition analysis for broken-bar detection on squirrel cage induction motors", *IEEE Trans. Instrum. Meas.*, vol. 64, no. 5, pp. 1118-1128, May 2015.
- [32] Ayhan, B., Mo-Yuen Chow, B. and Myung-Hyun Song, B. "Multiple Discriminant Analysis and Neural-Network-Based Monolith and Partition Fault-Detection Schemes for Broken Rotor Bar in Induction Motors," *IEEE Trans. Industrial Electronics*, Vol.53 (4), pp.1298-1308, June 2006.
- [33] M. Hernandez-Vargas, E. Cabal-Yepez, A. Garcia-Perez, "Real-time SVD-based detection of multiple combined faults in induction motors", *Comput. Elect. Eng.*, vol. 40, no. 7, pp. 2193-2203, Oct. 2014.
- [34] Arlot, Sylvain, and Alain Celisse. "A survey of cross-validation procedures for model selection," *Statistics surveys*, vol. 4, pp. 40-79, 2010.
- [35] Mallat S. *A wavelet tour of signal processing: the sparse way*. 3rd ed. New York: Academic; 2008.
- [36] Chandran K S, Subhash, Mishra, Ashutosh, Shirhatti, Vinay and Ray, Supratim. "Comparison of Matching Pursuit Algorithm with Other Signal Processing Techniques for Computation of the Time-Frequency Power Spectrum of Brain Signals," *The Journal of neuroscience: the official journal of the Society for Neuroscience*, 23, Vol.36 (12), pp.3399-408, March 2016.

Chapter 5: Burg and Welch PSD analysis of Neighbouring and Spaced Broken Rotor Bar Faults for Induction Motors

The following manuscript is ready for submission to a conference. The research work is done under the supervision of Dr. Xiaodong Liang. Kenneth Edomwandekhoe conducted research, created models, and wrote the paper. Dr. Liang reviewed and modified the whole paper.

Figures and table numbers were revised in accordance with master's manuscript instruction by faculty of electrical engineering and computer science of Memorial University of Newfoundland.

**Burg and Welch PSD analysis of Neighbouring and Spaced Broken Rotor Bar
Faults for Induction Motors**

Kenneth Edomwandekhoe, *Student Member IEEE*, Xiaodong Liang, *Senior Member
IEEE*,

Faculty of Engineering and Applied Science, Memorial University of Newfoundland,
St. John's, Newfoundland, Canada.

***Abstract-* Broken rotor bar (BRB) faults of Squirrel cage induction motors, if unchecked, can interfere with motor operation. Improperly diagnosed fault can be a source of interruption to work flow and ultimately can have the same effect as unscheduled breakdown. The finite element software ANSYS is employed for the modeling and simulation of an induction motor at full load. In this paper, a new method is proposed to detect BRB faults. By finding the slope of two reference side lobes, the severity of fault can be easily determined. From the measurement of reference side lobes slope, it is proven that two BRB neighboring defect is more severe than spaced bar fault. If this is true, motor with neighboring BRB fault should be closely monitored for maintenance and repair so as to ensure unopposed work flow and more productivity in industrial settings.**

Index terms- Induction motor, ANSYS software, Finite element method, Signal analysis, FFT, PSD.

I.Introduction

Squirrel cage induction motors consume about 60% of electrical power used in industry today due to compactness, durability and simple design, and the minimal maintenance requirement. However, as an electromechanical device, a squirrel cage induction motor does experience various mechanical and electrical faults including broken rotor bar faults [1]-[3]. It is statistically found that BRB faults account for approximately 10% of induction motor failure. The traditional motor current signals analysis (MCSA) uses FFT to process motor current signal and can detect BRB faults by monitoring the amplitude of harmonics sidebands near the stator current fundamental frequency [3]. Nevertheless, it has been suggested in [4] that false alarms are most likely when traditional MCSA are employed because the unbalanced voltage can distort magnetic field uniformity, which then initiates asymmetrical condition in the motor. This could be mistakenly identified as BRB faults, leading to a false diagnosis of BRB faults.

Various signal processing methods have been reported in the literature for BRB fault detection [5] – [17]. In [5], the speed and current signal estimation approach is deployed on induction motors. The method uses a model reference adaptive system (MRAS) to estimate speed, and uses a logic-based technique in a β reference frame to improve a drive fault tolerant to current sensor failures. Since lower side bands harmonics are typical for BRB faults, Reference [6] establishes features to detect rotor asymmetries based on the presence of a qualitative Λ -shaped pattern observed in DWT low frequency signals. In [7], through a wavelet application it was asserted that the fault severity is reflected in an increased amplitude of the signal; however, no benchmark is defined for various degrees of fault

severity. Power spectral density (PSD) and a wavelet application capable of addressing speed and time varying conditions has been proposed in [9]. A higher mother wavelet is employed to reduce the effect of overlapping between neighboring frequency bands. The fault severity issue remains a contentious subject as various technique proposed by researchers are tentative and subjective. In [10] and [11], the signal decomposition wavelet energy is used as a yardstick for determining fault severity. Again, this method isolates other properties of the signal, leaving room for unreliability. Reference [12]-[14] present a method of isolating harmonics from the fundamental frequency for fault detection purpose. It uses a non-linear filter by the name Teager–Kaiser Energy Operator (TKEO). The TKEO technique transforms harmonics in the main signal to constant constituents, allowing for easy separation from fundamental constituents. Another method of separating the main supply harmonic from harmonic components for easy analysis is presented in [15]-[16]. The extended Park’s Vector approach requires that the supply harmonics are first transformed to a dc component and then separated before analysis for fault detection and diagnosis. Hilbert’s transform signal analysis technique has been proposed in [17]. This method provides good resolution and substantial information for the current signal envelop. It requires computation of direct and inverse FFT. Although this method promises better results than a classical FFT, the computation time and complexity remain a concern.

In this paper, a new method of discovering the onset of trouble from diagnosis of fault severity through motor current signal analysis. Although a single BRB fault could not immediately interrupt the motor operation, the following question is raised: when should the motor be stopped, and a maintenance is performed? (by monitoring the current or torque

signal, when the signal variation is becoming more apparent, then machine can be stopped for maintenance. A further deterioration to neighbouring BRB could be the onset of problem capable of raising worrying concern about the machine status. Therefore, this paper analyzes neighbouring broken bar fault and spaced bar fault, using Burg PSD and Welch PSD analysis techniques, for the purpose of differentiating neighbouring bar fault having more severe negative impacts in the machine than their counterpart spaced bar fault. By computation of the slope, motor conditions are easily identified.

This paper is organized as follows: Section II discusses the modeling of induction motor and fault formation; Section III presents the proposed method and parameter analysis; Section IV discusses results; and the conclusion and future work are provided in Section V.

II. ANSYS Models

The finite element analysis promises a better model representation by taking into consideration the full geometry of a motor. It can compute motor transient conditions and field distribution, which are quite elusive and not easily attained using other models [18]. In this paper, stator current signals of the induction motor under healthy and BRB fault conditions are obtained through the two-dimensional finite element analysis. The software ANSYS is used to build various simulation models for the motor under full load condition.

Neighbouring bar presents more threats to machine operation than spaced bar, as will be further substantiated from the analysis of result in a further section of this paper. In the event of neighbouring BRB fault, it is mandatory to correctly diagnose the fault, because failure to do so might lead to the faults spreading into neighbouring bar and further

degenerating motor condition and eventually leading to failure and irreparable machine damage. This is why it is crucial to accurately detect motor BRB conditions.

Fig. 5.1 shows the models for 2 and 3 neighbouring and spaced BRB faults. A BRB fault is implemented by deleting rotor bars in the ANSYS model. The simulated stator current signals for the four different BRB fault conditions are shown in Fig 5.2. The basic motor information used in the simulation is shown in Table 5.1.

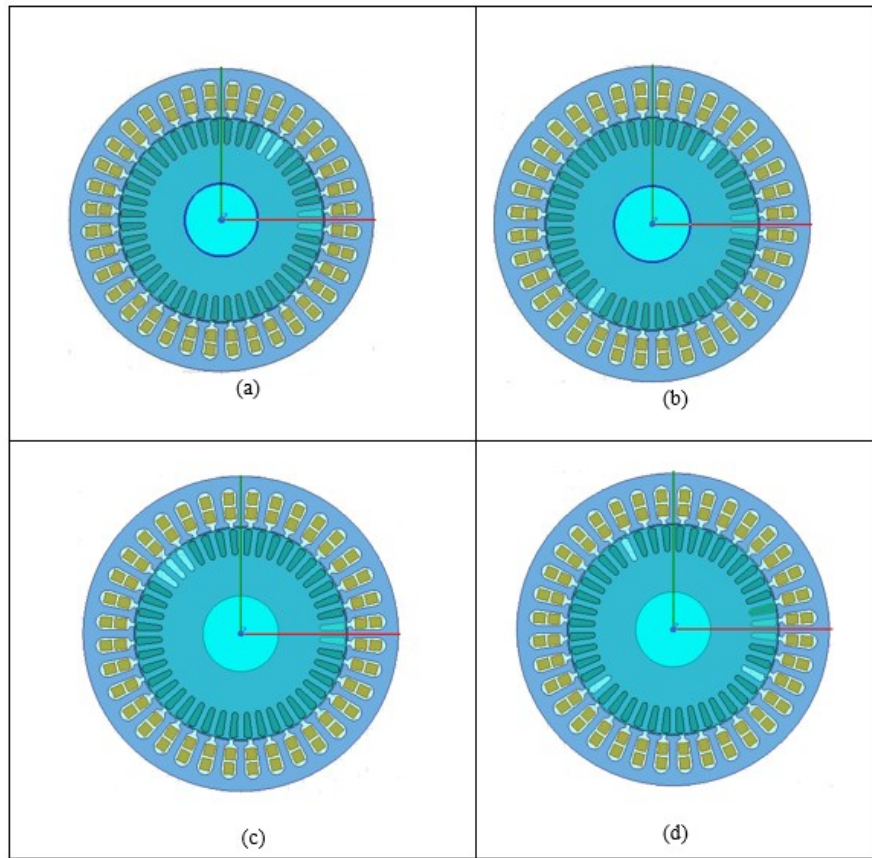


Figure 0.1. IM ANSYS Model under 100% loading; (a) 2-Neighbor BRB, (b) 2-Spaced BRBs, (c) 3-Neighbor BRB, and (d) 3-Spaced BRBs

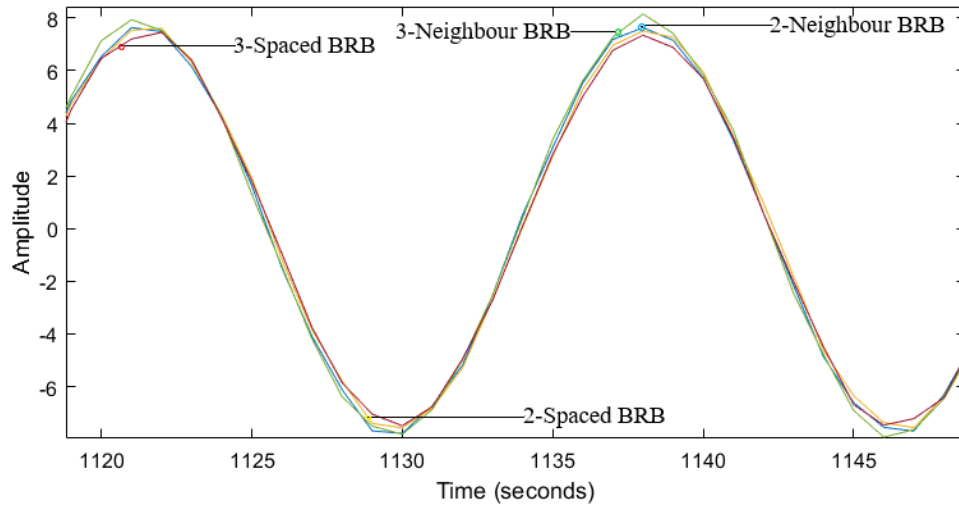


Figure 0.2. The stator current signal: Blue is 2-Neighboring BRB, Yellow is 2-Spaced BRB, Green is 3-Neighboring BRB, and Red is 3-Spaced BRB.

Table 0.1: The basic motor information used in the simulation

Rated voltage	230V
Rated power	3kW
Frequency	60Hz
Speed	1740
Number of stator slot	44
Number of rotor slot	36

III. PSD Analysis

5.1 Burg PSD Signal Analysis

The Burg PSD signal analysis is a parametric approach that involves the minimization of forward and backward prediction in accordance with the Levinson-Durbin recursion [19]. This approach slightly differs from the Auto Regressive (AR) estimation procedure because it sidesteps computation of the auto correlation function and directly estimates the reflection

coefficients and PSD of the signal. This technique offers the advantage of better resolution of closely spaced sinusoids of the signal with the minimal noise level, correct estimate and a stable AR model. The mathematical algorithm for Burg PSD signal analysis is represented in Equations (1) – (4) [20]-[21]. In this paper, the model order was chosen to be 10 in accordance to the Akaike information criterion (AIC) grade [22].

The forward minimization error can be determined by

$$e_f^p(n) = x(n) + \sum_{k=1}^p a_{pk} x(n - k) \quad (1)$$

The backward minimization error can be determined by

$$e_b^p(n) = x(n) + \sum_{k=1}^p a_{pk}^* x(n - p + k) \quad (2)$$

Where, $e[n]$ is the unobserved input data, $x[n]$ is the observed output of the system. p represents model order.

The reflection coefficient estimation can be calculated as follows:

$$k_p = \frac{-2 \sum_{n=p}^{N-1} e_{p-1}^f(n) e_{p-1}^{b*}(n-1)}{\sum_{n=p}^{N-1} |e_{p-1}^f(n)|^2 + |e_{p-1}^{b*}(n-1)|^2} \quad (3)$$

The Burg PSD is computed as follows:

$$P_{Burg}(f) = \frac{e_p}{|1 + \sum_{k=1}^p a_p(k) e^{-j2\pi f k}|^2} \quad (4)$$

Where, E_p is the total least-square error of the order p , $\hat{a}_p(k)$, are estimates of AR parameters obtained from the Levinson-Durbin recursions.

In this paper, Burg PSD is employed for the comparative analysis of 2 and 3 neighbouring and spaced BRB faults in induction motors. The PSD of the stator current signals from the simulation models is computed using the Matlab tool box. Using the slope of side-lobe peaks numbered 1 and 2 in the stator current signal, it is found that spaced BRB faults can be distinguished from the neighbouring BRB faults. The neighbouring BRB faults present more threats to the working conditions of induction motors. The simulation results are displayed in Fig. 5.3 (a)-(d) below.

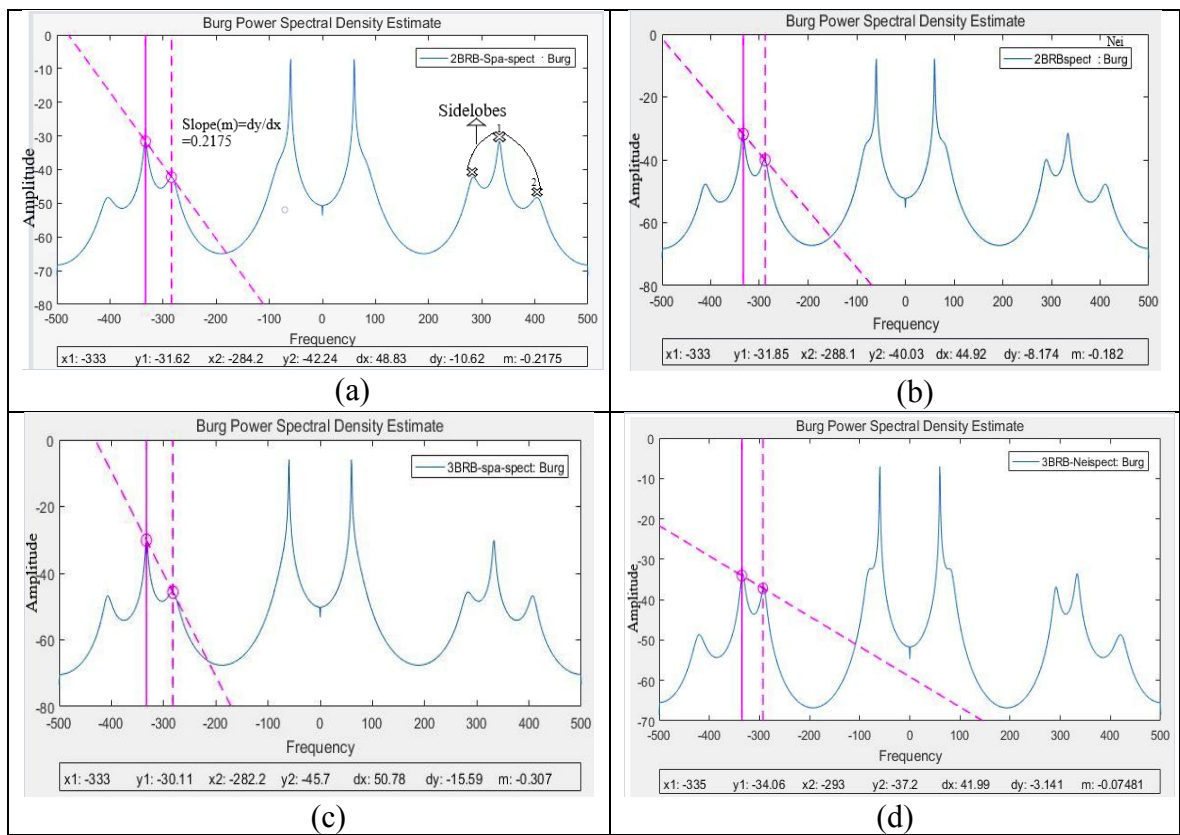


Figure 0.3. Burg PSD Estimate; (a) 2-Spaced-BRB; (b) 2-Neighbour-BRB; (c) 3-Spaced-BRB; and (d) 3-Neighbour-BRB

Table 0.2: Comparative Features of Burg and Welch PSD Technique.

	Burg	Welch
Technique	Parametric	Non Parametric
Property	No window, indirect method	Direct method, Windowed signal Averaging modified periodogram of signal.
Advantages	<ul style="list-style-type: none"> ✓ High resolution for short data records. ✓ Guarantees Stable model 	<ul style="list-style-type: none"> ✓ Uniform Variance ✓ Application of Taper to segmented signal. ✓ Welch estimate is biased, but asymptotically unbiased
Disadvantages	<ul style="list-style-type: none"> ✓ Peak condition depends on prior phase. ✓ Susceptible to spectral line-splitting in the presence of noise and large order ✓ There is frequency preference for estimates of sinusoids in noise 	Limited Resolution

5.2 Welch PSD Technique

To further validate the conclusion using the Burg PSD Estimate, the Welch PSD technique is implemented in this paper using the signal processing Matlab toolbox. This technique involves segmenting time series signal data, computing a modified periodogram of each segment, and averaging PSD estimates. In this paper, a non-rectangular window Barlett and long data from the simulated stator current signal model are used to improve redundancy introduced by overlapping and to manage the resolution deficiency. The effect of averaging modified periodogram is that variance is reduced. The output from the implementation of Welch PSD technique are displayed in Fig 5.4 and Fig 5.5 (a)-(d).

The mathematical computation algorithm for the Welch spectral estimate is shown in Eqs. (5) - (9) according to [23].

$$B_{xx}^W(w) = \frac{1}{K} \sum_{i=1}^K J_M^{(i)}(w) \quad (5)$$

Where $B_{xx}^W(w)$ is the biased spectral estimate, $J_M^{(i)}(w)$ is periodogram, and K is 1, 2, 3... n.

$$J_M^{(i)}(w) = \frac{1}{MU} \left| \sum_{n=0}^{M-1} w[n] x^{(i)}[n] e^{-jwn} \right|^2 \quad (6)$$

$$U = \frac{1}{M} \sum_{n=0}^{M-1} w[n]^2 \quad (7)$$

$$J_M^{(i)}(w) = \frac{1}{U} \left| \sum_{l=-(M-1)}^{M-1} C_{vv}^{(i)}[l] e^{-jwl} \right|^2 \quad (8)$$

The Welch estimate can be determined as follows:

$$W(e^{jw}) = \frac{1}{MU} \left| \sum_{n=0}^{M-1} w[n] e^{-jwn} \right|^2 \quad (9)$$

Where, U is the normalization factor, M depicts the length of sub samples, $w[n]$ is the applied window, and $W(e^{jw})$ represents the spectral window.

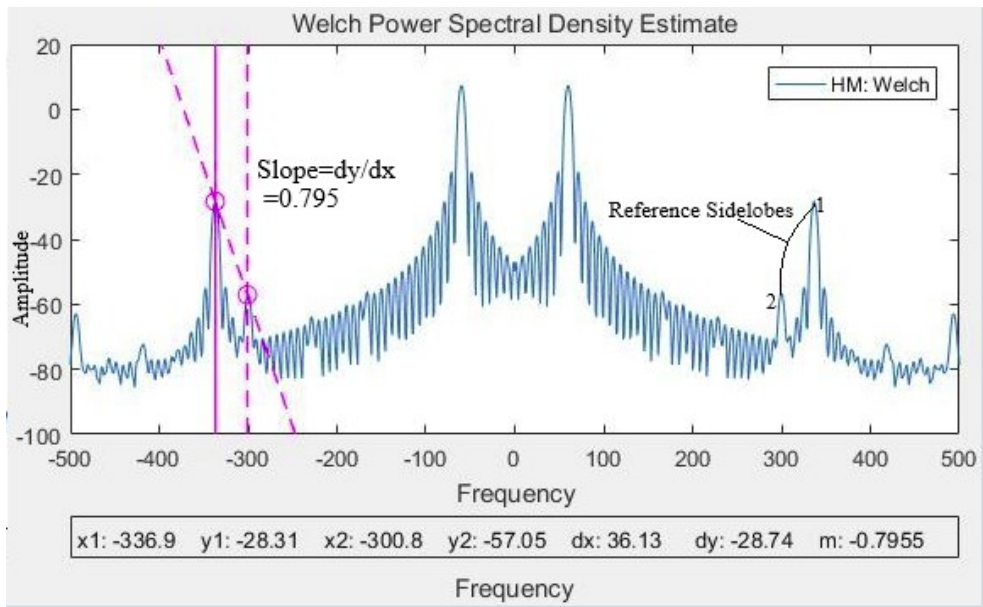
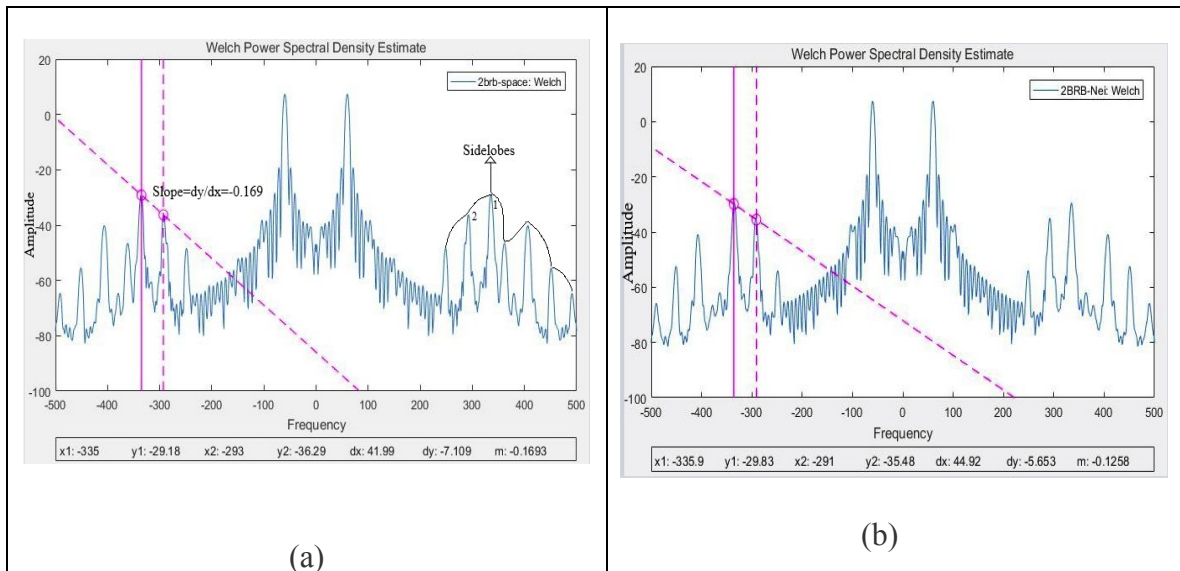


Figure 0.4. Welch PSD Spectrum for Healthy Motor Condition.



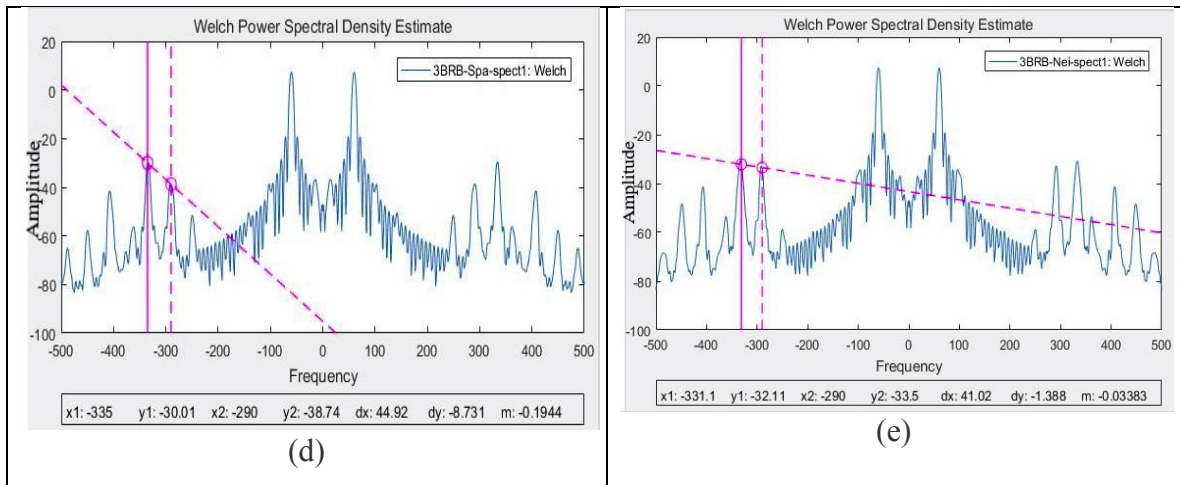


Figure 0.5. Welch PSD Estimate; (a) healthy motor; (b) 2 Spaced BRBs (c) 2 Neighbouring BRBs; (c) 3 Spaced BRBs; (d) 3 Neighbouring BRBs

Section IV. Result Analysis

In the presence of BRB faults, side band harmonics abound [24]. As it can be observed in Tables 5.3 (III) and 5.4 (IV) and the corresponding graphs, it is distinctively clear that the motor with neighboring BRB faults has a lower slope between the referenced side lobes, which is indicative of change in terms of amplitude to the frequency ratio (i.e. y and x axis) and this implies a greater field distortion incensed by the proximity of the broken bars. The spaced BRB fault expectedly has a higher slope which is indicative of a lower field distortion due to the distance of side bars. Dy and dx are the reference side lobes that emerge in the presence of BRB faults. The reference frequencies are determined by applying $f_b (1-2ks) f$, (where s represents slip, f_b depicts bar frequency, fundamental frequency is denoted as f, and $k=1, 2, 3, \dots$). Harmonic frequency due to BRBs is predictable as illustrated in [26]. dy in the estimates depicts change in amplitude of the earmarked sidelobes and dx denotes change in the frequency of the earmarked side lobes. Since BRB faults introduce asymmetry, which in

turns alter the uniform field distribution, field unevenness distorts the torque uniform rotary motion and eventually the speed is affected. The Relationship between the fault related field and torque is shown in Equ. (10) [25].

The details of the effect of the fault on motor speed and mathematical computation follows the order described in [25]. Asymmetry is reflected in non-uniformity of the signal, and by finding the slope of the reference side lobes, the PSD's spectrum estimate for neighboring and spaced BRB faults shows changes in the slope that can provide information of the motor fault condition. By using slope as a yardstick for the analysis of neighboring and spaced BRB faults, it is easy to see that both frequency spectrum and amplitude changes constitute the criteria for ascertaining the fault severity.

Through Burg and Welch PSD analysis techniques, it is shown that a neighboring BRB fault has more severe effects than a spaced BRB fault. Both techniques maintain consistent changes from a small slope for neighboring to a large slope for spaced BRB faults

$$C_{e_{tot}} = C_{e_{srp}} + C_{e_{srn}} = \pi \frac{RL_{em}}{\mu_0} k_s I_s [k_r \sin(\phi B_s + \phi B_r) + k_r I_{rn} \sin(2s\omega t + \phi B_s - \phi B_r)] \quad (10)$$

Where R connotes the average radius of the air-gap, L represents the active length of the magnetic circuit, and μ_0 is the magnetic permeability of the air. The mean of the torques due to interaction of stator and rotor normal field is denoted as C_{e_srp} C_{e_srn} . This represents the pulsating torque of pulsation $2s\omega$ fault field due to BRB. ϕB_s , ϕB_{rp} , and ϕB_{rn} depicts respective phases relative to the stator phase one current of the stator flux density, the rotor flux densities for both healthy motor field and fault field; k_s represents the coefficient and a

function of the stator winding arrangement, and k_r is a coefficient and a function of the cage rotor assembly. I_s , I_m and I_r depicts stator current, negative rotor current and positive rotor current.

Table 0.3: (III) Burg PSD analysis

	2-Neighbouring BRB	2-Spaced BRB	3-Neighbouring BRB	3-Spaced BRB
Frequency(dx-axis)	44.92	48.83	41.99	50.78
Amplitude(dy-axis)	-8.174	-10.62	-3.14	-15.59
Slope (m)	-0.182	-0.2175	-0.0748	-0.307

Table 0.4: IV Welch PSD analysis

	2-Neighbouring BRB	2-Spaced BRB	3-Neighbouring BRB	3-Spaced BRB
Frequency(dx-axis)	41.99	41.99	41.02	44.92
Amplitude(dy-axis)	-6.609	-5.628	-1.388	-8.731
Slope (m)	-0.1574	-0.134	-0.0338	-0.194

Section IV Conclusion

In this paper, two types of BRB faults, neighbouring and spaced BRBs, are investigated through Burg and Welch PSD estimate algorithms. The fault severity can be obtained by examining the slope of two reference side lobes. It was observed that neighboring BRB fault has a smaller slope than a spaced BRB fault. The consistent result obtained from the implementation of both PSD (Burg and Welch PSD respectively) methods shows that neighboring BRB fault has more severe effects than a spaced BRB fault. The implication of smaller slope means more proximity between bars field and asymmetry within the rotor field chamber. This is due to the interaction between the fields produced by individual bar, resulting in greater distortion of the field and motor operation. Although same trend can be

seen for both methods, as observed in Table 5.3 and 5.4, Welch PSD method offers more reliability in terms of results because the averaging of the segmented signals minimizes variances and errors. Burg PSD method, on the other hand, can vary with the type of the window applied. For a spaced bar the larger slope means less field distortion and less devastating effects on the motor operation. As neighboring broken bar increased from 2 to 3, the slope reduced even further for both PSD techniques. This phenomenon justified that the slope can be used to ascertain the severity effect on the field distribution and entire operation of motor. Future work will involve modeling more fault conditions, such as four and five BRBs, and use the slope as a feature to automatically diagnose fault conditions.

References

- [1] A. H. Bonnett, G. C. Soukup, "Cause and analysis of stator and rotor failures in three-phase squirrel-cage induction motors", *IEEE Trans. Ind. Appl.*, vol. 28, no. 4, pp. 921-937, Jul./Aug. 1992.
- [2] J. Yun, J. Cho, S. B. Lee, J. Yoo, "On-line detection of high-resistance connections in the incoming electrical circuit for induction motors", *IEEE Trans. Ind. Appl.*, vol. 45, no. 2, pp. 694-702, Mar./Apr. 2009.
- [3] Xiaodong Liang, and Kenneth Ik Edomwandekhoe, "Condition Monitoring Techniques for Induction Motors", *Proceedings of 2017 IEEE Industry Applications Society (IAS) Annual Meeting*, pp. 1-10, Cincinnati, OH, USA, October 1- 5, 2017.
- [4] A. Stefani, F. Filippetti, A. Bellini, "Diagnosis of induction machines in time-varying conditions", *IEEE Trans. Ind. Electron.*, vol. 56, no. 11, pp. 4548-4556, Nov. 2009.
- [5] Chakraborty, Chandan and Verma, Vimlesh "Speed and Current Sensor Fault Detection and Isolation Technique for Induction Motor Drive Using Axes Transformation" *IEEE Transactions on Industrial Electronics*, Vol.62 (3), pp.1943-1954. March 2015.
- [6] J. A. Daviu, S. Aviyente, E. G. Strangas, M. R. Guasp, "Scale invariant feature extraction algorithm for the automatic diagnosis of rotor asymmetries in induction motors", *IEEE Trans. Ind. Informat.*, vol. 9, no. 1, pp. 100-108, Feb. 2013.
- [7] J. Antonino-Daviu, M. Riera-Guasp, J. Roger-Folch, M. P. Molina, "Validation of a new method for the diagnosis of rotor bar failures via wavelet transformation in industrial induction machines", *IEEE Trans. Ind. Appl.*, vol. 42, no. 4, pp. 990-996, Jul./Aug. 2006.

- [8] B. Akin, S. Choi, U. Orguner, H. A. Toliyat, "A simple real-time fault signature monitoring tool for motor-drive-embedded fault diagnosis system", *IEEE Trans. Ind. Electron.*, vol. 58, no. 5, pp. 1990-2001, May 2011.
- [9] Y. Gritli et al., "Advanced diagnosis of electrical faults in wound-rotor induction machines", *IEEE Trans. Ind. Electron.*, vol. 60, no. 9, pp. 4012-4024, Sep. 2013.
- [10] J. Cusido, L. Romeral, J. A. Ortega, J. A. Rosero, A. G. Espinosa, "Fault detection in induction machines using power spectral density in wavelet decomposition", *IEEE Trans. Ind. Electron.*, vol. 55, no. 2, pp. 633-643, Feb. 2008.
- [11] M. Riera-Guasp, J. A. Antonino-Daviu, M. Pineda-Sanchez, R. Puche-Panadero, J. Perez-Cruz, "A general approach for the transient detection of slip-dependent fault components based on the discrete wavelet transform", *IEEE Trans. Ind. Electron.*, vol. 55, no. 12, pp. 4167-4180, Dec. 2008.
- [12] D. Vakman, "On the analytic signal the Teager-Kaiser energy algorithm and other methods for defining amplitude and frequency", *IEEE Trans. Signal Process.*, vol. 44, no. 4, pp. 791-797, Apr. 1996.
- [13] M. P. Sanchez et al., "Application of the Teager-Kaiser energy operator to the fault diagnosis of induction motors", *IEEE Trans. Energy Convers.*, vol. 28, no. 4, pp. 1036-1044, Dec. 2013.
- [14] D. Dimitriadis, A. Potamianos, P. Maragos, "A comparison of the squared energy and Teager-Kaiser operators for short-term energy estimation in additive noise", *IEEE Trans. Signal Process.*, vol. 57, no. 7, pp. 2569-2581, Jul. 2009.

- [15] S. M. A. Cruz, A. J. M. Cardoso, "Stator winding fault diagnosis in three-phase synchronous and asynchronous motors by the extended Park's vector approach", *IEEE Trans. Ind. Appl.*, vol. 37, no. 5, pp. 1227-1233, Sep./Oct. 2001.
- [16] G. Acosta, C. Verucchi, E. Gelso, "A current monitoring system for diagnosing electrical failures in induction motors", *Mech. Syst. Signal Process.*, vol. 20, no. 4, pp. 953-965, 2006.
- [17] R. Puche-Panadero, M. Pineda-Sanchez, M. Riera-Guasp, J. Roger-Folch, E. Hurtado-Perez, J. Perez-Cruz, "Improved resolution of the MCSA method via Hilbert transform enabling the diagnosis of rotor asymmetries at very low slip", *IEEE Trans. Energy Convers.*, vol. 24, no. 1, pp. 52-59, Mar. 2009.
- [18] Fiser, R. and Ferkolj, S. "Application of a finite element method to predict damaged induction motor performance" *IEEE Transactions on Magnetism*, Sept. 2001, Vol.37 (5), pp.3635-3639.
- [19] Marple, S. Lawrence *Digital Spectral Analysis*. Englewood Cliffs, NJ: Prentice Hall, 1987.
- [20] S. Beheshti, "A new approach to order selection and parametric spectrum estimation," *IEEE Proceeding, ICASSP*, Vol. 3, pp. 520-523, May 2006.
- [21] Akben, S. B., Subasi, A. and Kiyimik, Mahmut K. "Comparison of sub-space based MUSIC and AR BURG methods in diagnosis of migraine by support vector machines" 2010 *IEEE 18th Signal Processing and Communications Applications Conference*, April 2010, pp.192-195.

- [22] H. Akaike, A new look at the statistical model identification, IEEE Trans. Autom. Control AC. 19 (1974) 716-723
- [23] Silvia Maria. Alessio author. SpringerLink (Online service) “Digital Signal Processing and Spectral Analysis for Scientists Concepts and Applications” Springer eBooks Cham: Springer International Publishing: Imprint: Springer 2016.
- [24] G. B. Kliman, J. Stein, R. D. Endicott, "Noninvasive detection of broken rotor bars in operating induction motors
- [25] Ceban, A., Pusca, R. and Romary, R. “Study of Rotor Faults in Induction Motors Using External Magnetic Field Analysis” IEEE Trans. Industrial Electronics, May 2012, Vol.59 (5), pp.2082-2093.

Chapter 6: Conclusion and Future Work

6.1 Contribution

The objective of the research is to achieve fault diagnosis for broken rotor bar faults in induction motors. The finite element analysis method is used to create various models for healthy motors and the motors with different numbers of BRBs. The finite element software ANSYS is used to create such models. The models can output various parameters such as stator current, speed and torque. The simulated stator current is used in signal processing algorithms for BRB fault detection.

The thesis comprises four manuscripts that employed various parametric MCSA diagnosis technique, such as FFT, Burg PSD estimate, Welch PSD estimate, and Multitaper, for the identification of different BRB faults. Also, non-parametric method, such as YUL-AR method were also used for fault detection. The MP decomposition technique proved effective for diagnostic and classification purposes. Welch PSD was the most effective of the various non parametric methods deployed for fault discovery and classification. Peaks of the Welch PSD estimate serve as features for training and classification purposes. YUL-AR on the other was able to clearly identify fault behaviour. Results obtained for this method agreed with result obtained from traditional FFT method. The Multitaper technique also proved very effective for demonstrating amplitude and frequency behaviour in the presence of BRB fault. Although these various methods did not prove successful for classification purposes, the consistent result obtained from the application of the various method showed

that methods were able to diagnose faults through monitoring of the sidebands, amplitude peaks and characteristic harmonics associated with BRB faults.

ANN and SVM were the artificial intelligence tools used in this thesis. Both techniques were used to train features collected from PSD and MP screening methodology for the purposes of training and classification. SVM used the quadratic model and obtained 100% fault prediction accuracy for MP and 96% fault prediction accuracy for PSD features. Through scripts (codes) ANN successfully trained and classified motor various condition in four quadrants. A 95% fault prediction accuracy was obtained.

Chapter 4 of this thesis demonstrates the effectiveness of using MP decomposition method for diagnosis and real-time classification purposes. MP has never been deployed for motor signal analysis. The successful application of this method for diagnosis and classification of IM BRB faults opens new possibilities for researchers to explore this method for other machine fault detection and real-time monitoring. As seen from the results obtained, The MP technique is able to approximate signals for distinct feature selection and fault classification. Moreover, in Chapter 3; it can be seen that PSD side lobes peaks serve as features and proved very effective in BRB severity classification. However, this technique could only classify 1, 2, and 3 BRB faults.

Lastly, Chapter 5, which is yet to be published offers a promising method, that can easily separate neighbouring bar from spaced bar by monitoring reference side lobes and computing the slope of the side lobes.

6.2 Future Work

Future work will entail comparing result obtained from the model analysis with machine in the real world. Without comparing with experimental case or real operation machine condition, the work will not be totally complete. Comparison with real machine is required for validation of all techniques employed in this thesis. A 3-D ANSYS modeling for induction motors allows room for various implementation of near real life scenarios, so it is recommended to be used in the future.